UNIVERSITAT POLITÈCNICA DE CATALUNYA
BARCELONATECH
Escola Superior d'Enginyeries Industrial,
Aeroespacial i Audiovisual de Terrassa

Effect of the diurnal heating on urban street canyons: a CFD study

Document:
Report

Author:
Javier Ferrón Rísquez

Director /Co-director:
Ivette Maria Rodríguez Pérez

Degree:
Master in Industrial Engineering

Examination session:
Autumn Extension, 2021

MASTER FINAL THESIS

Declaration of honour

Title of the Thesis: Effect of the diürnal heating on urban street canyons: a CFD study.

Author: Javier Ferrón Rísquez

Director: Ivette Maria Rodríguez Pérez

I declare that,

The work in this Master Thesis is completely my own work,

No part of this Master Thesis is taken from other people's work without giving them credit,

All references have been clearly cited,

I understand that an infringement of this declaration leaves me subject to the foreseen disciplinary actions by *The Universitat Politècnica de Catalunya.*

Javier Ferrón Rísquez	24/04/2022
Student Name	Date

Acknowledgements

The intention of the following lines is to express my gratitude to all people who has helped me to develop this project.

Firstly, I want to thank my thesis director, *Ivette María Rodríguez Pérez*, whose knowledge and support has helped me a lot to go in the right direction to carry out this study.

My colleague *Eric Olmo* deserves mention not for helping me to develop this thesis, but for sharing all these years of university and to help each other with unconditional support.

Also, a special mention to my nearest family, especially to *Arnau* who has stand there for me whenever I needed him, despite the distance that separates us.

Finally, but not less important, I would like to thank my parents and my little nurse *Laura*. Thank you for supporting me and for your patience during all these years because without your unconditional support I would not be able to overcome this road plenty of difficulties.

Abstract

In this study Computational Fluid Dynamics (CFD) are used to predict the air flow structure and pollutant retention inside urban canyons taking into account thermal effects due to solar radiation in order to imitate diurnal heating over a city. The diurnal heating induces buoyancy therefore the flow structure and pollutant concentration will be completely different depending on the daytime.

The presented method departs from a 2D domain comprised by eight urban canyons of aspect ratio 1 and different 2D transient RANS (Reynolds-Averaged Navier-Stokes) simulations that have been conducted using OpenFoam. Isothermal, single-surface heating and multi-surface heating cases are considered. For all of them, the results obtained have been post-processed using ParaView and Matlab to be able to analyse all the information related with velocity, pressure, temperature, pollutant concentration, streamlines, etc. These results have been also contrasted and validated with data obtained from wind-tunnel experiments and other CFD simulations which have been conducted using a 2D model and conditions similar to the ones used in this thesis.

Finally, the conclusions obtained for an airflow with a Reynolds number of 12000 are that for most cases, a single main vortex is formed which is strengthen for the cases where leeward or ground surfaces are heated up compared to the vortex formed in isothermal case. In all cases where the windward side is heated up, a second counter-rotating vortex appears due to buoyancy and displaces the main one from the center of the canyon. Also, when the windward side is heated, the concentration of pollutants increases at the pedestrian level which may be considered as the worst case.

Further improvements may be considered to continue with this work such as improving the mesh quality, considering an additional heat source, using another turbulence modelling (LES) or even considering a 3D model since the buoyant flows have an unsteady and 3D characteristc that require complex numerical models to obtain more accurate results.

Resum

En aquest estudi la dinàmica de fluids computacional s'utilitza per predir el moviment de l'aire i la retenció de contaminants a l'interior de canyons urbans tenint en compte efectes tèrmics provinents de la radiació solar per tal d'imitar l'escalfament diürn sobre una ciutat. L'escalfament diürn indueix la flotabilitat, de manera que l'estructura del flux d'aire així com la concentració de contaminants seran completament diferents segons el dia i l'hora en què ens trobem.

El mètode presentat parteix d'un domini 2D format per vuit canyons urbans d'aspect ratio 1 a partir del qual s'han realitzat diferents simulacions 2D transitòries RANS (Reynolds-Averaged Navier-Stokes) mitjançant OpenFoam: s'han considerat els casos isotèrmic, escalfament d'una única superfície i escalfament de múltiples superfícies. Per a tots ells, els resultats obtinguts han estat postprocessats mitjançant ParaView i Matlab per poder analitzar tota la informació relacionada amb la velocitat, la pressió, la temperatura, la concentració de contaminants, les línies de corrent, etc. Aquests resultats també s'han contrastat i validat amb dades provinents d'experiments de túnel de vent i d'altres simulacions CFD que s'han dut a terme mitjançant un model 2D i sota condicions similars a les utilitzades en aquesta tesi.

Finalment, les conclusions obtingudes per a un flux d'aire amb un nombre de Reynolds de 12000 són que en la majoria dels casos, es forma un únic vòrtex principal que s'intensifica pels casos en què s'escalfa la paret de sotavent o el carrer en comparació amb el vòrtex que es forma en el cas isotèrmic. En qualsevol cas en què el costat de barlovento s'escalfa, apareix un segon vòrtex en contra-rotació a causa de la flotabilitat i desplaça el principal prèviament ubicat al centre del canó. Així mateix, quan s'escalfa el costat de barlovento, la concentració de contaminants augmenta a nivell de vianants de tal forma que es pot considerar com el pitjor dels casos.

Es poden considerar millores addicionals per continuar amb aquest treball com ara millorar la qualitat de la malla, considerar una font de calor addicional, utilitzar un altre model de turbulència (LES) o fins i tot considerar un model 3D ja que la flotabilitat té una característica inestable i 3D que requereix d'uns model numèrics complexos per obtenir resultats més precisos.

Table of contents

List of tables

List of figures

Glossary

- ACH: Air Change per Hour.
- AR: Aspect Ratio.
- CAD: Computer Aided Design.
- CFD: Computational Fluid Dynamics.
- DNS: Direct Numerical Simulation.
- EVM: Eddy Viscosity Model.
- FVM: Finite Volume Method.
- LDA: Laser Doppler Anemometer.
- LES: Large Eddy Simulation.
- RANS: Reynolds-Averaged Navier-Stokes.
- RNG: Re-Normalized Group.
- TKE: Turbulent Kinetic Energy.
- UHI: Urban Heat Island

1. Introduction

1.1 Object

The main purpose of this project is to study how diurnal heating affects air movement and pollutant transport inside an urban street canyon comprised by buildings of the same height. A simplified two-dimensional street canyon will be studied using computational fluid dynamics (CFD).

This thesis will continue the studies carried out previously by Jordi Galí [1] and Pau García [2] on the same field. Here, temperature will be added in order to understand how it affects the air movement and pollutant removal in urban street canyons of aspect ratio 1.

1.2 Scope

The points that this project covers are the following:

- State of the art of urban street canyons and heat island effect.
- Prepare and run the ideal case where all walls are considered at the same temperature (Isothermal case).
- Study the results for the isothermal case.
- Validation of the results obtained with similar studies such as results from other simulations as well as experimental results.
- Prepare and run three different single-surface heating scenarios (direct ground floor heating, leeward heating and windward heating).
- Validation of the results obtained with other sources.
- Set up and run multi-surface heating scenarios in order to simulate the sunlight orientation and shadowing effects in the canyon.
- Analyse the obtained results as well as to validate them with other sources.
- Make a comparison and a discussion about results obtained.
- Explaining the environmental impact of the project.
- Conclusions and future improvements.

Some aspects that this study does not cover are the following:

- Three-dimensional CFD simulations.
- Radiation will not be considered in the CFD simulations.

1.3 Requirements

The requirements that should be achieved on this thesis are the following:

- Find an appropriate solver of OpenFoam to include and solve the energy equation in order to introduce temperature in the base case.
- Be able to create an initial simulation using this solver to analyze how is the airflow structure as well as the pollutant transport in an ideal heating case (Isothermal).
- Obtain results with physical sense for the non-isothermal cases which show that any change in temperature has an effect on the structure of the air flow as well as on the pollutant transport.
- Be able to make a comparison and obtain conclusions about the influence of the temperature difference between canyon walls and ambient air.
- Propose future improvements.

1.4 Justification

One of the main environmental problems world-wide known is pollution. Big cities are a constant emission of atmospheric pollutant sources (hydrocarbons, carbon monoxide, nitrogen oxides among others). They tend to increase their emissions as cities become larger due to the increases in vehicles, industrial processes, residual treatments, etc.

Nowadays some cities in developed countries are trying to decrease their emissions by applying traffic restrictions, while some other developing countries such as India or China has increased their emissions during last years.

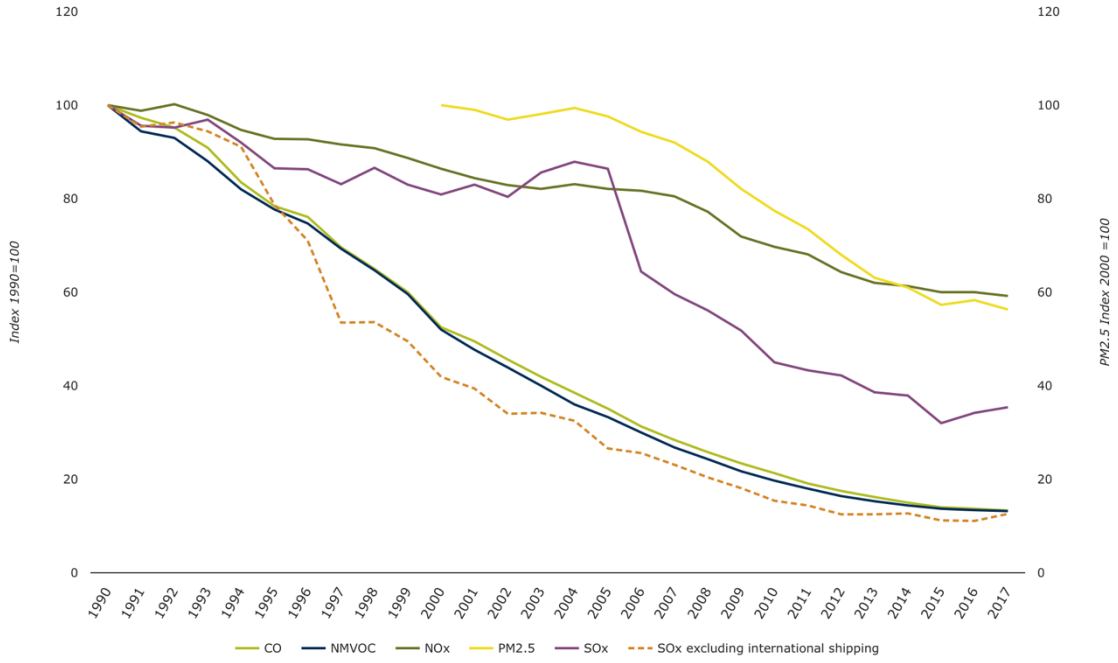

Figure 0-1. Trends in emissions of air pollutants from transport (Extracted from [3])

Nevertheless, the growth of cities coupled with the high density in some of them gives rise to bigger and taller buildings. Because of this, the quantity of urban canyons has increased all over the world.

There is an important problem related to these urban canyons which is the air quality that depends on the wind direction and also the temperature. On one hand, when the mean wind direction is

perpendicular to the canyon a vortex flow is created inside the canyon increasing the recirculation of the airflow, reducing dispersion of the pollutants and, therefore, increasing the pollutant concentrations. On the other hand, the temperature changes the velocity map field, thus affecting the pollutant concentration inside the canyon.

Summing up, the justification of this thesis is the need to understand how diurnal heating affects the air movement and distribution within urban canyons. There is also a need to comprehend how it can affect the distribution of atmospheric pollutants related to cities air quality linked with health problems of the inhabitants of the city.

2 Review of the state of the art

2.1 State of the art

Urban canyons are being studied since late years of 20th century. Among these studies, lots of CFD simulations have been carried out considering different types of urban canyons with different geometries and boundary conditions to obtain information about airflow distribution and the pollutant concentration. Some of these studies have included thermal effects in order to understand how temperature affects air movement and removal of air pollutants in urban canyons.

T. R. Oke conducted some of initial studies among which stand out: on one hand, the energy exchange balance within the mid-latitude urban canyons during summer weather in which he conclude that almost 30% of the midday solar energy received by the canyon is stored in the materials of the canyon [4]. On the other hand, the analysis of regular canyons where he define the existence of different regime flows that depend on their geometrical parameters.[5]

Later on, *Sini* [6] and *Kim J.J.* [7] made some of the first CFD studies in which temperature was included as they discussed the thermal effects over airflow and pollutant distribution considering heat exchange transfer in different urban canyons with different aspect ratios. In these studies, CFD simulations were carried out considering a RANS k-Epsilon model. Regarding the heat source, it was located in three different surfaces: upwind building (leeward surface), downwind building (windward surface) and ground. *Kim J.J.* concluded that the pollutant distribution and removal depends on the aspect ratio of the canyon as well as the heat source location. When the source is located in the upwind building, it appears one vortex regardless of the aspect ratio. The same performance was found when the source is located in the ground for aspect ratios lower than 3. Finally, when the source is located in downwind building, two contra-rotating vortex appears within the canyon.

During the first decade of 21st century, some studies were carried out using turbulence models that requires major computational cost than those performed with a RANS k-epsilon model. For example, Xian-Xiang Li performed a CFD simulation using a Large Eddy Simulations (LES) turbulence model [8].

It is important to note that some wind tunnel experiments have been carried out from the last years of XXth century to the current days. Examples of that are the experiment done by *Pavageau* to study the pollutant concentration in regular street canyons and the experiment performed by *Uehara* to study how thermal stratification affects the air flow in and above urban street canyons. These experiments are currently used in most of the CFD studies of urban canyons in order to validate CFD models. [9][10]

Undoubtedly, there are lots of studies that can be used as reference literature in order to validate, compare and prove the results obtained. The reports mentioned above are some of those that will be used as a reference.

2.2 Problem definition

From the 1920s to the present, the world population has increased by about 5.000 million people. This significant population growth has been accompanied by technological and industrial development worldwide, giving rise to widespread economic growth over the years that has also led to the need to create more jobs nearby the industrial and business centers.[11]

This has produced the creation of large cities around the world to accommodate more and more people. In addition, accumulating high population densities in cities with a limited land area has led to the need to create even higher structures in these cities, which have evolved to what is commonly referred as urban canyons.

There are two major problems related to the appearance of these urban canyons, which are the worsening of air quality in cities and the appearance of the well-known urban heat islands.

On the air quality side, it is important to note that as cities and populations have grown, the number of combustion vehicles circulating along the streets and emitting polluting particles has also increased. This is a problem that is aggravated when the wind direction is perpendicular to the streets of these canyons, since air vortices appears inside the canyons reducing the renewal of air inside the canyon, especially at pedestrian height.

The appearance of large cities has led to an increase in temperature compared to neighbouring non-urbanized areas, a phenomenon known as urban heat islands (UHIs). When a natural landscape is replaced by a large amount of artificial material, it absorbs part of the incident solar radiation and retains it for a long time. This effect can lead to increasing the temperature in urban areas in such a way that if the appropriate conditions are met, the increase of temperature in cities with respect to adjacent areas can reach between 10K and 15K.[40]

One of the most important factor for the appearance of UHIs is related with geometry, orientation and construction materials of urban canyons since they provide a large amount of surface for the reflection and absorption of sunlight. Moreover, when the wind is blowing in a perpendicular direction to them, the buildings block the action of the wind so that the cooling of the streets by convection is inhibited and the pollutant removal is prevented as well.

It is important to highlight the fact that there are many elements which may increase temperature inside urban canyons, not only solar radiation, such as the heat generated by the combustion of vehicles, air conditioning and even high levels of pollution which can trap solar radiation and increase temperature making the microclimate effect inside the canyons stronger.[12]

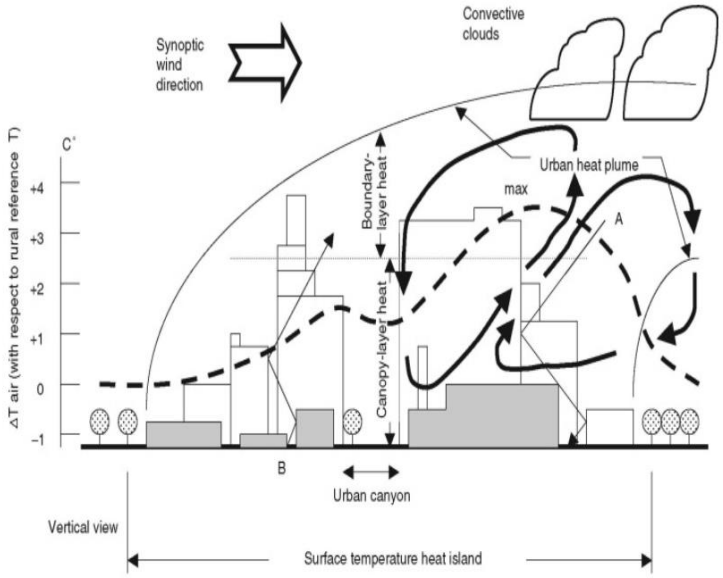

Figure 2-1. Diagram of the heat layers from an UHI (Extracted from: [13])

In this study, a two-dimensional model will be used to carry out simulations that will consist of different canyons with an identical aspect ratio, following a repetitive pattern that could be similar to those present in cities such as Barcelona. Also a pollutant source will be added as well as different scenarios including different temperatures between walls and ground in order to see how it affects the pollutant concentration and the air distribution inside canyons.

2.3 Main concepts of urban canyons

Firstly, there are some concepts and characteristics that will be presented below and serve to define an urban canyon [14]:

- Aspect ratio: is the ratio between the height and the width of the canyon (H/W). Depending on the ratio, they can be classified as:
    - Regular canyons: when the aspect ratio is approximately 1.
    - Avenue canyons: when the aspect ratio is lower than 0,5.
    - Deep canyon: when the aspect ratio is approximately 2.
- Upwind building: when the wind is blowing perpendicularly to the canyon, it is the building that receives beforehand the action of the wind.
- Downwind building: when the wind is blowing perpendicularly to the canyon, it is the building that receives later the action of the wind.
- Windward side: is the side of the building to which the wind is directly blowing.
- Leeward side: is the opposite side of the building to which the wind is directly blowing.

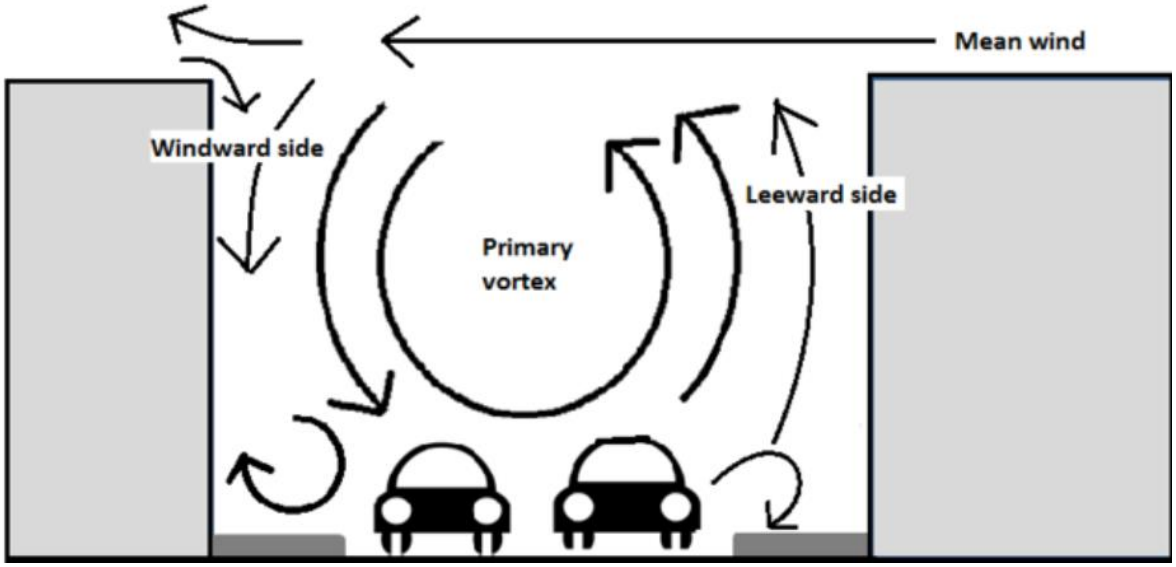

Figure 2-2. Parts of an urban canyon (Extracted from [14])

- Flow patterns: three different flow patterns in street canyons have been described by *Oke [5]:*
    - Isolated roughness flow: when the aspect ratio varies between 0.05 and 0.3 it indicates that the width of the canyon is enough to disturb the wakes of the low field.
    - Wake interference flow: this flow appears when the aspect ratio is approximately 0.5 and it is characterized by secondary flows in the canyon. The downward flow of the canyon is reinforced by deflection down the windward face of the next building downstream.
    - Skimming flow: when the aspect ratio is approximately 1 or even higher, the skimming flow appears. This flow is characterized by a stable single or multiple vortexes in the canyon and it is of special interest to investigate the pollutant removal to evaluate proposals for improving air quality of the city.

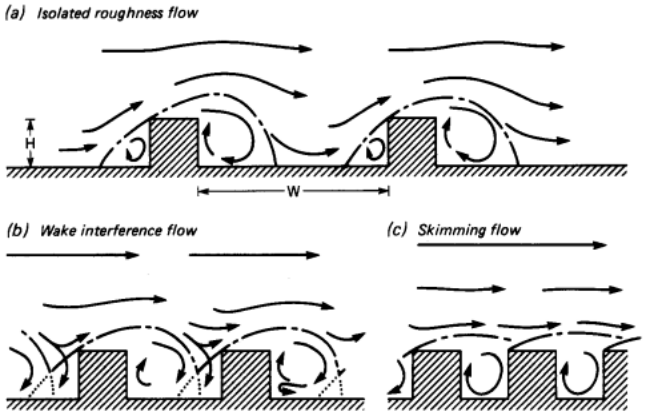

Figure 2-3. Interaction of different regime flows with buildings (Extracted from [5])

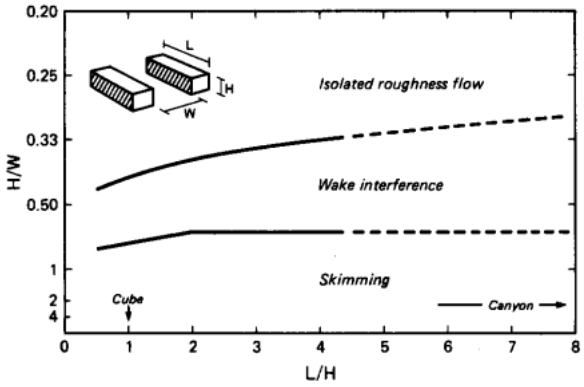

Figure 2-4. Classification of flow regimes depending on canyon parameters (Extracted from [5])

In addition to the previously mentioned flow patterns that depend on the aspect ratios H/W of the canyons, there are two more causes defined by Oke that are related with the temperature inside the canyon and the urban heat island effect. These causes are the increased absorption of solar radiation caused by multiple reflection and the reduction of long-wave radiation loss, directly related with the sky view factor. Regarding the solar radiation, it is important to note the relevance of surface albedo and solar access.

- Sky view factor [15]: the SVF is a dimensionless value from 0 to 1 and is calculated as the fraction of sky visible from the ground up. The SVF indicates the street geometry and building density; for example a value of 1 denotes that the sky is completely visible. Building's quantities and also its geometry limit the sky view factor results. A low SVF due to this reason increase the net heat storage as well as the UHI. The trees can also limit the SVF, but they do not store as much heat as buildings' materials.
- Surface albedo: is the ratio of radiosity (radiant flux per area unit that leaves the surface) to the irradiance received by a surface. The albedo of an urban canyon depends on the canyons materials as well as their geometry: it increases with the aspect ratio and is greater for East-West oriented canyons.
- Solar access: is the ability of buildings to receive sunlight without obstruction from other buildings, vegetation, etc. As shown in the figures below, the limit for solar access to urban canyons depends on the degree of penetration at the winter solstice.

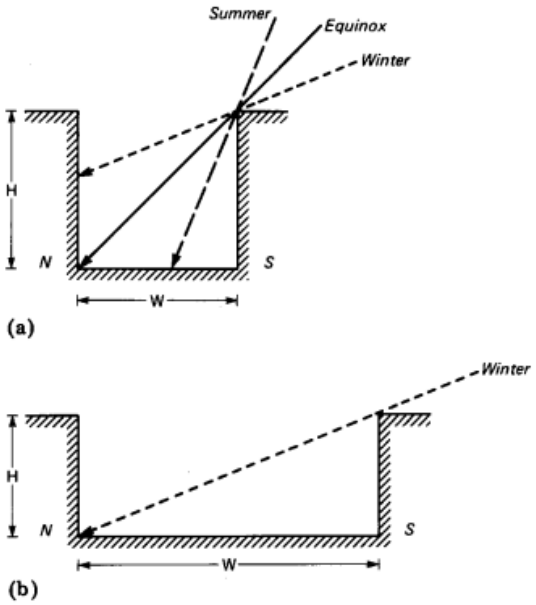

Figure 2-5. Solar access in canyons of different aspect ratios (Extracted from [5])

3 Theoretical framework

The mathematical models of this thesis are based on the numerical solution to the governing fluid flow equations as well as to the transport equations. They derive from basic conservation and transport principles in incompressible turbulent flows.

3.1 Convection-diffusion equation

The convection diffusion equation, also known as generic scalar transport equation, describes physical phenomena where particles, energy or other physical quantities are transferred inside a physical system due to diffusion and convection. [43]

$$\frac{\partial \rho\phi}{\partial t} + \nabla \cdot (\rho\vec{u}\phi) = \nabla \cdot (\Gamma \nabla\phi) + S_\phi \tag{3.1}$$

Where,

- $\frac{\partial \rho\phi}{\partial t}$ is the transient term. This term indicated the temporal variation of generic property ϕ in the control volume.
- $\nabla \cdot (\rho\vec{u}\phi)$ is the convection term and accounts for the transport of ϕ due to the existence of the velocity field.
- Γ is the diffusion coefficient or diffusivity.
- $\nabla \cdot (\Gamma\nabla\phi)$ is the diffusion term and accounts for the transport of ϕ due to its gradients.
- S_ϕ is the source term and accounts for any source that creates or destroys ϕ.

3.2 Navier-Stokes Equations

Due to the low velocities in street canyons, air is assumed to behave as an incompressible fluid. Thus, some of the following expressions that describes the motion of viscous fluid substances will be simplified.

- Mass conservation equation [16]:

$$\frac{\partial \rho}{\partial t} + \frac{\partial \bar{u}_i}{\partial x_i} = 0 \tag{3.2}$$

  Due to the fluid is incompressible:

$$\frac{\partial \bar{u}_i}{\partial x_i} = 0 \tag{3.3}$$

- Momentum conservation equations [16]:

$$\frac{\partial}{\partial t}(\rho\bar{u}_i) + \frac{\partial}{\partial x_j}\left(\rho\bar{u}_i\bar{u}_j\right) = \frac{\partial \bar{p}}{\partial x_i} + \rho g_i + \mu\left(\frac{\partial^2 \bar{u}_i}{\partial x_j^2}\right) \tag{3.4}$$

  The general momentum equation for an incompressible flow can be express as:

$$\frac{\partial \bar{u}_i}{\partial t} + \bar{u}_j\frac{\partial \bar{u}_i}{\partial x_j} = -\frac{1}{\rho}\frac{\partial \bar{p}}{\partial x_i} + \left(\frac{\rho - \rho_0}{\rho_0}\right)g + \mu\left(\frac{\partial^2 \bar{u}_i}{\partial x_j^2}\right) \tag{3.5}$$

  In this thesis, unlike those carried out by Jordi Galí and Pau García, the gravitational effects cannot be neglected since the buoyancy forces must be considered.

The term $\left(\frac{\rho-\rho_0}{\rho_0}\right) g_i$ describes the influence of buoyancy force on airflow, which adopts the Boussinesq approximation (see next chapter).

- Energy conservation equation [16]:

$$\frac{\partial \bar{\theta}}{\partial t} + \bar{u}_i \frac{\partial(\bar{\theta})}{\partial x_i} + \frac{\partial}{\partial x_i} \overline{u_i^{"} \theta^{"}} = 0 \tag{3.6}$$

Where Re and Pr are dimensionless numbers. Re is the Reynolds number which is the ratio of the scaling of the inertia of the flow to the viscous forces in the flow and Pr is the Prandtl number which is a similarity parameter that is the ratio of the viscous stresses to the thermal stresses:

- Reynolds number:

$$Re = \frac{uL}{\nu} \tag{3.7}$$

Where u is the flow speed [m/s], L is the characteristic dimension [m] and ν is the kinematic viscosity [m^2/s].

- Prandtl number:

$$Pr = \frac{c_p \mu}{k} \tag{3.8}$$

Where c_p is the specific heat [J/(kg·K)], μ is the dynamic viscosity [Pa·s] and k is the thermal conductivity in [W/(m·K)].

3.3 Boussinesq Approximation

The Boussinesq approximation is used to solve natural convection problems where the temperature of the fluid changes. Variations on fluid properties other than density are ignored, while the density only appears multiplying by the gravitational acceleration term of the fluid. [17]

The results obtained using this approximation are accurate when density variations are small so it is assumed that these variations do not affect the fluid except that they give rise to buoyancy forces.

Therefore, using a solver that implements this approximation allows to reduce computational resources since it is not necessary to solve the full compressible formulation of Navier-Stokes equation. [18]

By taking the Navier-Stokes equation of the general case of an incompressible fluid and considering that temperature and pressure-dependent density ρ is replaced by a constant density ρ_0 except in the body force term that represents buoyancy force, we get the following equation:

$$\rho_0 \left(\frac{\partial u}{\partial t} + u \cdot \nabla u\right) = -\nabla \mathrm{p} + \mu \nabla^2 \mathrm{u} + \rho \mathrm{g} \tag{3.9}$$

Where the ρ term can be divided into a reference density value and another one that has a linear dependence on temperature:

$$\rho = \rho_0 - \beta \rho_0 (T - T_0) \tag{3.10}$$

Introducing this term to the conservation of momentum equation:

$$\rho_0 \left(\frac{\partial u}{\partial t} + u \cdot \nabla u\right) = -\nabla(\mathrm{p} - \rho_0 \mathrm{g} \cdot \mathrm{z}) + \mu \nabla^2 \mathrm{u} - \mathrm{g} \rho_0 \beta (T - T_0) \tag{3.11}$$

3.4 Computational Fluid Dynamics (CFD)

Computational Fluid Dynamics is the process of mathematically modelling a physical phenomenon involving fluid flow and solving it numerically using computational prowess.[19]

CFD is widely used in a lot of engineering sectors where there is a physical problem related to a thermo-fluid flow which is governed by the three laws of conservation (Mass, Momentum and Energy). A discretization method shall be applied to get a numerical solution that cannot be solved by using analytic methods. The accuracy of the results is highly dependent on the quality of the discretization for which there are different methods. In this thesis the finite volume method (FVM) will be used.

The Finite Volume Method approach consists on transforming the differential equation to its integral form using the divergence theorem and, eventually, applying differences methods to translate the differential expressions. Then, the volume is discretized in a group of cells where properties can be evaluated in center of the cell or in a vertex.[20]

The CFD methodology is the same for every problem to be solved:

1) Preprocessing:
    a. Creating the geometry: this process can be done with different CAD softwares. For the current thesis, the chosen software is Gmsh.
    b. Meshing: consists on dividing the volume of the geometry into discrete cells to create a mesh. Gmsh will also be used to discretize the CAD model.
    c. Defining initial and boundary conditions: to specify how the fluid interacts with the surrounding surfaces of the model as well as to define which are the properties of the fluid. For this thesis, OpenFOAM will be used to set up the simulation and running it.
2) Simulating: the governing equations of the problem are solved on every discretized element.
3) Postprocessing: results obtained shall be analysed and validated in order to be ensure the accuracy of the model. In order to obtain map fields of each variable, ParaView will be used.

3.5 Turbulence

There are three different flow regimes which are laminar, turbulent and fully developed turbulent regime. The classification of a flow in one of these regimes is given by the previously mentioned Reynolds number: lamina flow for a $Re < 2500$; turbulent flow for a value $4500 < Re < 10^5$ and fully developed turbulent flow for values $Re > 10^5 – 10^6$.

In this case, since $Re = 12000$, the flow regime of the case will be turbulent.

The turbulent regime is characterized by unstable flow: irregular fluctuations of the flow appear; there is a large exchange of momentum between fluid particles. Although it is true that, in this type of flow, inertial forces are predominant, viscous forces still play a certain role.[21]

Thus, turbulent flows are chaotic, diffusive causing rapid mixing, time-dependent and involve three-dimensional vorticity fluctuations.

The most commonly known theory of turbulence is the energy cascade developed by Kolmogorov: turbulent flow is characterized by a large range of vortexes of different sizes that interact with each other exchanging energy. The main idea is that kinetic energy enters the turbulence at the largest scales of motion. This energy is transferred progressively to smaller scales until at smallest scales, energy is dissipated by viscous action into thermal energy. The process of energy transfer from large to small scales is known energy cascade and the smallest scales are called Kolmogorov length scale.[22]

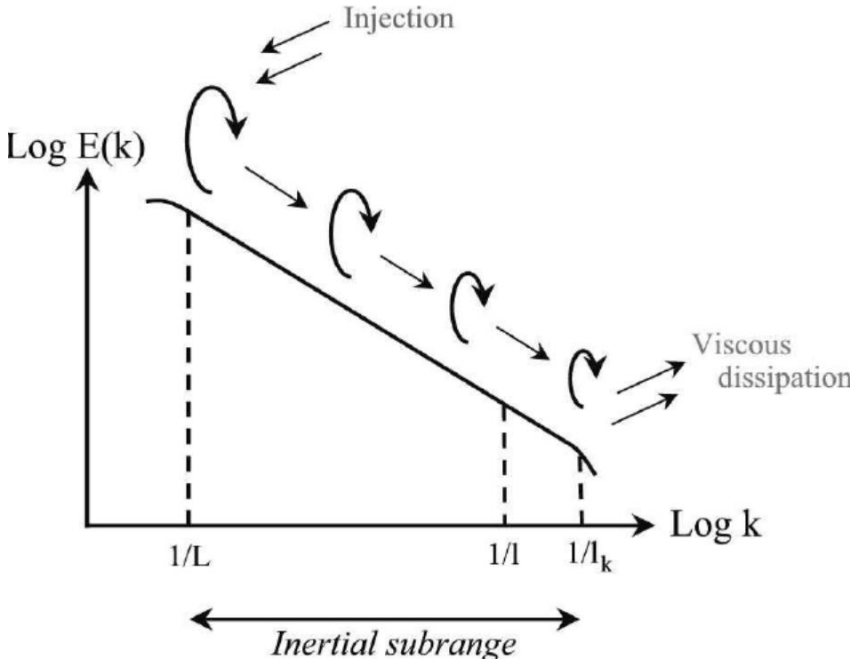

Figure 3-1. Schematic illustration of the energy spectrum of turbulent velocity cascade (Extracted from [42])

Most flows observed in nature are turbulent. This turbulence can be easily observed in many of them, but it is very difficult to predict and give an exact and precise definition of fluid motion since randomness is a characteristic of all turbulent flows.

For all these reasons, it is necessary to resort to turbulence models in CFD simulations that allow turbulence to be resolved and to obtain correct and reliable results.

3.6 Turbulence modelling in CFD

The governing equations of a fluid (Navier-Stokes equations) that have already been presented in this thesis can be directly solved without using any statistical approach. This type of simulations are called Direct Numerical Simulation (DNS) and they are used for very specific projects because they are the most cost demanding simulations since the computational resources needed are prohibitive in most cases. These simulations shall be carried out using very small time step as well as a fine mesh with a large number of grip points to get the complete range of turbulent scales involved in the problem.

Since DNS is an exception and they are not commonly used, there applying turbulence models is needed in order to reduce the large computational costs derived from them. One such method is the Large Eddy Simulation (LES) where large eddies are directly simulated whereas small turbulent scales are modelled using sub-grid scale models. The main concept of LES is to filter by size, choosing scales larger than the minimum filter set. Thus, larger eddies with the higher content of energy are directly resolved while the smallest eddies are simply modelled. This kind of simulation saves a lot of computational resources compared with DNS.

Another widely used approach to model turbulence is the one based on Reynolds Average Navier-Stokes equations where the statistical averaging is based not on spatial averaging but on a proper time. The main idea is to decompose the variables of the flow into time-mean value components and a fluctuating one. Since this thesis was developed using personal computational resources, simulations will be carried out under a RANS-based turbulence model.[23][24]

3.7 Reynolds Average Navier-Stokes (RANS)

Currently the most common used approach to solve turbulent flow problems is the one based on solving Reynolds Averaged Navier Stokes equations.

At a given time t and at vector position x, an instant value of any variable of the flow ϕ(x, t) can be decomposed into a mean value $\bar{\phi}$ (x, t) and a fluctuating component ϕ'(x, t):

$$\phi(x,t) = \bar{\phi}(x,t) + \phi'(x,t) \tag{3.12}$$

Applying this approach to decompose each variable of the flow:

$$u_i = \overline{u_i} + u_i{}' \tag{3.13}$$

$$p = \bar{p} + p' \tag{3.14}$$

$$T = \bar{T} + T' \tag{3.15}$$

Then, substituting these expressions by those present in Navier-Stokes equations presented in the previous section and assuming an incompressible Newtonian fluid, these equations are transformed to the following:

$$\frac{\partial \bar{u}_i}{\partial x_i} = 0 \tag{3.16}$$

$$\frac{\partial \bar{u}_i}{\partial t} + \frac{\partial}{\partial x_j}(\overline{u_i' u_j'}) = -\frac{1}{\rho} \cdot \frac{\partial \bar{p}}{\partial x_i} + \nu \cdot \frac{\partial^2 \bar{u}_i}{\partial x_i \partial x_j} \tag{3.17}$$

The nonlinear term can be decomposed as:

$$\overline{u_i' u_j'} = \overline{(\overline{u_i} + u_i')(\overline{u_j} + u_j')} = \overline{\overline{u_i}\,\overline{u_j}} + \overline{\overline{u_i} u_j'} + \overline{u_i{}' \overline{u_j}} + \overline{u_i' u_j{}'} = \overline{u_i}\,\overline{u_j} + \overline{u_i' u_j{}'} \tag{3.18}$$

Therefore, the resulting equation is:

$$\frac{\partial \bar{u}_i}{\partial t} + \bar{u}_j \frac{\partial \bar{u}_i}{\partial x_j} = -\frac{1}{\rho} \cdot \frac{\partial \bar{p}}{\partial x_i} + \nu \cdot \frac{\partial^2 \bar{u}_i}{\partial x_i \partial x_j} - \frac{\partial \tau_{ij}}{\partial x_j} \tag{3.19}$$

Where $\tau_{ij} = -\overline{u_i' u_j'}$ is the Reynolds stress term that incorporates the effects of turbulent motions on mean stresses. The Reynolds tensor is symmetric: the components out of the diagonal are shear stresses while those located at the diagonal are normal stresses. This introduces six new unknowns to the momentum equations.

Consequently the set of RANS equations is not a closed system, therefore, additional equations are required to solve the system. The process to solve these Reynolds stresses is called turbulence modelling.[25]

3.8 RANS-based turbulence modelling

Turbulence modelling is the construction and use of a mathematical model to predict the effects of turbulence. For most real life turbulent flows, CFD simulations use turbulent models to predict the evolution of turbulence.

As it has been mentioned above, RANS equations are obtained when averaging the governing equations of Navier-Stokes. To close the system of equations obtained, Boussinesq introduced the concept of eddy viscosity to model Reynolds stress term.

$$-\overline{u_i'u_j'} = \mu_t\left(\frac{\partial\overline{u_i'}}{\partial x_j} + \frac{\partial\overline{u_j'}}{\partial x_i}\right) - \frac{2}{3}k\delta_{ij} \tag{3.20}$$

And it can be also written introducing the mean rate of strain tensor:

$$-\overline{u_i'u_j'} = 2\mu_t S_{ij} - \frac{2}{3}k\delta_{ij} \tag{3.21}$$

Where μ_t is the turbulence eddy viscosity, S_{ij} is the Strain tensor, k is the turbulent kinetic energy (TKE) and δ_{ij} is the Kronecker delta.

Models of this type are known as Eddy Viscosity Models (EVMs). These can be classified in different subcategories depending on the number of transport equations solved to compute the eddy viscosity coefficient.[26]

- Zero-equation models: this class does not use additional partial differential equations so, it only uses a system of partial equations to solve the mean field. These models are not proper to solve generic problems. However, they are useful for simpler flow geometries or initial phases of computation.
- One-equation models: this class requires one transport equation to calculate the turbulence velocity scale (usually this transport equation is the turbulent kinetic energy, *k*).
- Two-equation models: this class requires to introduce two additional transport equations to calculate the energy of the turbulence and the turbulence length scale, usually the first one is the turbulent kinetic energy k and the second one may vary depending on what type of two-equation model is used. Common equations for this second transport equation are dissipation rate of turbulent kinetic-energy (ϵ) or specific turbulence dissipation rate (ω).

On this thesis the RNG k-epsilon model will be used since it is a statistical method similar to Standard k-epsilon model and is useful for most homogenous turbulence cases. Furthermore, RNG model has some refinements that Standard does not include. These refinements makes the RNG k-epsilon model more accurate and useful for a wider class of flows than the Standard model. In addition to this, the values for *k* (0.19 m^2/s^2) and *epsilon* (5.57 m^2/s^3) will be obtained from Jordi Galí thesis.

3.9 RNG k-Epsilon model

The modelled transport equations for k and ϵ are the following:

- **k (turbulent kinetic energy):**

$$\frac{\partial}{\partial t}(\rho k) + \frac{\partial}{\partial x_i}(\rho k u_i) = \frac{\partial}{\partial x_j}\left[\left(\mu + \frac{\mu_t}{\sigma_k}\right)\cdot\frac{\partial k}{\partial x_j}\right] + P_k + P_b - \rho\epsilon - Y_M \tag{3.22}$$

- **Epsilon (dissipation rate):**

$$\frac{\partial}{\partial t}(\rho\epsilon) + \frac{\partial}{\partial x_i}(\rho\epsilon u_i) = \frac{\partial}{\partial x_j}\left[\left(\mu + \frac{\mu_t}{\sigma_\epsilon}\right)\cdot\frac{\partial\epsilon}{\partial x_j}\right] + \frac{C_{1\epsilon}\epsilon}{k}(P_k + C_{3\epsilon}P_b) - \frac{C_{2\epsilon}\rho\epsilon^2}{k} - R \tag{3.23}$$

Where,

  - P_k represents the generation of turbulence kinetic energy due to the mean velocity gradients.
  - P_b represents the generation of turbulence kinetic energy due to buoyancy. This will be further explained in the following section.

- Y_M represents the contribution of the fluctuating dilatation in compressible turbulence to the overall dissipation rate.

- **Turbulent viscosity:**

$$\mu_t = \frac{\rho C_\mu k^2}{\epsilon} \tag{3.24}$$

3.10 Buoyancy effects on turbulence in k-epsilon models

In this study it is important to mention the effects of buoyancy in k-epsilon models since, unlike those carried out by Jordi and Pau previously on the same field, a gravitational field and a temperature gradient are taken into account in this thesis. Therefore, the buoyancy term inside turbulent kinetic energy transport equation cannot be neglected on this thesis.

The generation of turbulence due to buoyancy is given by the following equation:

$$P_b = \beta g_i \frac{\mu_t}{Pr_t} \frac{\partial T}{\partial x_i} \tag{3.25}$$

Where:

- Pr_t is the turbulent Prandtl number for energy.
- g_i is the component of the gravitational vector in vertical direction.
- β is the coefficient of thermal expansion which is defined as:

$$\beta = -\frac{1}{\rho}\left(\frac{\partial \rho}{\partial T}\right)_p \tag{3.26}$$

From the transport equation of the kinetic energy, it can be seen how it is affected by the buoyancy term: k tends to be augmented in unstable stratification, while in stable stratification, buoyancy tends to suppress turbulence.

3.11 Pollutant source

One of the main concepts that this thesis aims to study is how the diurnal heating will affect to the air quality inside the street canyons. Therefore it is important to introduce a source of particles in the model that injects particles into the control volume to be able to see how its concentration is affected in each of the scenarios that will be studied in further sections.

Different cases will be simulated, the first one will be an isothermal case while the next scenarios will consider different walls of the street at different temperatures; then, a comparison will be done to understand how the temperature may affect the pollutant retention in urban street canyons.

The mathematical equation that governs the pollutant transport, can be obtained from the generic scalar transport equation explained before, the same way that was done to obtain RANS equations in previous chapters:

$$\frac{\partial c}{\partial t} + U_i \frac{\partial c}{\partial x_i} = \frac{\partial}{\partial x_i}\left(D \frac{\partial c}{\partial x_i}\right) - \frac{\partial}{\partial x_i}\left(\overline{u_i' c'}\right) + S \tag{3.27}$$

Where:

- c: scalar.
- S: pollutant source.
- D: molecular diffusion coefficient [m^2/s]. The molecular

The standard gradient-diffusion hypothesis (SGDH) where the turbulent scalar flux is assumed to be proportional to mean scalar gradient will be used in this study:

$$\overline{u_i' c'} = -D_t \frac{\partial c}{\partial x_i} \tag{3.28}$$

This equation will allow to obtain the mean pollutant concentration fluxes. And, introducing this hypothesis in previous equation:

$$\frac{\partial c}{\partial t} + U_i \frac{\partial c}{\partial x_i} = \frac{\partial}{\partial x_i}\left((D + D_t) \frac{\partial c}{\partial x_i}\right) + S \tag{3.29}$$

Where, on one hand, D_t is the turbulent diffusion coefficient $D_t = \frac{\nu_t}{Sc_t}$, knowing that Sc_t is the Schmidt turbulent number, it can be seen that this is dependent with the turbulent eddy viscosity and turbulent viscosity. Then, it is defined by a turbulent flow and has no universal value. According to literature, the value of the turbulent Schmidt number is acceptable in a range of 0.7 – 0.9. However, in this case it will be used 0.72 which is the same than Schmidt number. On the other hand, D is the molecular diffusion coefficient.[27]

4 Isothermal case

4.1 Experimental study

The experimental study that will be used to validate the obtained results for the isothermal case is called "Physical Modeling of Flow Field inside Urban Street Canyons" [28] and it was conducted by Xiang-Xiang Li, Dennis Y. C. Leung, Chun-Ho Liu and K.M. Lam. The experiment was carried out with a physical model using a water channel in a laboratory to study the characteristics of the air flow inside urban street canyons of different aspect ratios (AR = 0.50, 1.00 and 2.00).

The length, width and height of the water channel used are 30 cm, 10 m and 50 cm respectively. The water is driven by a closed circuit thanks to a pump that drives it from the reservoir, at a constant flow rate of 28 L/s, up to the water channel. Also, there is a flowmeter in the circuit to measure the flow rate.

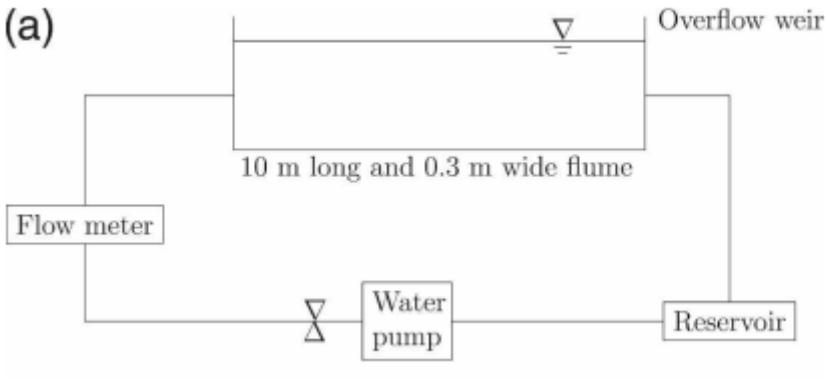

Figure 4-1. Experiment's scheme (Extracted from [28])

A laser Doppler anemometer was used to measure the two-component flow velocities as well as the turbulent intensities in the streamwise and vertical directions. The LDA is a fiber-optic system that uses a 4-W argon ion laser as laser source and as mentioned before, it is able to measure velocity in X and Y direction. This measurement methodology is a non-intrusive method which means that the flow field is not disturbed by the presence of measurement devices. However, some seeding particles were used to obtain results. These particles were polycrystalline powders with a nominal diameter of 30 μm.

The model of aspect ratio 1.00 is comprised by 8 identical buildings of 0.3-m-width, 10-cm-length and 10-cm-height. These buildings were aligned perpendicular to the streamwise direction and the width of the canyon varies depending on the aspect ratio, which for case AR = 1.00 is fixed to 10 cm. Also, the depth of the water is approximately 40 cm.

The Reynolds number based on the freestream velocity and building height is about 12,000. It is important to note that measurements have been carried out in three different vertical lines (x/H 0.25, x/H=0.50 and x/H=0.75) as well as in two horizontal ones (y/H=0.50 and y/H=1.00). These same measurements locations will be used in this thesis to obtain values in order to carry out the post-processing stage.

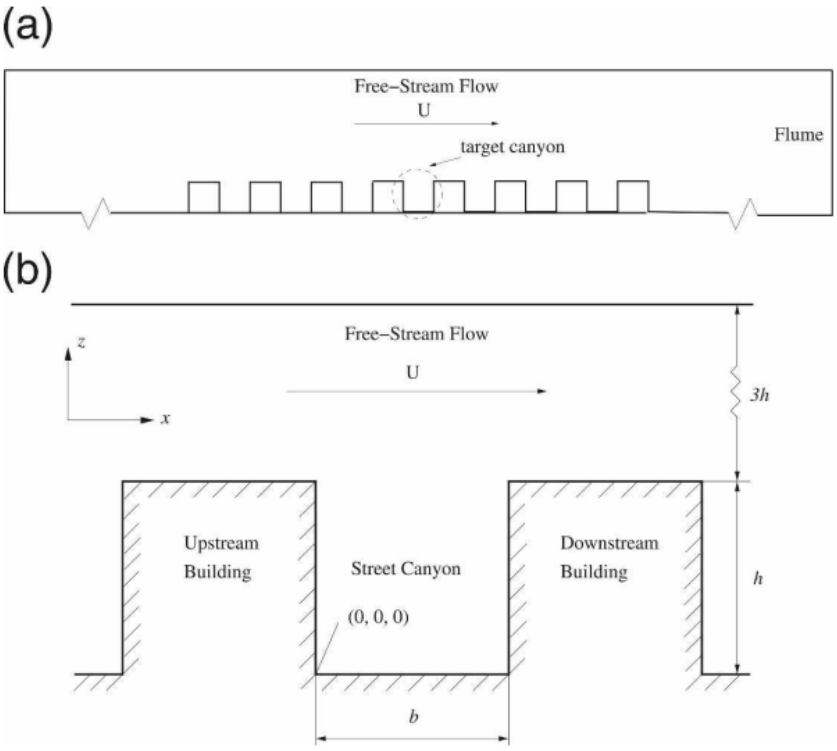

Figure 4-2. Scheme of the model and detail view of the experiment's street canyon (Extracted from [28])

4.2 Geometry

The CAD model used to carry out the simulations has been generated using the Gmsh version 4.4.1. This model has been built taking into account the geometry of the physical model used in the experiment explained in section 4.1 of this thesis: it is made up of eight equal buildings of 1-m-long by 1-m-high and all of them have a width of 3 meters; the distance between them is equal to one meter resulting in an aspect ratio of the urban canyons is equal to 1.

The total length of the model is 35 meters: the inlet is located on the left side and the outlet on the right side. The distance between the inlet and the windward wall of the first building is 5 meters, while the distance between the leeward wall and the outlet is 15 meters. Finally, it is important to note that the height of the domain is 4 meters.

Also, even though the study is based on a 2D model, it must be extruded in the Z direction in order to have at least one cell in this direction. This is a necessary condition to be able to simulate in OpenFOAM. However, front and back faces will be defined as empty patches so this direction must not be resolved (Z direction).

The target canyon is the fourth one in a row so the airflow that enters the domain through the inlet face will be fully developed and stabilized at this point. Thus, the suction region generated in the first buildings will have been overcome. Also, in this canyon a pollutant source has been modelled at the center of the street as a surface of 0.015-m-wide by 3-m-long.

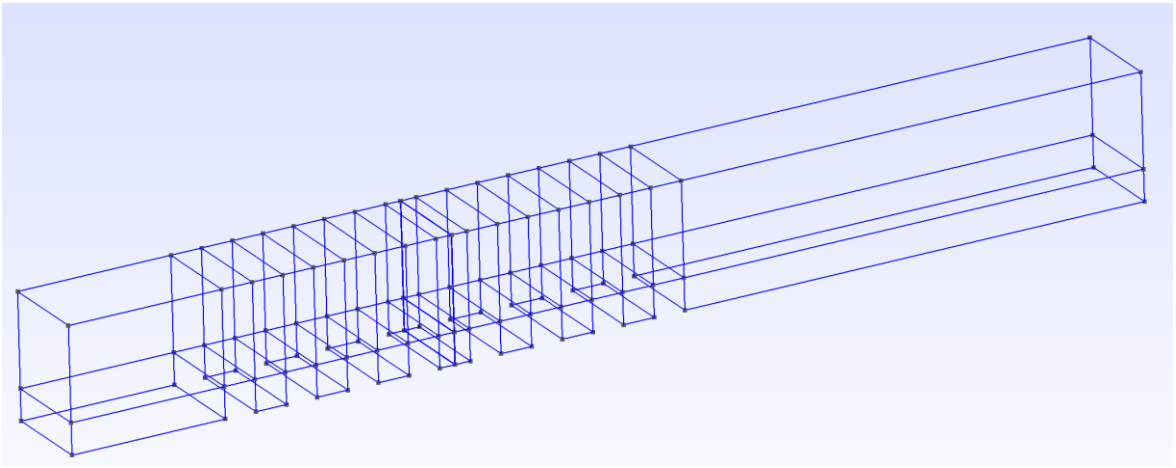

Figure 4-3. CAD model obtained with GMSH

4.3 Meshing

The spatial discretization of the domain, commonly known as meshing, is an important and necessary part when solving CFD simulations since the computational time and the accuracy of the results obtained will depend, among other things, on the type of mesh used to solve the problem.

The choice of the mesh will affect the accuracy of the results and the computational resources used: the greater the refinement of the mesh, the more precise the results will be, but the longer the required time to obtain converged results; while the lower the refinement of the mesh, the less accurate the results and the less computational time required. For this reason, a balance must be found between accuracy and computational cost, especially, when carrying out thesis projects like this one in which using personal resources.

To develop this master thesis, two types of mesh were considered: unstructured and structured meshes.

On one hand, regarding structured meshes, the points of an elemental cell can be easily addressed by double indices (i,j) in two dimensions or triple indices (i,j,k) in three dimensions. The connectivity is straightforward because cells adjacent to a given elemental face are identified by the indices, and the cell edges form continuous mesh lines that begin and end on opposite elemental faces. In 2-D meshes, the central cell is connected by four neighbouring cells, while in 3-D it is connected to six neighbouring cells. Therefore, for geometries with lower degree of complexity such as in that case, they are a good option.[29]

On the other hand, the unstructured meses can be defined as those with no explicit relationship between their nodes. Thus, the cells are allowed to be assembled freely within the computational domain and the most typical shape of an unstructured element is a triangle (2D element) or a tetrahedron (3D element).

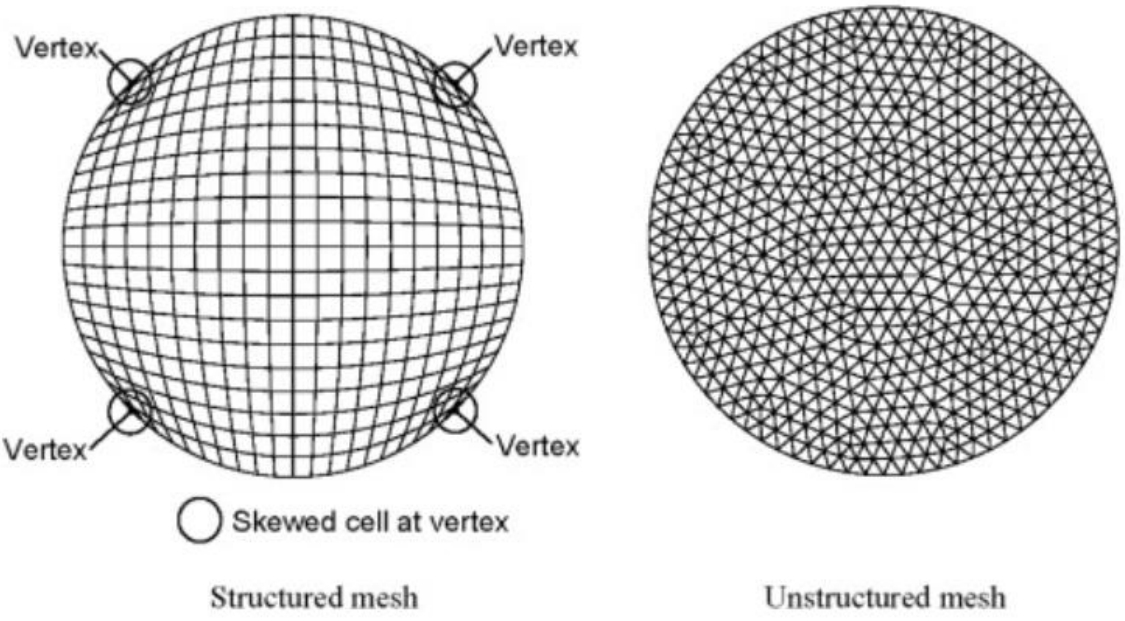

Figure 4-4 Structured mesh vs unstructured mesh (Extracted from [29])

The final decision is to make a structured mesh because of the simplicity of the model's geometry so it can be perfectly adjusted to quadrilateral 2D elements and hexahedral 3D elements.

Two meshes with different sizes have been created to asses which of them fits better the balance between accuracy and computational time. These two can be classified as coarse mesh and fine mesh according to the smallest cell size that correspond to cells within the urban street canyons since it is the region of interest in this thesis.

Table 4-1. Mesh sizes

Mesh	Minimum cells size		Number of cells
	Minimum length [m]	Minimum area [m^2]	
Coarse	0.015	$2.25 \cdot 10^{-4}$H	83,207
Fine	0.01	$1 \cdot 10^{-4}$H	137,845

The properties of the mesh have been checked with the *checkMesh* function in OpenFoam. This functionality checks statistics, topology and geometry of the mesh. Among geometry tests, this functionality checks the aspect ratio, cells volumes, mesh non-ortogonality, skewness… Finally, it provides a conclusion of "Mesh OK" if no warnings are detected.

As it can be seen in the following figures, the smallest cell size is found in the seven urban canyons of the model: a linear refinement has been carried out in the vertical direction so that the cells closest to the top face of domain are taller than those located nearest to the canyons. In addition, an horizontal refinement has also been carried out in order to accumulate a greater number of cells in the centre of the model where buildings and urban canyons are located. Thus, for this reason it is observed that the largest cells are found at the inlet and outlet, especially at the domain's corners.

Figure 4-5. Fine mesh

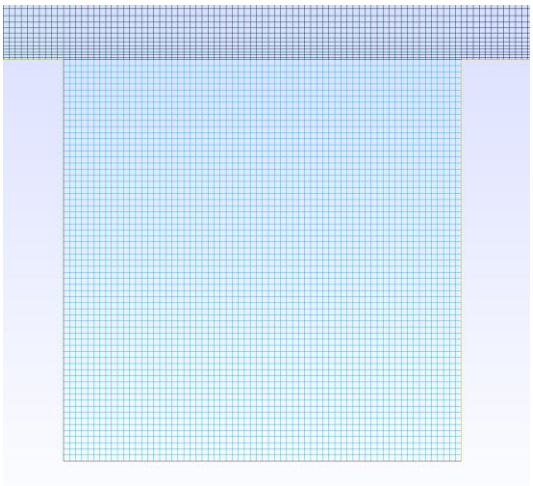

Figure 4-6. Detail view of the mesh inside a canyon

4.4 Case configuration

4.4.1.1 OpenFOAM directories

As mentioned before, the software that will be used to carry out the simulation is OpenFOAM. All the information is saved in a main directory with the name of the case and this folder contains subdirectories that are common for all cases. In these subfolders, the necessary scripts to initialize the simulation are stored. The subdirectories are the following:

- ***0 directory***: In this folder the text files in which the initial conditions of the fluid are defined are saved as well as the boundary conditions defined for every patch of the domain with respect to all variables of the problem (pressure, velocity…).
- ***constant directory***: In this folder the text files that define the physical properties that characterize the fluid to be used in the simulation are saved as well as the polyMesh folder that includes all scripts of the mesh.
- ***System directory***: contains all data for setting parameters related to the solution procedure. It shall contain at least three scripts: controlDict, fvSchemes and fvSolution.

4.4.1.2 Constant directory

The first step that was done with OpenFOAM was to import the mesh created with Gmsh through the *gmshToFoam* function which takes the text file created with Gmsh and creates a new subdirectory called polyMesh where all the mesh information is saved.

In the boundary file, the different surfaces of the model were imported and they had to be defined as patch, wall or empty. All surfaces of the model were called as *Inlet*, *Up*, *Outlet*, *Down*, *Windward*, *Leeward*, *Pollutant*, *streetc*, *Back* and *Front*

Down, *Pollutant*, *streetc*, *Windward* and *Leeward* surfaces were defined as walls, while *Inlet*, *Up* and *Outlet* were defined as patches. Note that *Back* and *Front* surfaces were considered empty since 2D simulations need to be carried out, so this consideration is interpreted by OpenFOAM as if the canyons were infinite long in the Z direction.

The *transportProperties* and *turbulenceProperties* files are also located in this same directory:

- *transportProperties*: in this script the fluid is defined as Newtonian and the kinematic viscosity is set to $8.3 \cdot 10^{-5}$ m^2/s and the Prandtl number is set to 0.72. Furthermore, unlike for the isothermal case should not be necessary, since the solver used will be the same than for the rest of cases, here it has been defined the reference temperature (T_{ref} = 296 K), the thermal expansion coefficient (β) is set to 0.003 1/K and the turbulent prandtl number which has been set to 0.85 (usually varies between 0.7 and 0.9).
- *turbulenceProperties*: this dictionary is read by the solver in order to know which turbulence model shall be applied. The *simulationType* will be defined as RAS since as it was previously mentioned the simulations carried out in this thesis will use Reynolds-averaged Navier-Stokes (RANS) modelling. In addition to the type of simulation, the turbulence model that is going to be used is the RNG k-Epsilon. Finally, the turbulence is switch on in order to solve the turbulence modelling.

4.4.1.3 Initial and boundary conditions

In folder 0 there are the text files that includes the initial conditions and the boundary conditions for each particular field.

In this simulation, the files that can be found in this directory refer to the variables of pressure (*p* and *prgh*), velocity (*U*), temperature (*T*), *k*, *epsilon*, *alphat*, pollution concentration (*s*), *nut* and *nuTilda*.

- Pressure (*prgh*): on one hand, the boundary condition that is defined for all surfaces inside the domain, except for the outlet, is a Von Neumann condition (*zeroGradient*). On the other

hand, a *fixedValue* condition (0 m^2/s^2) is defined for the *Outlet* patch. Therefore, the airflow will enter the domain through the surface marked as *Inlet* since as it will be stated later, a velocity condition is established at this patch so the air will be forced to flow from the left hand side to the right hand side of the domain.

At the beginning of the simulation, the domain volume is filled with air at a fixed pressure value of 0 m^2/s^2.

- Pressure (p): As it will be explained in next section, the pressure is calculated as $p = p_{rgh} + \rho g h$, therefore in this script a calculated condition is established for each domain's surface, except for the outlet. The *internalField* as well as the outlet are fixed to a uniform value of 0 m^2/s^2.

- Velocity (U): the air velocity is set at the inlet equal to 1 m/s in the X direction (1 0 0) m/s. At the outlet patch a *zeroGradient* condition is established while the bottom surfaces marked as *Down*, *Leeward*, *Windward*, *Roof*, *Pollutant* and *streetc* a *no-slip* condition is established (0 0 0) m/s. Regarding to the *Up* surface, a *slip* condition is defined.

  At the beginning of the simulation, the domain is filled with motionless air, thus the internal field speed is set to 0 m/s.

- Temperature (T): for the isothermal case, whole domain is considered at the same temperature T = 296K. Therefore, a *fixedValue* condition with a value equal to 296 K is applied for all surfaces. Also the walls of the buildings and the ground could be considered as adiabatic walls, then a *zeroGradient* condition should be applied. Despite these differences, the results should have been the same.

  The *internalField* is set to a uniform value of 296 K.

- *alphat*: this script refers to the turbulent thermal diffusivity, so the necessary wall functions to calculate it are applied. For all the walls of the model (*Leeward*, *Windward*, *Ground*, *streetc*, *Pollutant* and *Roof*) the same wall function is applied: *alphatJayatillekeWallFunction* with a value of Prt equal to 0.85. In the rest of surfaces (*Inlet*, *Up* and *Outlet*) a *calculated* boundary condition is applied.

  The *internalField* is set to a uniform value of 0.

- Pollutant concentration (s): in this case, as mentioned in section 3, a dimensionless source of contaminants has been used in order to validate and compare the results obtained with other reports that can be found in the literature. Regarding the boundary conditions of this variable, a *fixedValue* condition equal to 1 is applied at the surface defined as *Pollutant*, while a *zeroGradient* boundary condition is applied to the rest.

  At the beginning of the simulation it is considered that there are no pollutant particles inside the domain, so the internal field is equal to 0.

- Turbulent kinetic energy (k): at the inlet patch, a boundary condition of Turbulent Intensity Kinetic Energy of 5% has been applied, while at the *Outlet* and *Up* patches a *zeroGradient* condition has been defined. At the bottom walls (*Ground*, *Roof*, *Leeward*, *Windward*, *streetc* and *Pollutant*) a wall function has been applied *kqRWallFunction* with a value of 0.19 m^2/s^2.

  Regarding the internal field, it has been defined uniform with a value of 0.19 m^2/s^2.

- Dissipation rate (*Epsilon*): at the inlet patch a *fixedValue* condition has been applied with a uniform value of 5.57 m^2/s^3, while at the *Outlet* and *Up* patches a *zeroGradient* condition has been considered. The boundary condition applied at the bottom walls is an *epsilonWallFunction* with a uniform value of 5.57 m^2/s^3.

  Eventually, the internal field has been defined as uniform with a value of 5.57 m^2/s^3.

It is necessary to mention that *Front* and *Back* boundary conditions have been defined as *empty* for all above mentioned variables. Also, the *nut* and *nuTilda* which are related to the turbulent viscosity are set to a uniform initial value of 0.

4.4.1.4 System directory

In this directory, there are scripts related to run control parameters, discretisation schemes used in the solution, equation solvers, tolerances and other algorithm controls.

- *controlDict*: this dictionary is used to specify the main case controls such as timing information, write format and optional libraries. In this first case, a solver which did not take into account temperate could have been chosen, however, it was decided to use the same solver for all scenarios. In the current case, a turbulent and transient simulation of incompressible flow is carried out, thus the chosen solver is *buoyantBoussinesqPimpleFoam*. It is important to note that a steady-state simulation using *bouyantBoussinesqSimpleFoam* solver was also considered and the results obtained were similar as to what was expected due to no transient phenomena being present in that case. Nevertheless, as it will be explained later, in next case including temperature the results with a steady-state solver did not converge and were not as good as those obtained with a transient solver.
- *fvSchemes* and *fvSolution*: the finite volume discretization schemes are specified in *fvSchemes* file, while the *fvSolution* file is used to specify the linear equation solvers, algorithms and residual control.

4.5 *BuoyantBoussinesqPimpleFoam* solver

The solver that is going to be used is *BuoyantBoussinesqPimpleFoam* since it is a transient solver for buoyant turbulent flow of incompressible fluids. In this section a brief explanation of how the solver solves the governing equations.

The source code of the solver may be found in the annex of this thesis.

The *createFields.H* script creates the thermo-physical properties (pressure, velocity and temperature) and transport properties fields (kinematic density for buoyancy force and kinematic turbulent thermal conductivity) used by solver. Density is calculated using the Boussinesq approximation:

$$\rho_k = 1 - \beta \cdot (T - T_{ref}) \tag{4.1}$$

This script calls to the *singlePhaseTransportModel.H* file in order to calculate the absolute viscosity through a viscosity-based model defined in *transportProperties* file. In this case the viscosity model is set to Newtonian.

Regarding the governing equations:

- Momentum equation (*UEqn.H*):

$$\frac{\partial u}{\partial t} + \nabla(\rho u u) + \nabla\left(\nu_{eff}\nabla u\right) + \nabla\left(\nu_{eff}(\nabla u)^T - \nu_{eff}\cdot\frac{2}{3}\cdot tr(\nabla u)^T I\right) = -(\nabla\rho)ghf - \nabla p_{rgh} \tag{4.2}$$

  Where $(\nabla\rho)ghf$ and ∇p_{rgh} represents the body force acting on the fluid and the pressure gradient term respectively. Furthermore, the effective viscosity is obtained as $\nu_{eff} = \nu + \nu_t$.

  The following terms $\nabla\left(\nu_{eff}\nabla u\right) + \nabla\left(\nu_{eff}(\nabla u)^T - \nu_{eff}\cdot\frac{2}{3}\cdot tr(\nabla u)^T I\right)$ represent the viscous shear stress term.

- Pressure (*pEqn.H*): In here the PIMPLE algorithm is used to couple the pressure and velocity. The pressure is calculated as:

$$p = p_{rgh} + \rho g h \tag{4.3}$$

- Temperature (*TEqn.H*):

$$\frac{\partial(\rho T)}{\partial t} + \nabla(\rho u T) - \nabla\alpha_{eff}\nabla T = S_{radiation} + S_T \tag{4.4}$$

  Where $\alpha_{eff} = \frac{\nu_t}{Pr_t} + \frac{\nu}{Pr}$, S_{rad} and S_T are source terms due to radiation and thermal sources. Since they are not consider for this simulation, the equation will be as follows:

$$\frac{\partial(\rho T)}{\partial t} + \nabla(\rho u T) = \nabla\alpha_{eff}\nabla T \tag{4.5}$$

4.6 Validation

One of the fundamental parts when carrying out simulations is the validation of the model that is going to be used with results obtained from other reports that can be found in the literature in order to verify that the results obtained in your own report are acceptable.

In this first case, in which there are no differences of temperature between walls, average speed values in X direction and Y direction as well as the air velocity fluctuations will be compared. To make the comparison, these values must be dimensionless so, they will be divided by the flow stream air velocity U_{ref} = 1 m/s.

The measurements of these variables are obtained in three vertical lines in the fourth canyon that are located at the points x = 12.25m, x= 12.5m y x=12.75m. Between the ground level and the roof of the buildings, one hundred equidistant points are measured and saved. This vertical component must also be dimensionless so it is divided by the height of the canyon's buildings (H=1m).

Next, the legend of the graphs is related to the literature sources from which results have been obtained to carry out the validation:

- Blue bullets: experimental data from experiment conducted by Liu. [28]
- Red line: LES simulation from [28].
- Yellow lines: LES simulation provided by the director of this thesis Ivette García.
- Magenta line: RANS simulation from [2]
- Green line: RANS simulation from this thesis.

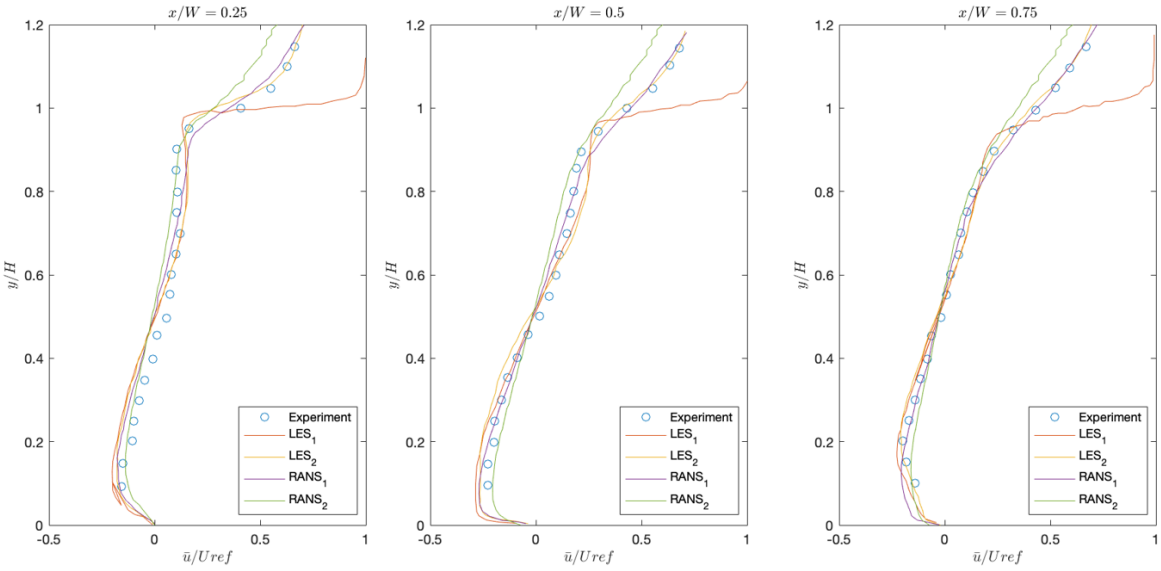

Figure 4-7. Comparison of the mean velocity in X direction

Regarding the air velocity in the horizontal direction, it can be seen how the model is quite precise, especially inside the canyon, giving values very similar to those obtained in the experimental results. Note that all the simulations used for the comparison deviate very little from the experimental results. The greatest difference exists at the top of the canyon.

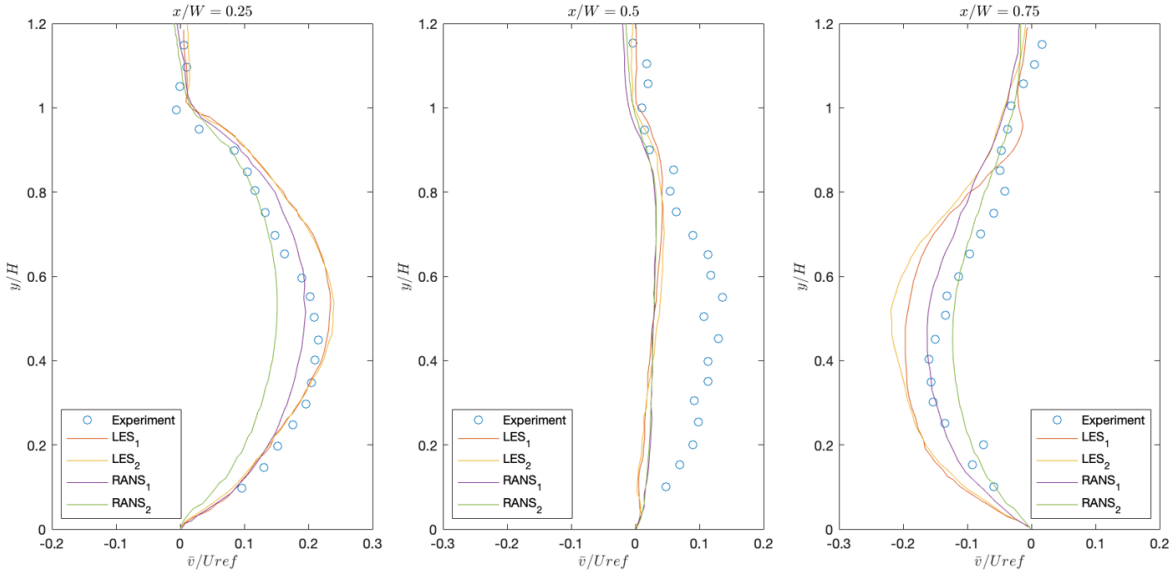

Figure 4-8. Comparison of the mean velocity in Y direction

Concerning the Y velocity, the graphs show that the results obtained are close to the experimental ones. Nevertheless, the model does not give as accurate results as the ones obtained for the horizontal velocity. The same thing happens to all the CFD simulations included in the comparison. However, these differences are minimal at lines x/W = 0.25 and x/ = 0.75.

The values obtained in the central line of the canyon are noteworthy, where all the simulations agree that the vertical component of the velocity is practically null. On the other hand, in the experimental results it is positive and reaches a maximum at the center of the canyon. This may be due to the face that the center of the vortex is slightly deviated towards the windward side.

Below are the graphs of the velocity fluctuations, which have been obtained using the openFoam R postprocessing function in order to obtain the modelled Reynold Stress tensor components. In these graphs it can be seen that the results are very accurate along the height of the canyon until they reach the top of the building, where the canyon connects with the air flow stream.

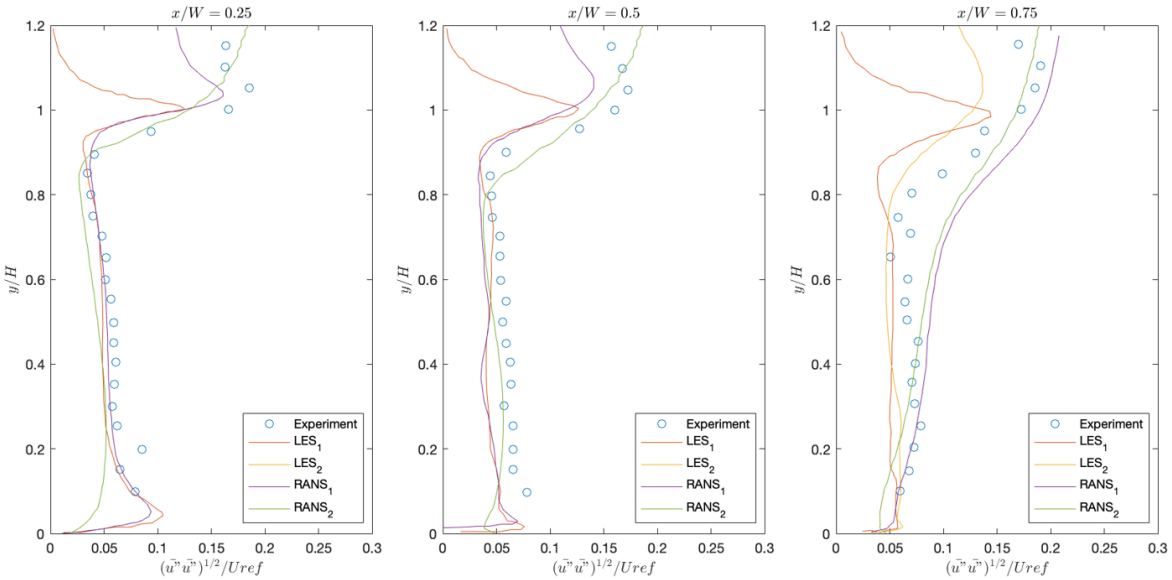

Figure 4-9. Comparison of the velocity fluctuations in X direction

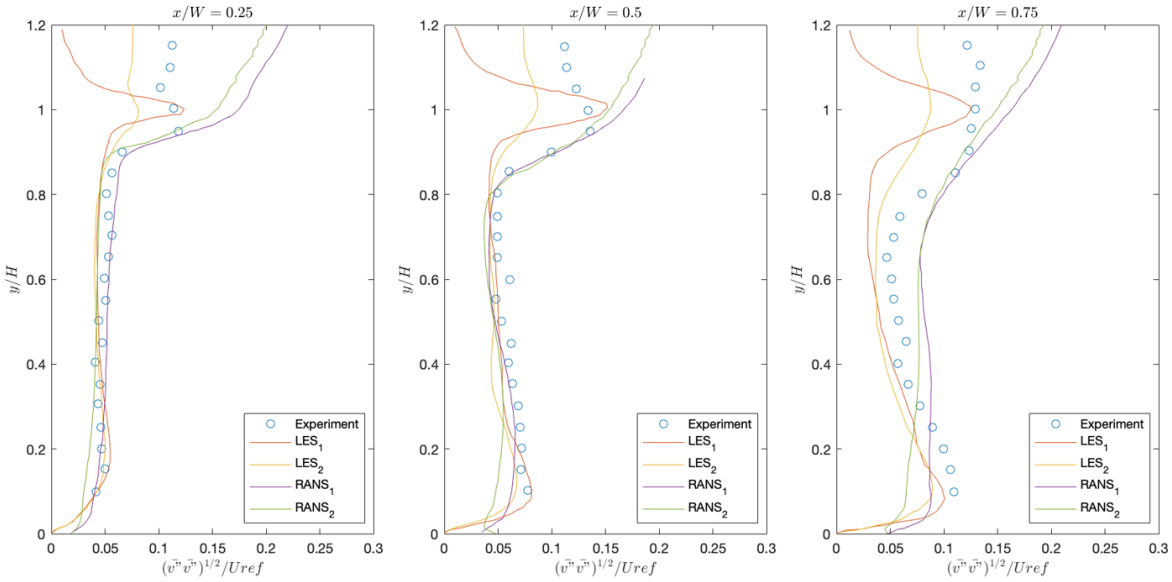

Figure 4-10. Comparison of the velocity fluctuations in Y direction

The following figures show the comparison of mean velocity and velocity fluctuations at roof level. It can be seen how the horizontal velocities are under-predicted compared to the experimental results and the other CFD simulations. However, the vertical velocities are in line with results obtained in all the other sources. Also, the fluctuating velocities in vertical direction, which are the responsible of the contaminants removal from street canyon are better predicted with the current CFD model if they are compared with the results obtained from the other CFD RANS-based simulations and the experimental ones. Probably, this is due to the use of smaller cells inside the canyon, i.e. a finer mesh.

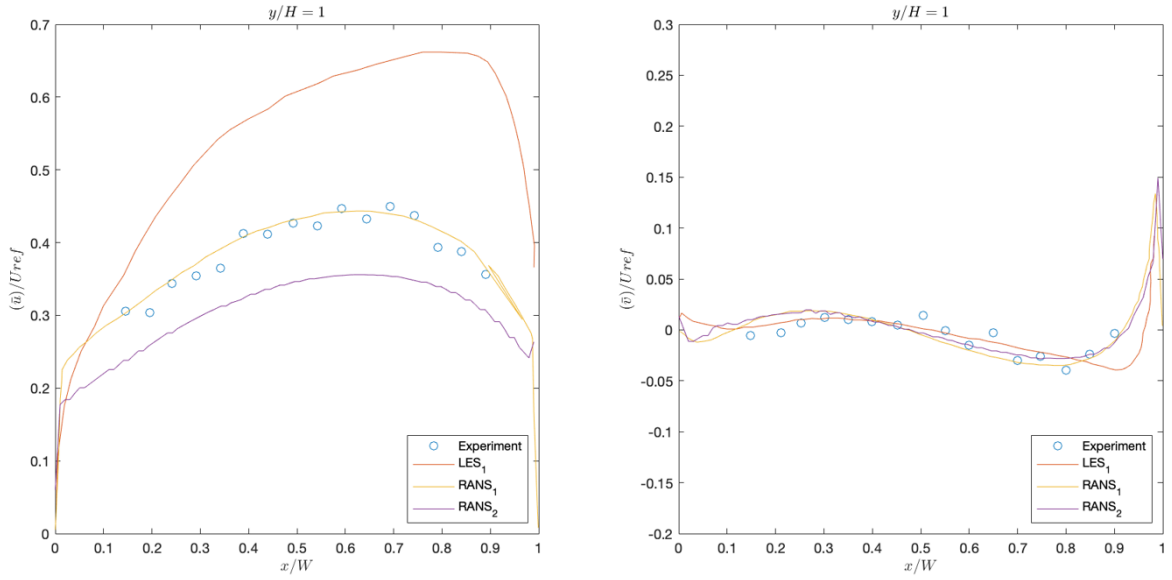

Figure 4-11. Comparison of the mean velocity in X and Y direction at roof level

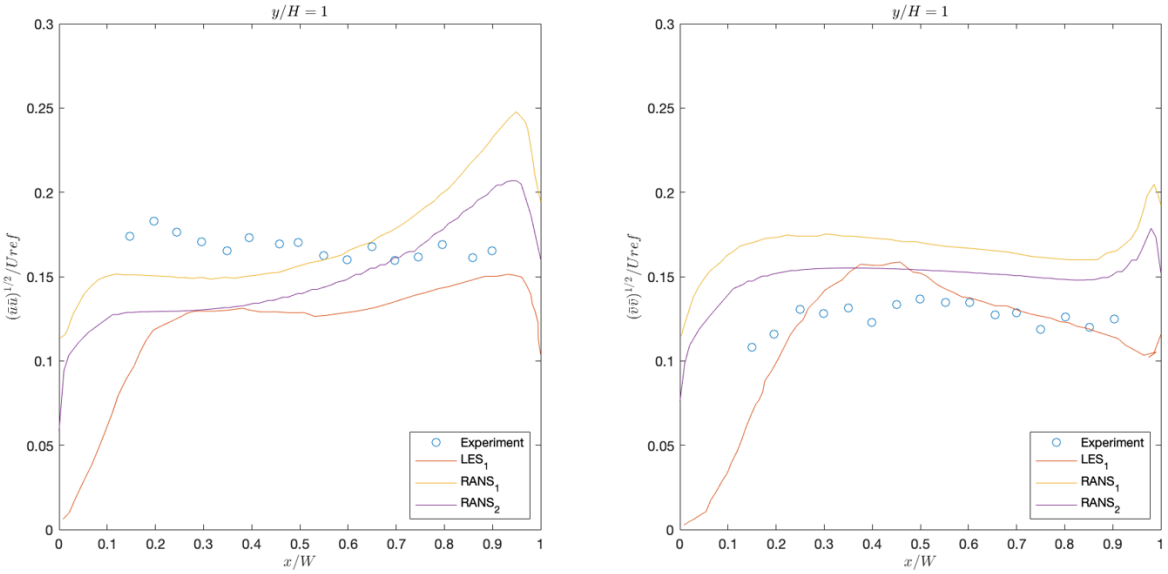

Figure 4-12. Comparison of the velocity fluctuations in X and Y direction at roof level

4.7 Results

4.7.1.1 Residuals

An important aspect when analyzing the results of a CFD simulation are the residuals. Residuals are the error of the variables so they are employed to monitor the behaviour of the numerical process. Importantly, they implicate whether the solution shows a trend of convergence or divergence.

It is important that the residuals of the variables that are being monitored converge since it will be indicative about the stability of the results obtained. In addition, the smaller the value of the residual, the smaller the error committed so the greater the accuracy of the results obtained.

In *Figure 4-13* it has been plot the residuals of the pressure variables and each velocity component on a logarithmic scale (Y axis) against simulation time (X axis). It can be seen how each variable has been completely converged. The values reached by all of them are good enough: pressure has an approximate value of 10^{-6}, vertical velocity component (Uy) reaches a value of 10^{-10} and the horizontal velocity component (Ux) reaches a value of 10^{-11} approximately.

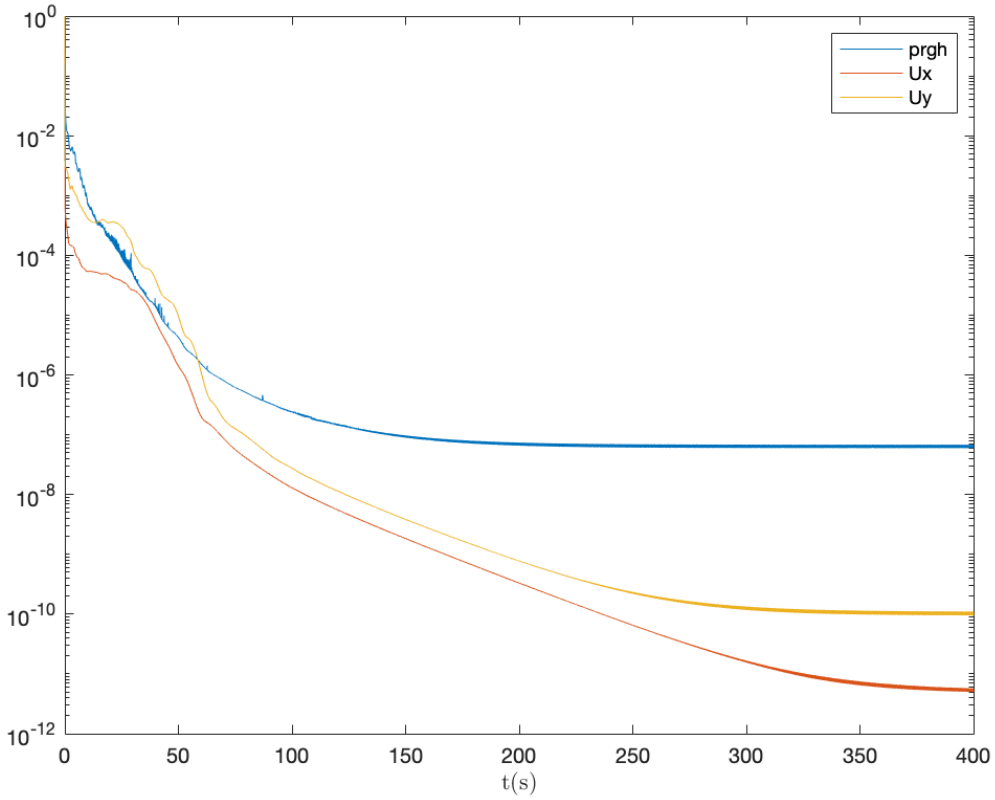

Figure 4-13. Residuals for the isothermal case

4.7.1.2 Pressure

The pressure map down below shows how the streamwise pressure is positive before reaching the first building and once it reaches the first building, a suction zone appears where the minimum pressure is approximately -1.3 m^2/s^2 between the first and the second building. Then, the pressure increases although it remains at a constant approximate value of -0.25 m^2/s^2 until the streamwise leaves the eight buildings behind. From there until the outlet, pressure tends to zero as *zeroGradient* condition has been imposed at the outlet of the domain.

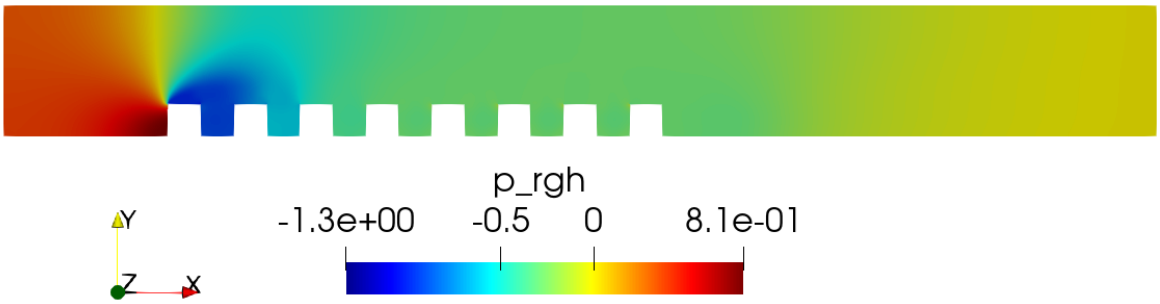

Figure 4-14. Pressure map field

4.7.1.3 Velocity

The velocity map down below shows different velocity regions in the streamwise flow: on one hand, there is an area between the inlet and the first building where the air velocity is maintained at approximately 1 m/s as it was imposed at the inlet boundary conditions. When the airflow arrives to the first building, it is disturbed and three different regions can be appreciated. A zone with a lower air speed in the bottom side of the domain, especially inside urban canyons where the speed is below 0.5 m/s, meaning the air of this area slows down. A second region just above the urban canyons with an air speed that remains around the entrance speed of 1 m/s. Finally, there is a region above the last one and until the top of the domain in which the air accelerates reaching a peak value of 1.8 m/s approximately.

It can be clearly seen that from the fourth canyon until the outlet's domain, the velocity map stabilizes and follows the same pattern for the last four canyons.

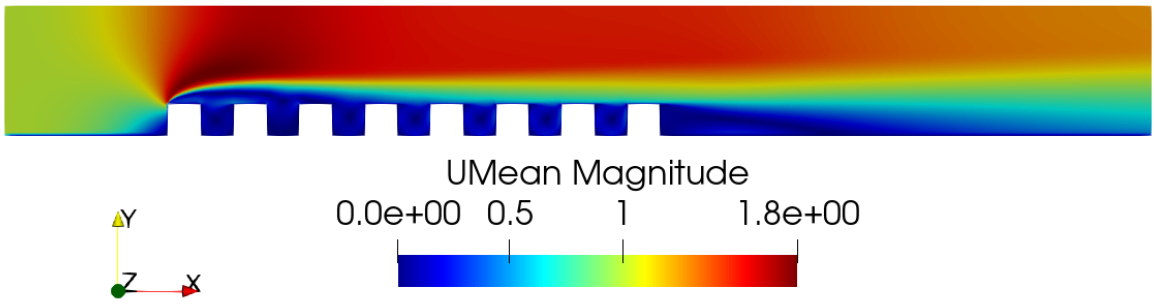

Figure 4-15. Mean velocity map field (in m/s)

Observing in detail the air velocity in Y direction inside the fourth canyon, it can be seen that the air moves in opposite directions on the opposite sides of the canyon. While on the windward side, the vertical component of the air speed indicates that air is moving towards the street, on the leeward side, it indicates that the air is moving towards the roof of the buildings. In addition, this velocity map confirms the existence of a vortex within the canyon which will contribute to having a lower

number of air changes per hour inside the canyon and, as consequence, there will be an increase of pollutant concentrations.

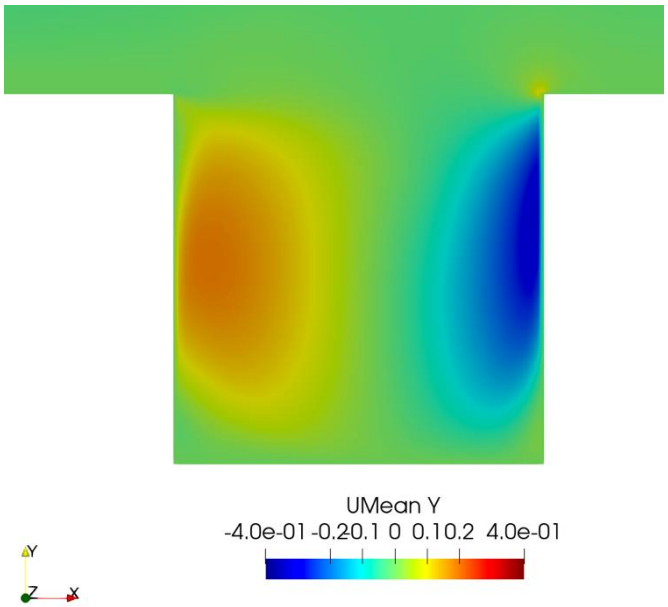

Figure 4-16. Mean velocity map (Y direction) in 4th canyon (in m/s)

4.7.1.4 Streamlines

The streamlines help to visually understand how the air is behaving inside the flow domain. The turbulence generated in the first and second canyons due to the disturbance of the air caused by the first building of the row can be observed. They also allow to observe the zones with local air recirculation, for example, the great vortex that is generated after the last building reaching the end of the domain.

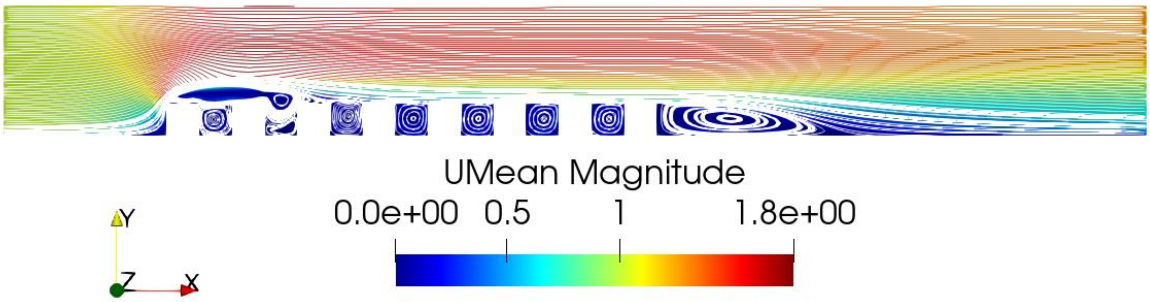

Figure 4-17. Streamlines in the domain

The appearance of vortices inside urban canyons has been previously discussed. The streamlines are the trajectories followed by air particles and they show the air recirculation regions in a clearer way: a centered vortex located in the middle of the canyon does indeed appear. In addition, the existence of two smaller secondary counter-rotating vortices can be seen in the lower corners; these vortices had not been possible to discover with the detail of *Figure 4-18*.

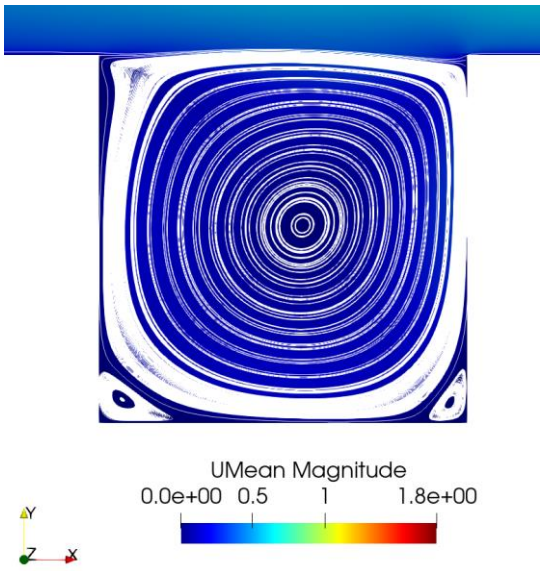

Figure 4-18. Streamlines in 4th canyon

4.7.1.5 Mean pollutant concentration

Figure 4-19 shows the map of average concentration of pollutants, while *Figure 4-20* shows the same map with a scale change to better appreciate the amount of pollutants in the fourth canyon where the source of pollutants is located, how they leave the canyon, the average concentration in the rest of the subsequent canyons and the average amount of contaminants that reaches the end of the domain following the streamwise.

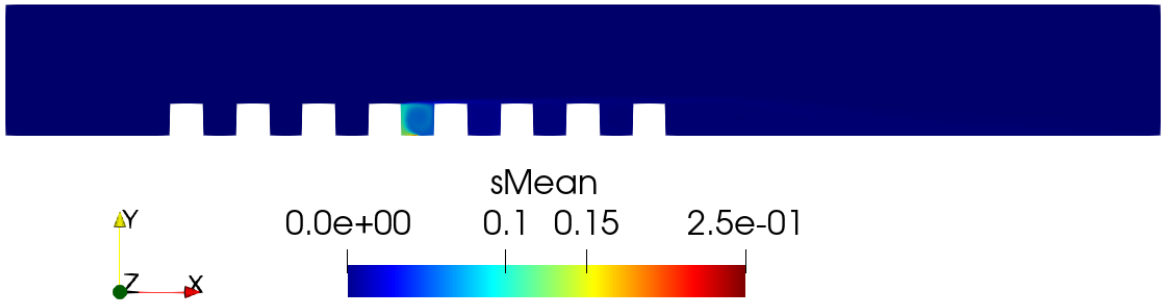

Figure 4-19. Mean pollutant concentration

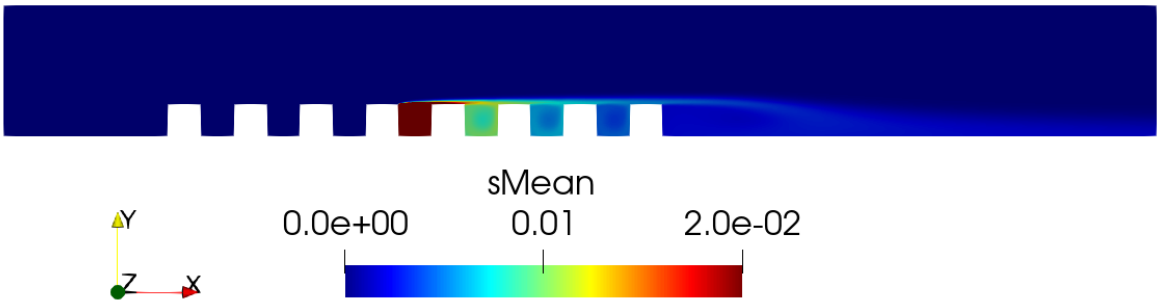

Figure 4-20. Mean pollutant concentration with a scale change

According to the detailed views, it can be observed what happens with the average pollutant concentration inside the target canyon: the concentration is higher on the leeward side than on the windward side due to the vortex created in the canyon having a clockwise direction and at the lower point, the air velocity component in X direction is negative which means that the air is moving from right to left or, what is the same, from the windward side to leeward side, a fact that implies a major concentration levels of contaminants on the left wall of the canyon than on the right one.

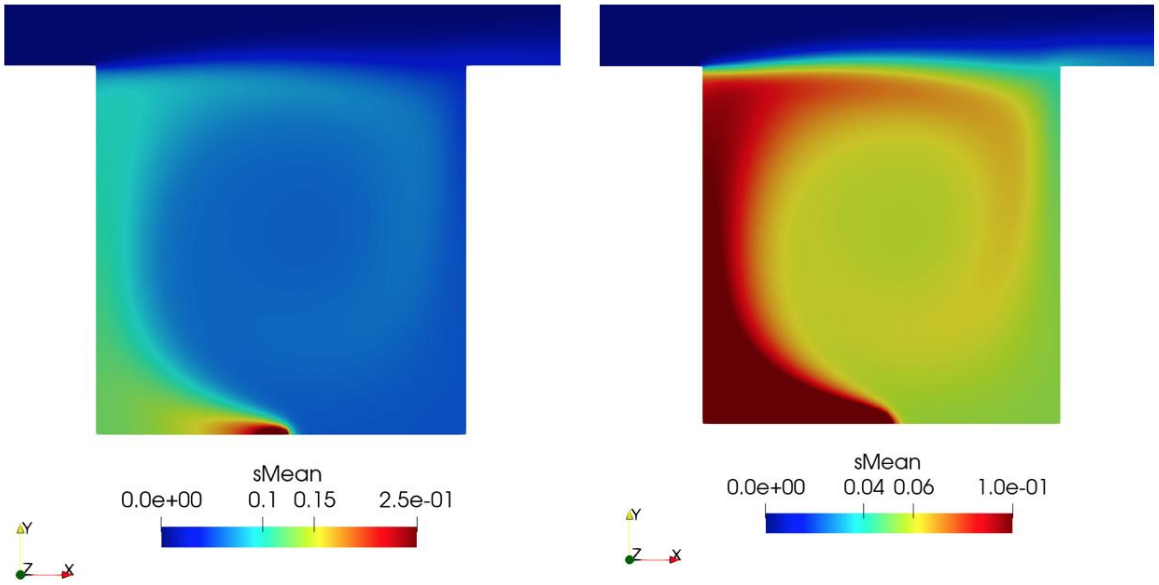

Figure 4-21. Mean pollutant concentration with a scale change in 4th canyon

4.7.1.6 *Mean pollutant concentration fluxes*

To further examine the pollutant transport within the urban canyon the previously explained Simple Gradient Diffusion Hypothesis (SGDH) will be applied in order to calculate the mean pollutant concentration fluxes. These can be calculated since the fluctuating velocities as well as the pollutant gradient are obtained with post-processing tools.

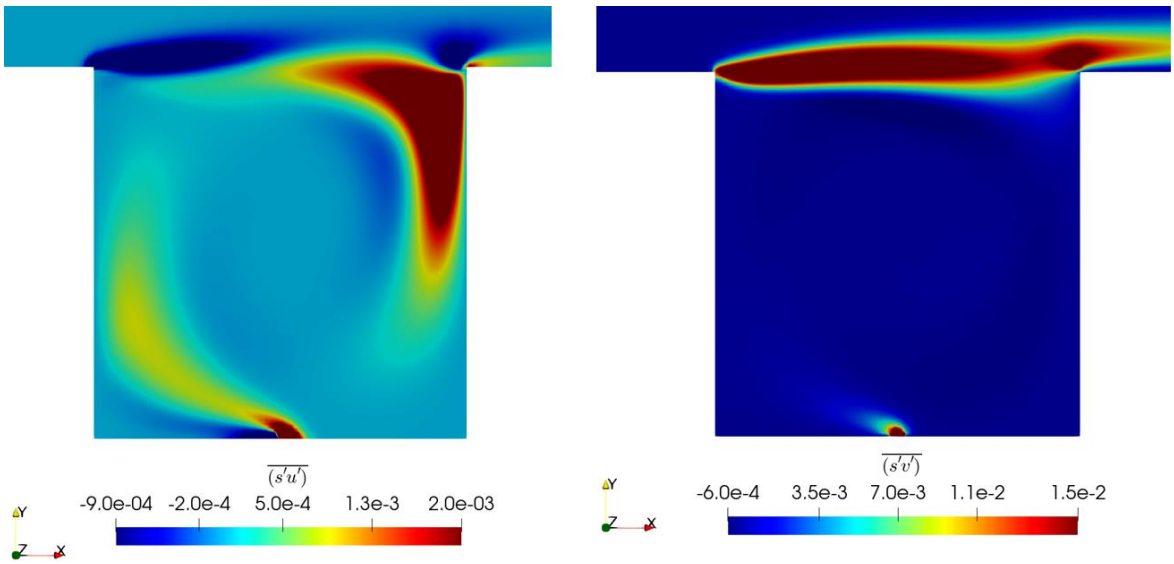

Figure 4-22. Mean pollutant concentration fluxes in horizontal and vertical direction in 4th canyon.

Left-hand figure represents the mean pollutant fluxes in the horizontal direction and it is noticeable that peak values are located at pedestrian level where pollutant source is located as well as at the top corner of windward side.

The right-hand figure represents the mean pollutant fluxes in vertical direction and they are a visual representation of the pollutant removal from the urban canyons. According to this figure high values of pollutant fluxes may be observed along the line of roof level and how the turbulent transport is responsible for removing pollutants from canyon and moving them to the freestream.

5 Case: Including thermal effects

5.1 Experimental study

In that case the experimental study used to validate the results is based on a wind tunnel experiment and it was conducted by K. Uehara, S. Murakami, S. Oikawa and S. Wakamatsu in 1999. The experiment was carried out in a thermally stratified wind tunnel in order to study the flow characteristics inside street canyons and how are they affected by atmospheric stability.[10]

The length, width and height of the wind tunnel where the experiments were conducted are 24 m, 3 m and 2 m respectively. The wind speed range is 0.2 - 10 m/s. Regarding thermal stratification, the wind temperature can be controlled in the range of 10 – 90 ºC, while the wind tunnel floor temperature between 0 and 110 ºC.

There are roughness elements distributed along horizontal direction of the wind tunnel, from X = 2m to X = 12m. These elements are blocks made of Styrofoam, are spaced 100 mm on all sides and their dimensions are 100 x 100 x 50 mm. They are intended to create a turbulent boundary layer.

Unlike the experiment in the previous case, the buildings of the street canyons are made up of blocks of 100-mm-length, 100-mm-width and 100-mm-hight. These blocks are distributed from X = 12m to X = 14.8m and they are spaced 100 mm in the X direction and 50 mm in the Y direction. Therefore, the aspect ratio of the street canyons is 1.

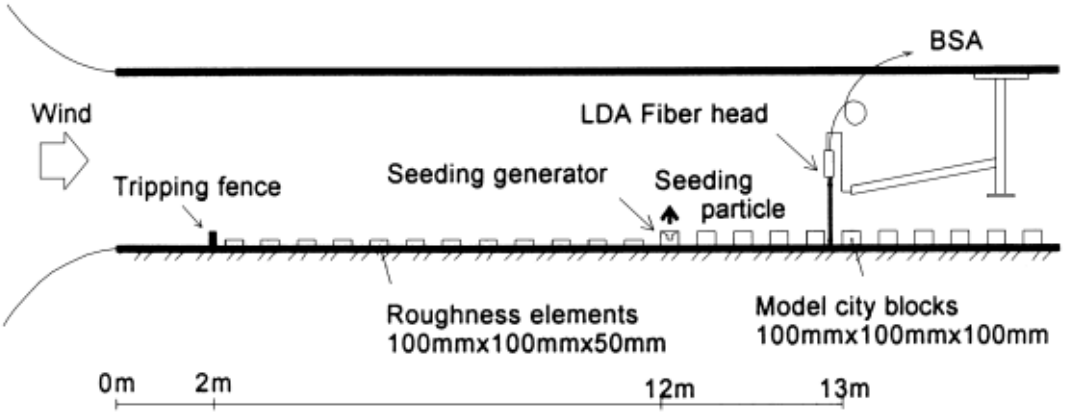

Figure 5-1. Scheme of the wind tunnel experiment (Extracted from [10])

In order to carry out the measurements in this experiment, an LDA and a cold wire were used to measure the wind speed components as well as the temperature within and above the street canyon. Also, the turbulence intensity, shear stress and heat flux distribution were measured.

As it was used in the experiment of the previous case, some seeding particles were released into the air to get results. These were Magnesium carbonate powder with a nominal diameter of 5 μm.

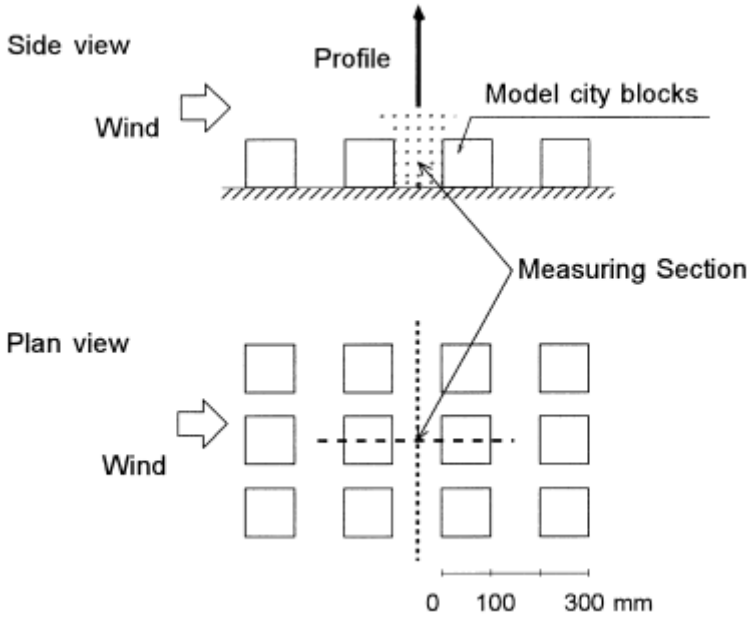

Figure 5-2. Measuring points (Extracted from [10])

5.2 Case setup

5.2.1 Scenarios simulated

Two types of non-isothermal setups will be considered: single-surface heating and multi-surface heating.

First, three cases will be simulated and analysed in which only one of the canyon walls is at a higher temperature than ambient air and the rest of walls: ground, leeward or windward. The difference of temperature considered is: $\Delta T = 6K$.

Once the results for a single-surface heating have been presented and analysed, the multi-surface heating scenarios will be simulated, presented and analysed. These will consider different gradients between walls and air temperature in order to imitate the diurnal heating scenario by sunlight in an urban street canyon.

The first all heated surfaces scenario is a night-time scenario where according to Nakamura and Oke [32] the temperature difference between building walls and ground is higher than the air temperature. Then, on this scenario all solid walls of the model are going to be defined with same temperature.

The other two scenarios will take place between 10.00 LST and 12.00 LST and around 18.00 LST due to the consideration that in these times is when windward and leeward facades reaches their highest temperature. It has been considered that for these scenarios the ground will be heated at the same level than these walls, while the opposite wall will remain at the same temperature than ambient air.

Three different temperature gradients were considered for these scenarios: 2K, 6K and 12K.

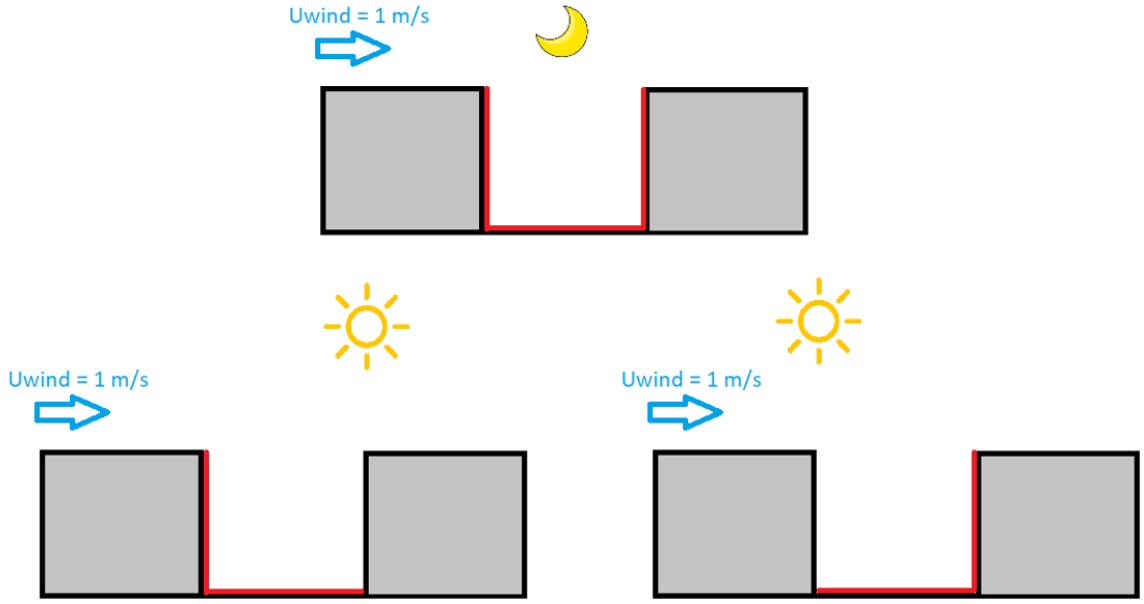

Figure 5-3. Schematic diagram of the multi-surface heating scenarios considered

5.2.2 Openfoam implementation

This section will specify the main changes to set up the case compared with the isothermal case. Refer to section 4.4 to observe the main differences between both cases.

5.2.2.1 Constant directory

The first step should be to import the mesh into OpenFOAM. Nevertheless, as the mesh used is the same than in previous case, the *polyMesh* folder does not change.

Regarding the *transportProperties* and *turbulenceProperties* files, there are no changes.

5.2.2.2 Initial and boundary conditions

The boundary conditions of the cases mentioned in section 5.2.1.1 and taking into account scripts used for the isothermal simulation, only the temperature script shall be modified:

- Temperature (*T*):
    - Single-surface heating:

- Ground heated: in this case, all surfaces are set to 296 K using a *fixedValue* type boundary condition except *streetc* and *Pollutant* surfaces which have been set to 302 K.

  The ambient air has been set to 296 K, so the *internalField* has been fixed to 296 K.

- Leeward side heated: in this case, all surfaces are set to 296 K using a *fixedValue* boundary condition except *Leeward* surface which has been set to 302 K.

  The ambient air has been set to 296 K, so the *internalField* has been fixed to 296 K.

- Windward side heated: in this case, all surfaces are set to 296 K using a *fixedValue* boundary condition except *Windward* surface which has been set to 302 K.

  The ambient air has been set to 296 K, so the *internalField* has been fixed to 296 K.

    - Multi-surface heating:

- Case 1 (All bottom surfaces heated): in this case, the *Inlet*, *Outlet* and *Up* surfaces are set to 296 K using a *fixedValue* type boundary condition whereas at the rest of surfaces defined as walls (*Ground*, *Roof*, *Leeward*, *Windward*, *Pollutant*, *streetc*) have been also applied a *fixedValue* condition.

  Since three different heating scenario shall be simulated, the temperature of these walls have been set to three different values 298 K, 302 K and 308 K.

  The ambient air has been set to 296 K, so the *internalField* has been fixed to 296 K.

- Case 2 (*Leeward*, *Ground* and *Roof* surfaces heated): in this case, the *Inlet*, *Outlet* and *Up* surfaces are set to 296 K using a *fixedValue* type boundary condition as well as the windward walls which are considered to be in the shade. The rest of surfaces (*Ground*, *Roof*, *Leeward*, *Pollutant*, *streetc*) have been considered to be at a higher temperature, therefore, a *fixedValue* condition with three different values have been applied in order to get results for these three different scenarios: 298 K, 302 K and 308 K.

  The ambient air has been set to 296 K, so the *internalField* has been fixed to 296 K.

- Case 3 (*Windward*, *Ground* and *Roof* surfaces heated): in this case, the *Inlet*, *Outlet* and *Up* surfaces are set to 296 K using a *fixedValue* type boundary condition as well as the leeward walls which are considered to be in the shade. The rest of surfaces (*Ground*, *Roof*, *Windward*, *Pollutant*, *streetc*) have been considered to be at a higher temperature, therefore, a *fixedValue* condition with three different values have been applied in order to get results for these three different scenarios: 298 K, 302 K and 308 K.

  The ambient air has been set to 296 K, so the *internalField* has been fixed to 296 K.

As it has been mentioned before, the surfaces of the model defined as empty have also been defined as *empty* conditions inside temperature scripts.

5.2.2.3 System directory

In this directory, there are scripts related to run control parameters, discretisation schemes used in the solution, equation solvers, tolerances and other algorithm controls.

- *controlDict*: the time step contemplated for the isothermal case had to be modified, it has been reduced to $\Delta t = 0.005s$ since the velocity components, pressure and temperature variables did not converge. Before that, a refinement of the mesh was tried, however, the results still did not converge and the computational resources used to carry out the simulation increased significantly.
- *fvSchemes* and *fvSolution*: there are no changes from previous case.

5.3 Single-surface heating results

In this section the results obtained for single-surface heating will be shown using paraView. As it has been done in section 4.7, the velocity, pressure and pollutant concentration map fields will be presented and commented. In addition to these, a new map field showing the normalized temperature will be included.

It is important to mention that for these simulations, the comments will be focused on the map fields of canyon 4th since there are no major changes in the complete domain compared to those presented for the isothermal case.

5.3.1.1 Residuals

According to the following figures, it can be seen that the residuals have converged at approximately 350s: the pressure is the first one to converge at a value around 10^{-3}, then the velocities in Y and X direction at values between 10^{-6} and 10^{-8} and, finally, the temperature at a value between 10^{-8} and 10^{-9} approximately.

It can be seen that for ground heating scenario, the residuals plot starts from 280s; this can be explained because the simulation stopped and then it had to be continued from this last saved point. The windward side heating scenario was also started from 20s due to the same fact.

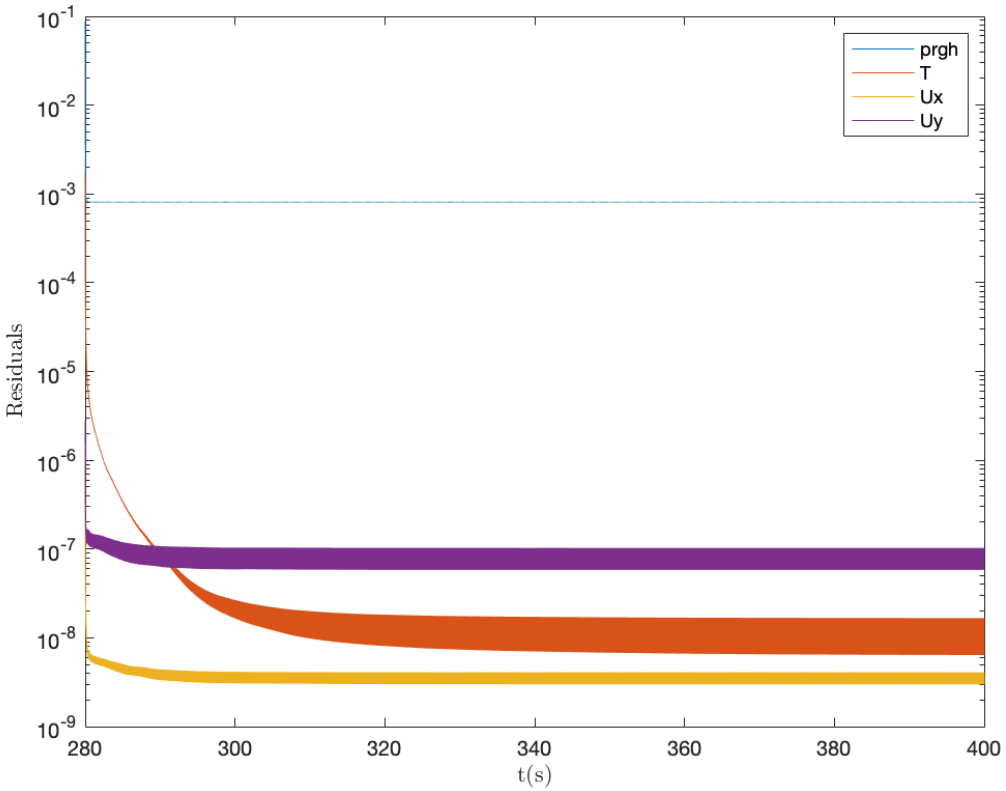

Figure 5-4. Residuals of direct ground heating scenario (ΔT = 6 K)

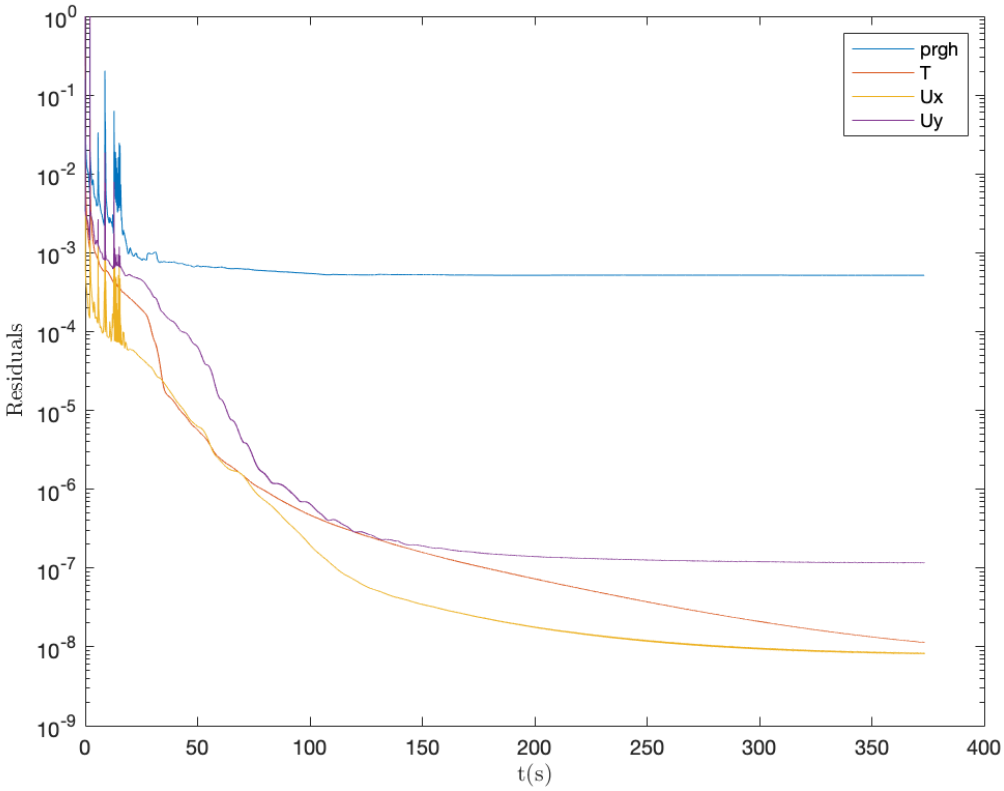

Figure 5-5. Residuals of leeward side heating scenario (ΔT = 6 K)

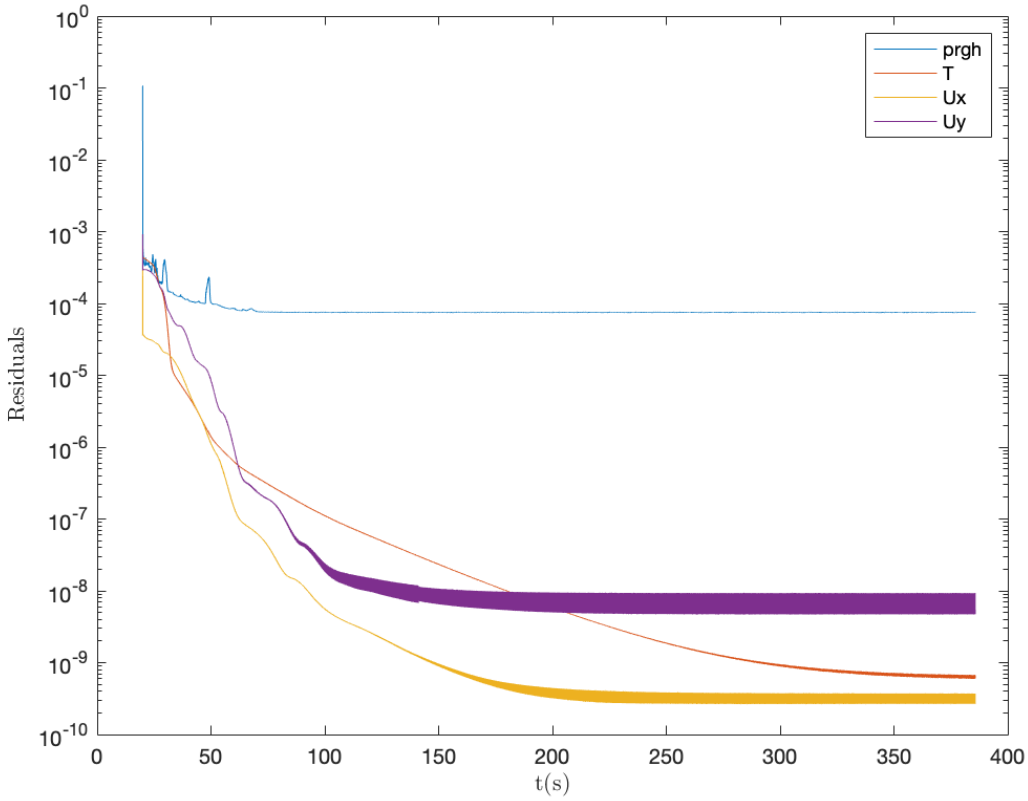

Figure 5-6. Residuals of windward side heating scenario (ΔT = 6 K)

5.3.1.2 Temperature

Figure 5-7 show the normalized temperature on each considered case. It can be appreciated how the air flow at the bottom corner of leeward side has a higher temperature for direct ground heating than for leeward heating. In addition to this observation, the scenario where the leeward is heated up show a higher air temperature at the top left corner of the canyon. Eventually, when the windward side is heated up, the temperature increases throughout the canyon; this, as will be mentioned later, is indicative of a greater permanence of the air inside the canyon which causes a generalized increase of the ambient temperature, especially in the lower windward corner.

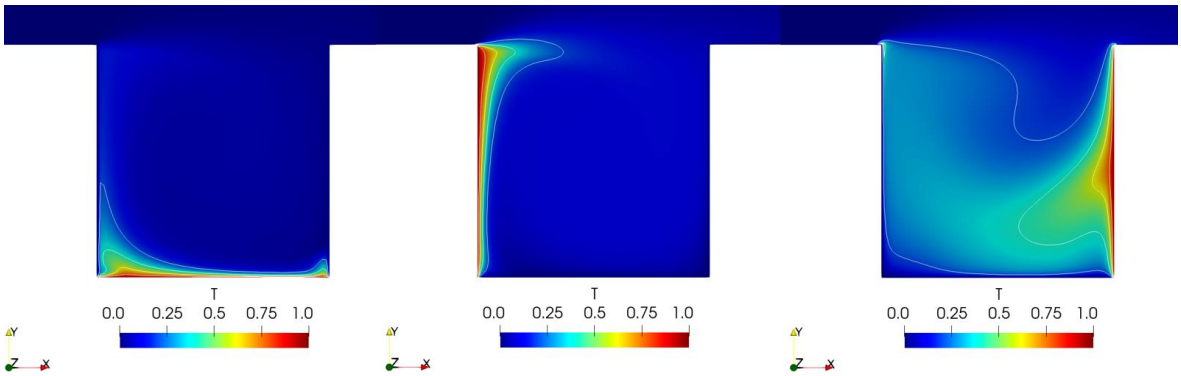

Figure 5-7. Normalized temperature in 4th canyon (From left to right: Ground, LW side and WW side heated)

5.3.1.3 Velocity

One of the main changes regarding the isothermal case is the velocity map field inside urban canyon. Such as it can be observed in next figures, it is not only a question of changes in the air velocity magnitude, but depending on the wall side that is heated, the structure of the airflow inside the canyon is also modified.

Figure 5-8 show the mean velocity map in vertical direction while *Figure 5-9* show the mean velocity map in horizontal direction. It can be appreciated how the vortex is strengthen when the ground is heated compared to the rest of scenarios, included the isothermal case.

For leeward heating scenario, the air distribution has more or less the same structure than former case, however, the increase of the air velocity is not as strength as for direct ground heating scenario. This may be due to the fact that in this scenario the air is heated only when it reaches the leeward side, while in direct ground heating scenario, the air at the lower corner of leeward side already has a high temperature. Moreover, the air velocity in this scenario is higher than isothermal case.

Regarding windward heating scenario, it can be appreciated how the main vortex is displaced upwards inside the canyon since a second counter rotating vortex is formed at the lower corner of windward side due to the upward buoyancy force. The presence of this secondary vortex affects the velocity components inside the canyon which are lower than the others scenarios, included the isothermal case.

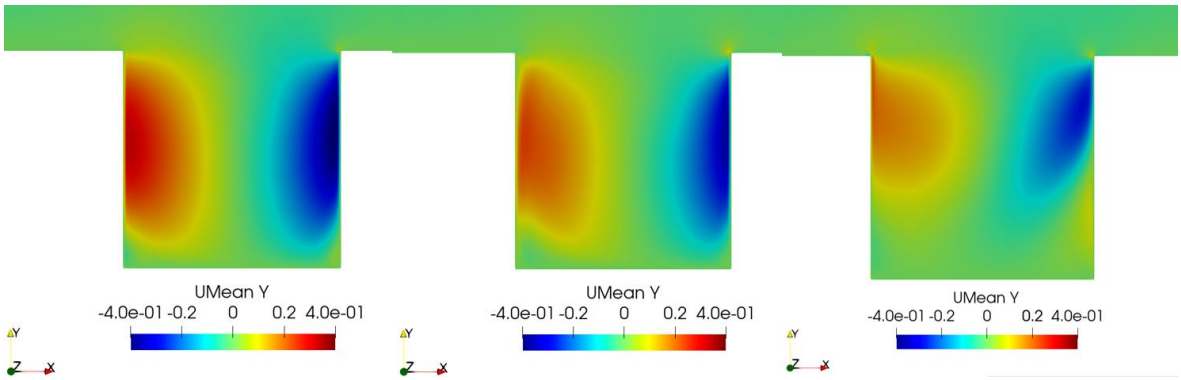

Figure 5-8. Mean velocity map (Y direction) in 4th canyon (in m/s) (From left to right: Ground, LW side and WW side heated)

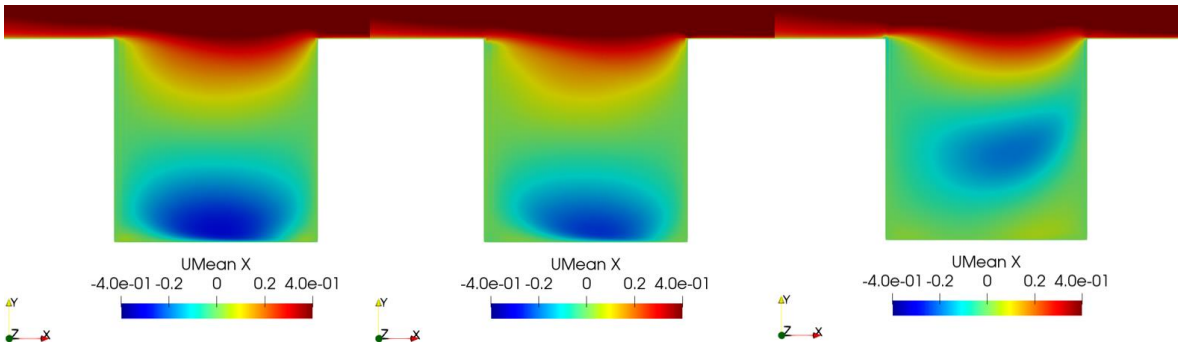

Figure 5-9. Mean velocity map (X direction) in 4th canyon (in m/s) (From left to right: Ground, LW side and WW side heated)

5.3.1.4 *Streamlines*

Figure 5-10 show the air flow structure inside 4th canyon. These pictures illustrates what it has been previously mentioned: on one hand, for scenarios where ground or leeward are heated, the flow structure is the same than for the isothermal case, despite there are some differences in the strength of the main vortex. On the other hand, when windward side is heated up, buoyancy changes the vortex structure since the main vortex is displaced towards the top-right corner of the canyon as well as a major secondary counter-rotating vortex appears in windward side.

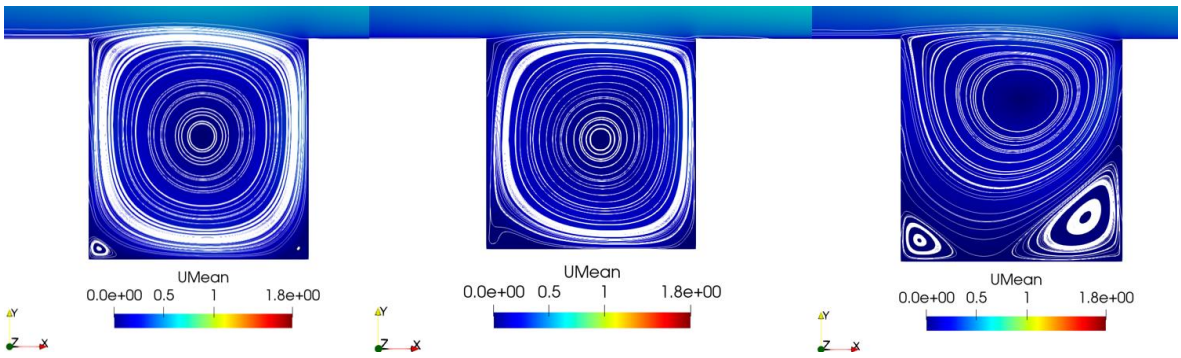

Figure 5-10. Streamlines in 4th canyon (From left to right: Ground, LW side and WW side heated)

5.3.1.5 *Mean pollutant concentration*

In *Figure 5-11*, it can be observed how the mean concentration of pollutants is higher in the scenario where the leeward side is heated. Similarly, it is observed that when the leeward side or ground surface are heated, the concentration is greater in the leeward side, while when the windward side is heated, the concentration increases more in the lower corner of the downwind building. In *Figure 5-*

12, a scale change is shown and it can be better appreciated that for the leeward heating scenario, the transport of pollutants outside the canyon is higher, followed by the direct ground heating scenario and, finally, the windward one.

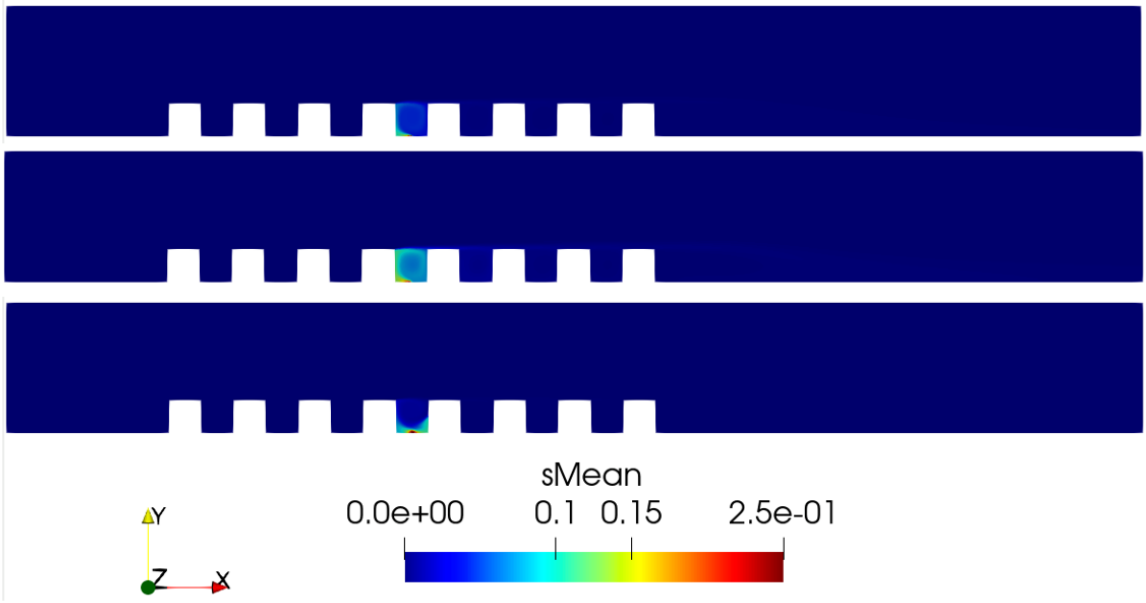

Figure 5-11. Mean pollutant concentration (From top to bottom: Ground, LW side and WW side heated)

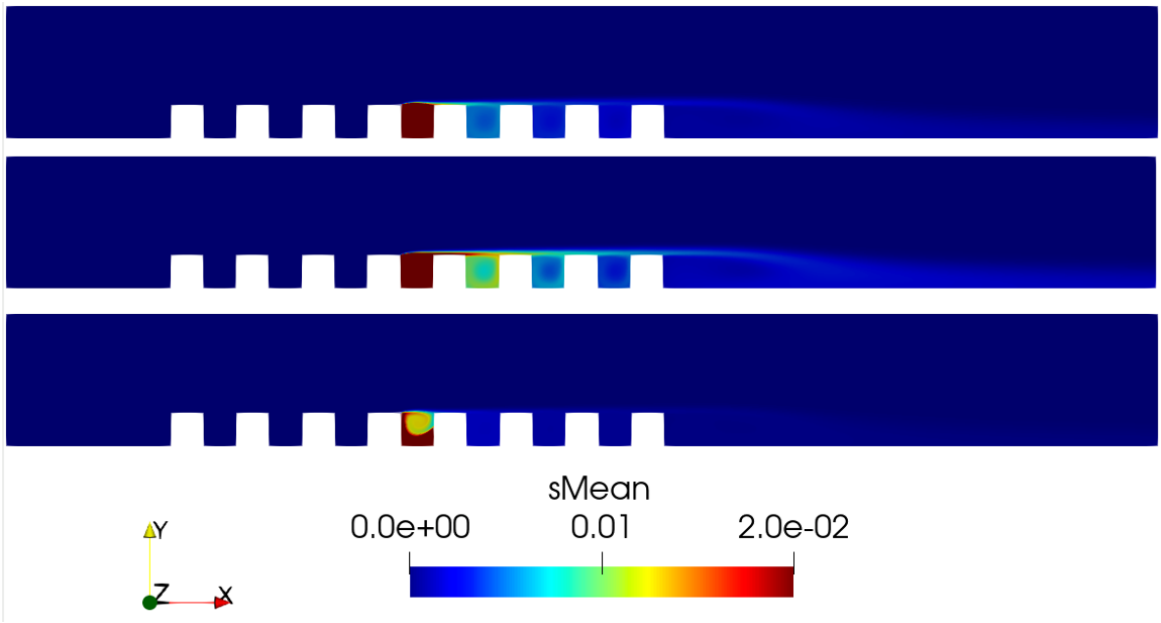

Figure 5-12. Mean pollutant concentration (From top to bottom: Ground, LW side and WW side heated)

Pollutant concentration inside canyons is also modified due to thermal effects since there are changes in the velocity fields that will modify the pollutant transport, thus, the pollutant concentration will be different on each case.

Considering all the scenarios simulated, in *Figure 5-13* it can be seen that the scenario with a lowest concentration of pollutants is the direct ground heating scenario which is reasonable due to the fact that for this case the air velocity inside the canyon is the highest.

Regarding the leeward heating scenario, the pollutant concentration is higher than isothermal case in spite of the vortex is more intense. This might be produced due to most of the air leaving the street canyon at the leeward side is re-entrained again instead of be mixed up with main flow stream.

Regarding the windward heating scenario, the pollutant concentration is higher at the bottom side of the canyon as it was expected since there is a secondary counter-rotating vortex which will increase the retain of pollutants and will decrease the air exchange rate.

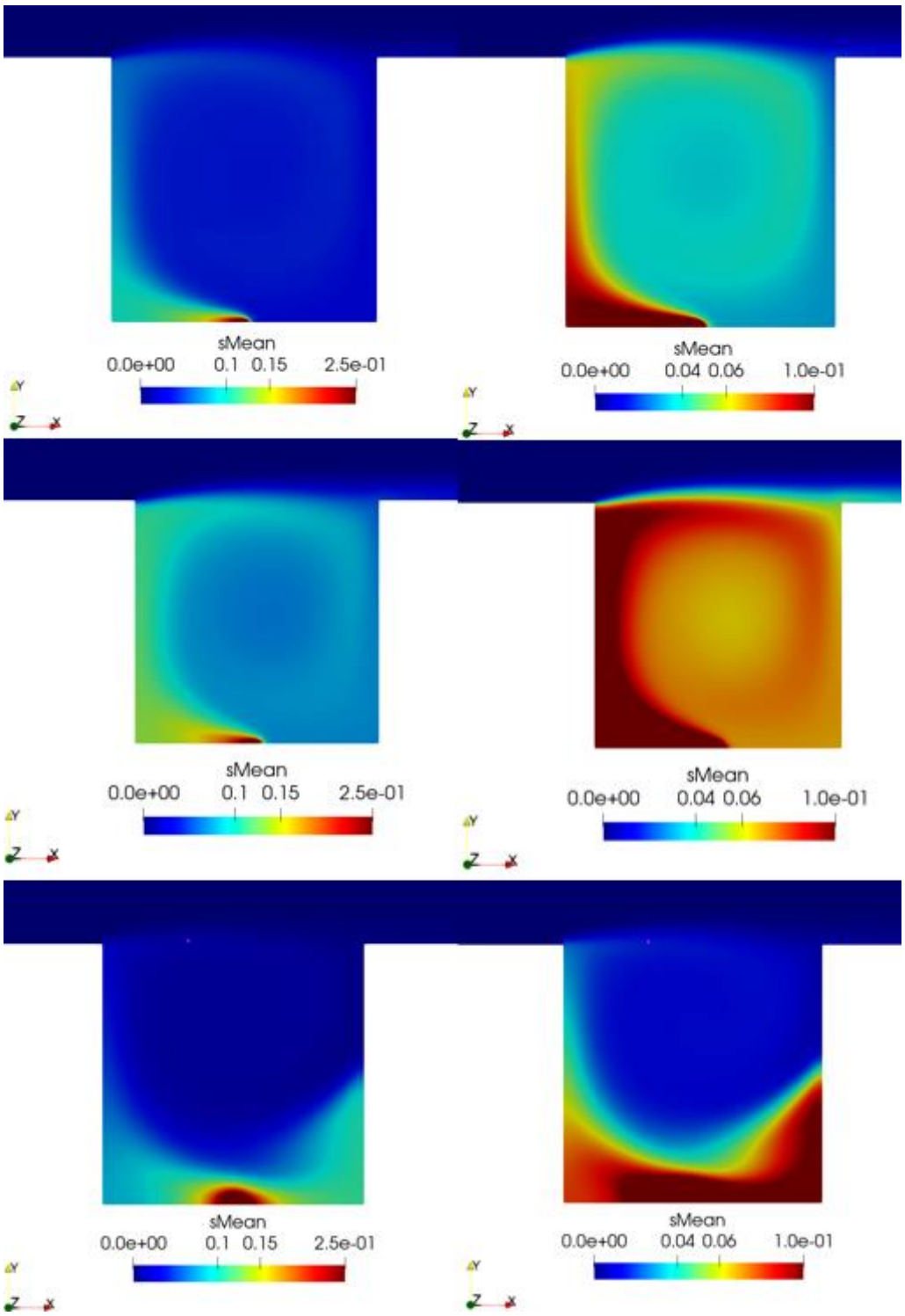

Figure 5-13. Mean pollutant concentration in 4th canyon with a scale change included (From top to bottom: Ground, LW side and WW side heated)

5.3.1.6 *Mean pollutant concentration fluxes*

In *Figure 5-14* the horizontal fluxes are shown. It can be appreciated that there are practically no differences between the ground and leeward scenarios, the only difference is in the leeward side where there is a stronger horizontal flux when ground is heated. While for the windward heated scenario, it is observed how the source of contaminants has a greater opposition by the counter-rotating vortex located in the lower corner of the leeward side, which favours a bigger amount of pollutants to enter the counter-rotating vortex of the windward side before moving on to the main vortex.

Vertical concentration fluxes show that the air pollutants leaving the canyon is higher in the case of the leeward side than in the rest of cases. This can be contrasted in *Figure 5-12* where it is shown that the transport of contaminants outside the canyon is higher in the scenario where the leeward side is heated. However, comparing these results with *Figure 5-13*, it is concluded that part of the pollutants that leaves the canyon by the leeward side are re-entrained so, the mean concentration throughout the canyon is greater despite the vertical mean pollutant fluxes are greater for this case.. Regarding the case where the windward side is heated, a new vertical flux is observed in the downwind building façade where some pollutants are transported from the windward counter-rotating vortex to the main one since, as mentioned before, contaminants are forced to enter the secondary vortex, they are moved upwards through the windward side and pass to the main vortex at the connection area of both vortexes.

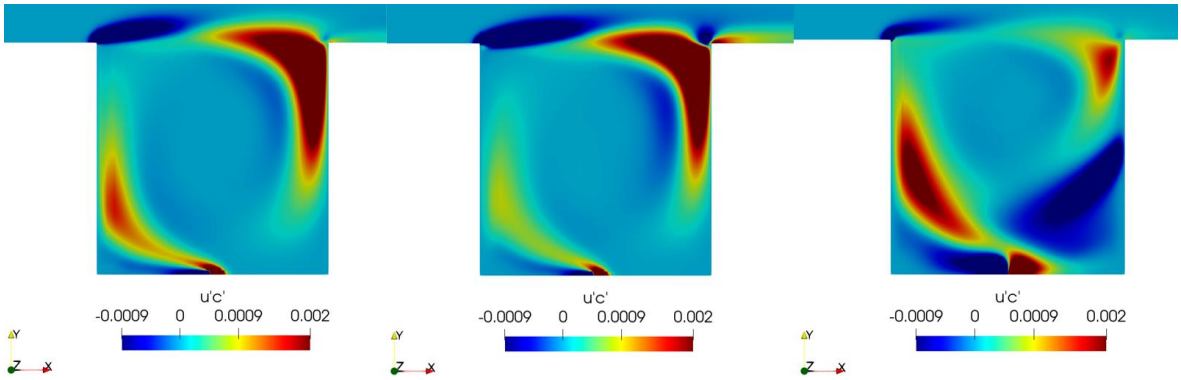

Figure 5-14. Mean pollutant concentration fluxes in horizontal direction in 4th canyon (From left to right: Ground, LW side and WW side heated)

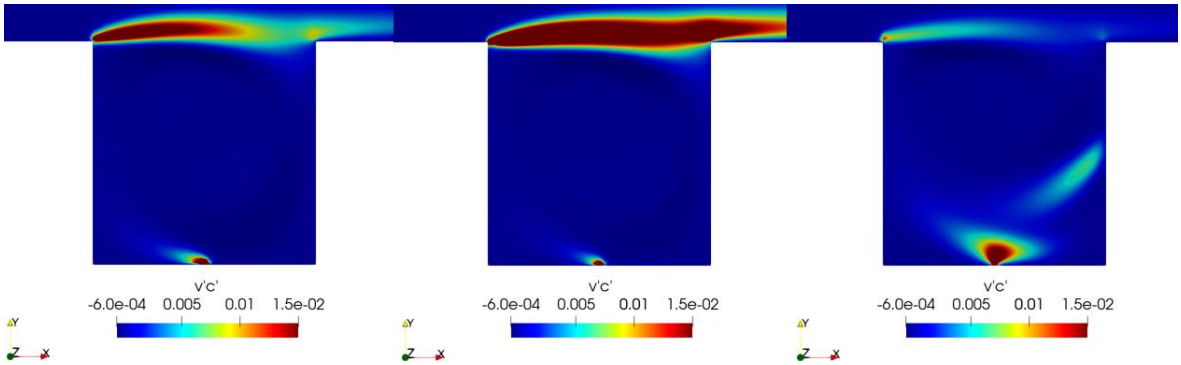

Figure 5-15. Mean pollutant concentration fluxes in vertical direction in 4th canyon (From left to right: Ground, LW side and WW side heated)

5.4 Multi-surface heating results

In this section the results obtained for multi-surface heating will be shown using paraView.

5.4.1 Case 1: All bottom surfaces heated

5.4.1.1 Residuals

It is important to know if the solution obtained by OpenFoam has converged or not. For that, the error (residuals) of velocity, pressure and temperature must be plotted in order to see if they tend to zero while the simulation is running and, also, if they stand stable at some value.

According the next figures below, the residuals of the variables of each scenario have converged approximately at 350s. The first variable to converge is the pressure at a value around 10^{-3}, then the velocities in Y and X direction at a values of 10^{-7} and 10^{-8} respectively and finally, the temperature at a value of 10^{-9} approximately. It is considered that the solution has arrived at a stationary zone in 350s.

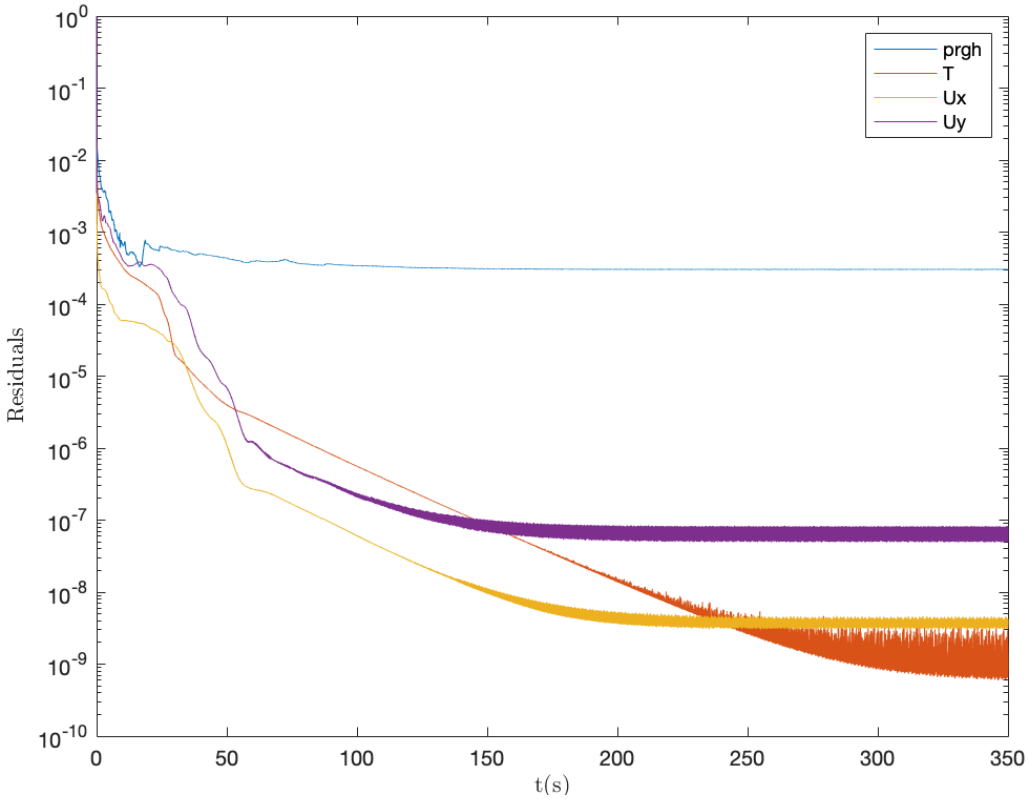

Figure 5-16. Residuals of all bottom surfaces heated scenario (ΔT=2K)

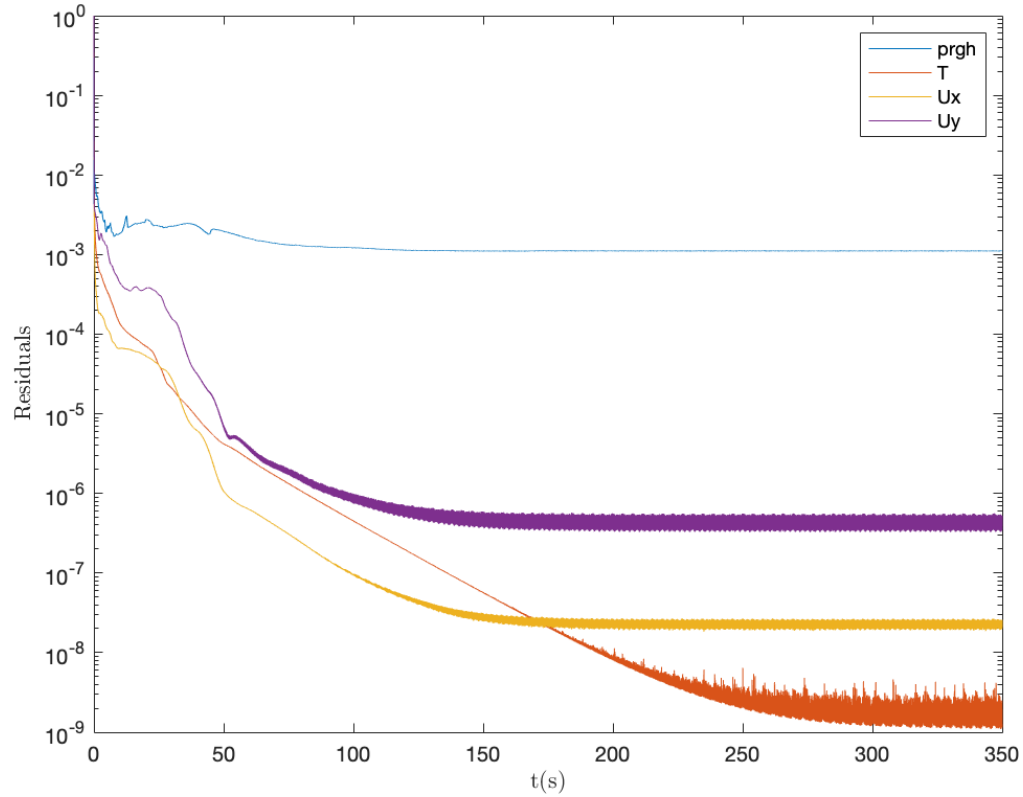

Figure 5-17. Residuals of all bottom surfaces heated scenario (ΔT=6K)

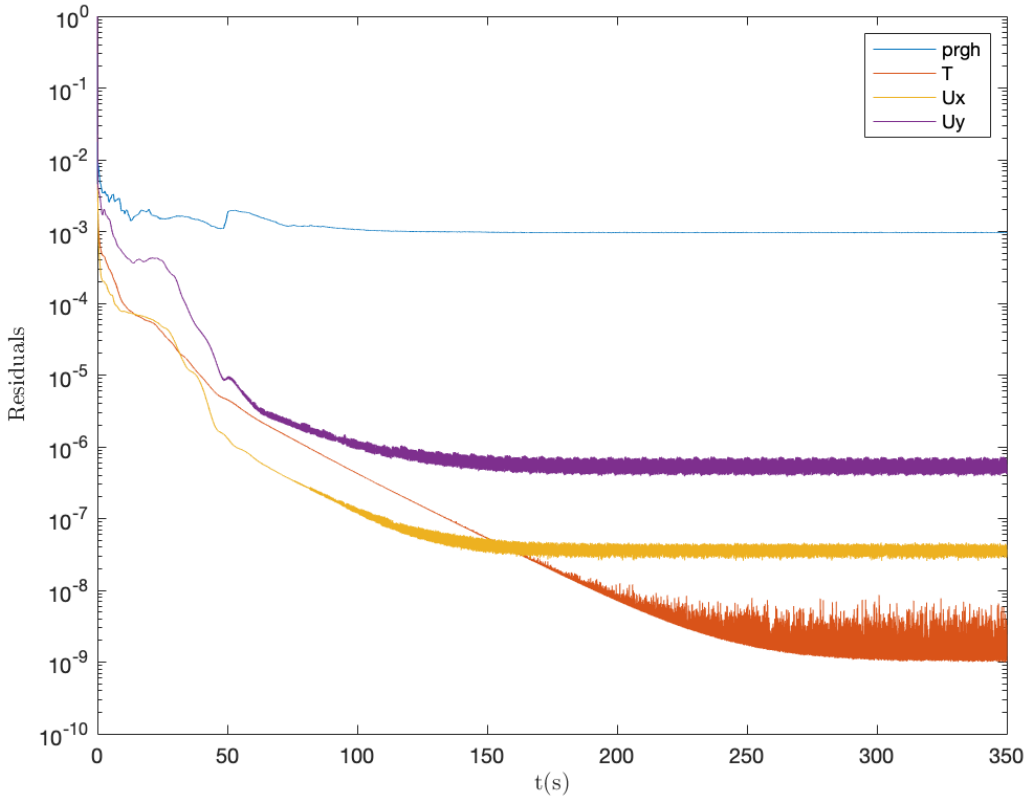

Figure 5-18. Residuals of all bottom surfaces heated scenario (ΔT=12K)

5.4.1.2 Pressure

The pressure maps show a similar distribution to the one presented in previous isothermal case. The suction region is present in all of them, however it seems that the suction bubble flatter while temperature gradient raises. Furthermore, the pressure is maximum between the inlet and the first building and the peak value decreases as the temperature difference increases: for a difference of 2 degrees, the maximum pressure value is 0.96 m^2/s^2 while for a difference of 12 degrees this value increases to 1.3 m^2/s^2.

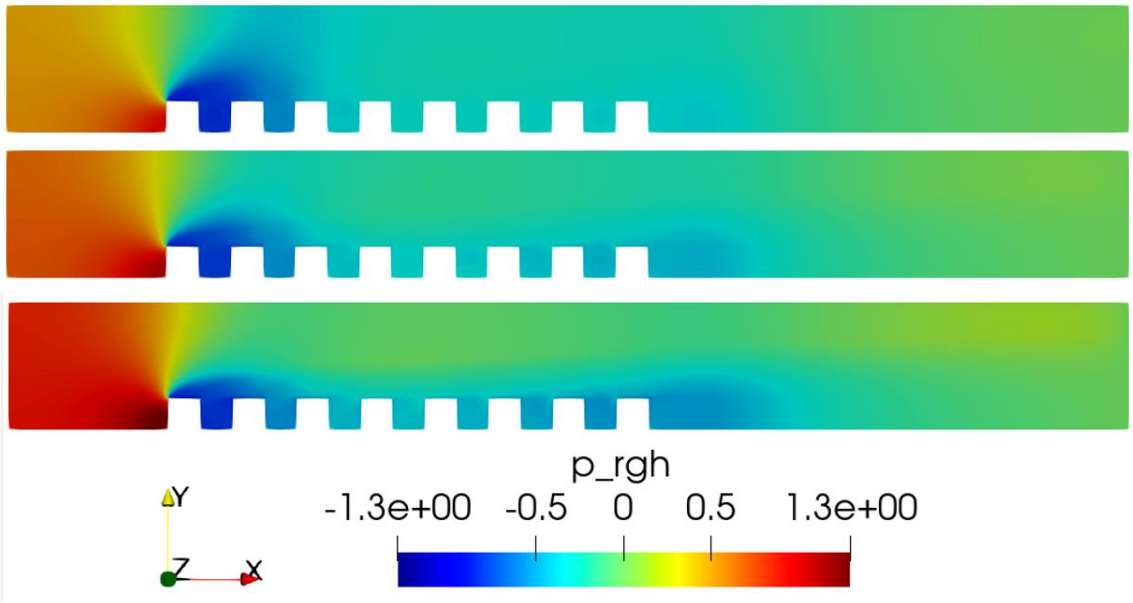

Figure 5-19. Pressure for case 1 (From top to bottom: ΔT=2K, ΔT=6K, ΔT=12K)

5.4.1.3 Temperature

In this section, new map fields showing temperature distribution along the complete domain are going to be presented since the scenarios simulated consider heating not only inside canyon 4th but also in the rest of walls of the domain. The following images show the temperature distribution on the whole domain. It can be appreciated how the canyons are the areas with a higher temperature due to the recirculation of the air. The particles of air that are trapped inside the canyons are not being able to mix themselves up with the fresh air of the flow stream in order to reduce its temperature by convection. Thus, the temperature inside the canyons increases as heating also increases.

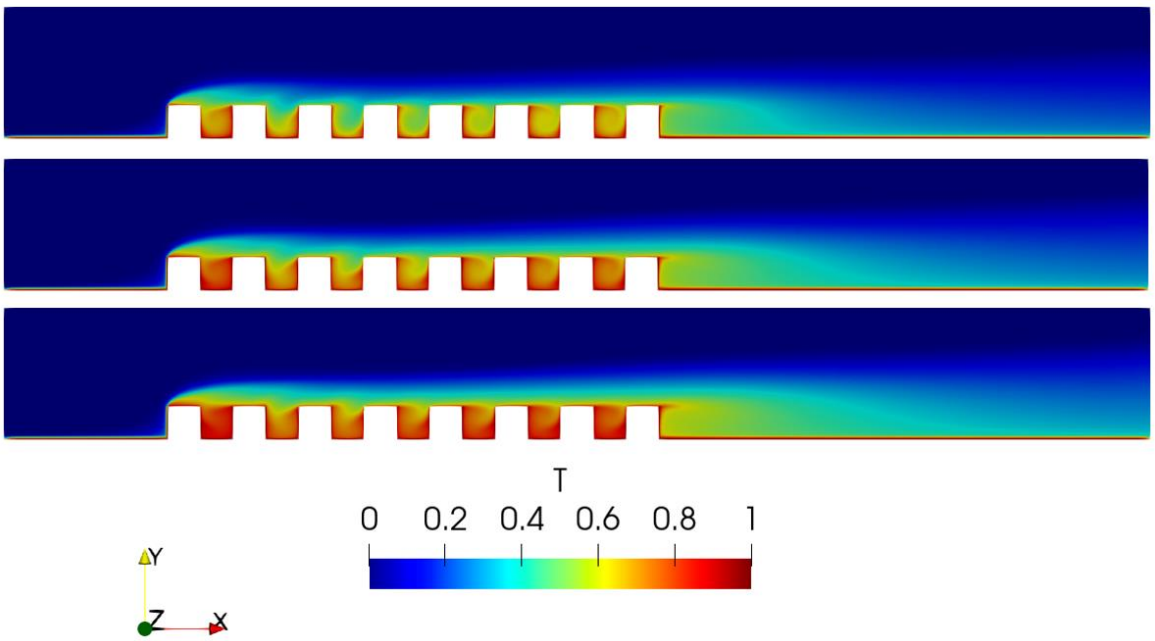

Figure 5-20. Normalized temperature map field for case 1 (From top to bottom: ΔT=2K, ΔT=6K, ΔT=12K)

5.4.1.4 Velocity

The velocity maps of *Figure 5-21* show that there are minor changes as the temperature differential between the walls and ambient air increases in the scenario where all the lower surfaces are heated.

The main difference is that as the wall temperature increases compared to ambient air temperature, the air velocity also increases: this can be easily seen at the top side of the domain where the higher velocities are found. However, the flow structure does not vary between these three cases, nor does it compared to the previously studied case in which the temperature was not included.

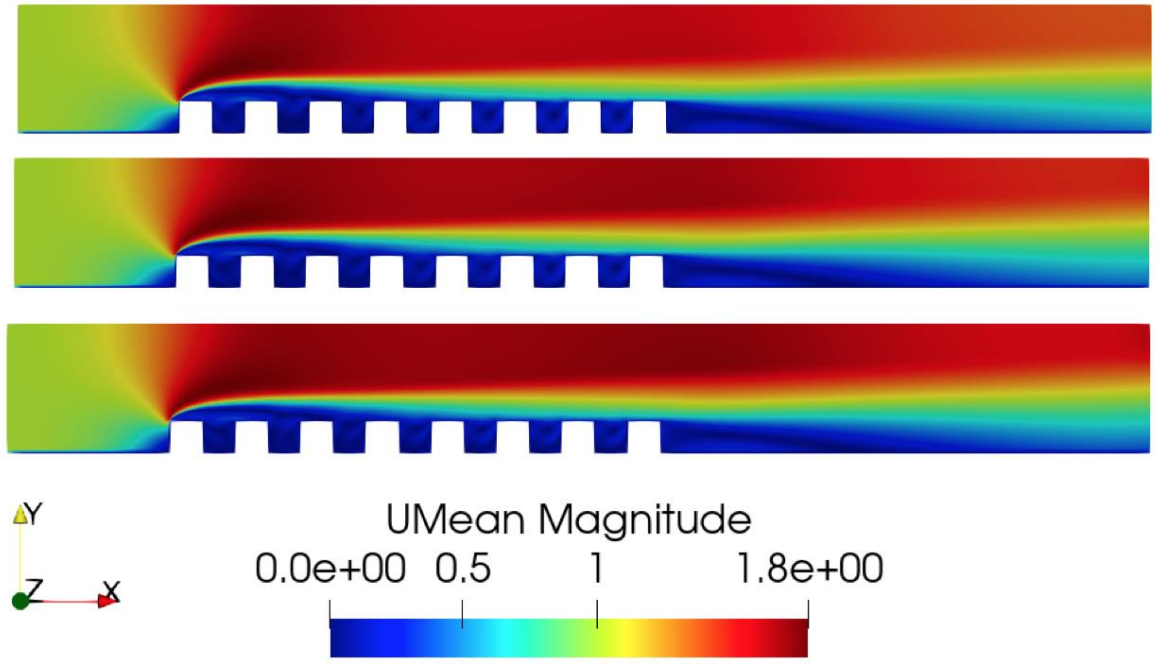

Figure 5-21. Mean velocity maps for case 1 (From top to bottom: ΔT=2K, ΔT=6K, ΔT=12K).

The detailed views of the mean velocity in vertical direction inside the target canyon show that the velocity's vertical component of main vortex decreases as long as the difference of temperature between the ambient air and the bottom walls increases. Also, it can be appreciated how the

secondary vortex, located in the bottom corner of the windward side, increases its velocity as the walls are warmed up.

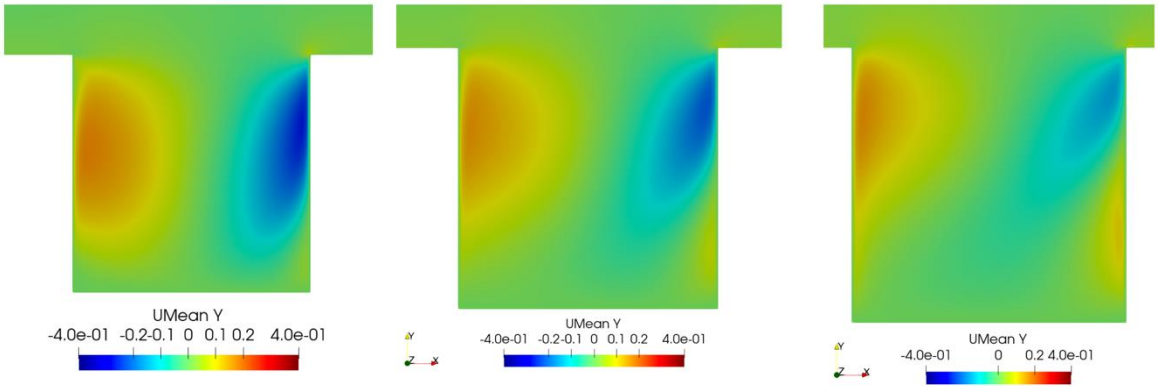

Figure 5-22. Mean velocity maps (Y direction) in the 4th canyon for case 1 (From left to right: ΔT=2K, ΔT=6K, ΔT=12K)

5.4.1.5 Streamlines

The streamlines show the trajectory followed by a particle in the domain, so it can be seen how the complete domain is swept from inlet surface to the outlet surface as well as the areas with a higher recirculation can be seen in a clearer way.

Analyzing the streamlines in the complete domain, a certain stability is observed from the third canyon onwards. Between the first and the third canyon there is a zone of higher vorticity.

The most interesting results are those related to the detail views of the streamlines in the fourth canyon: for a temperature difference of 2K between the walls and the air, there is a main vortex located approximately at the center of the canyon and two smaller vortices in the lower corners of the canyon. As the temperature difference increases, the leeward vortex disappears while the windward vortex grows, displacing the main vortex upwards and affecting the mean concentration of pollutants as will be discussed later.

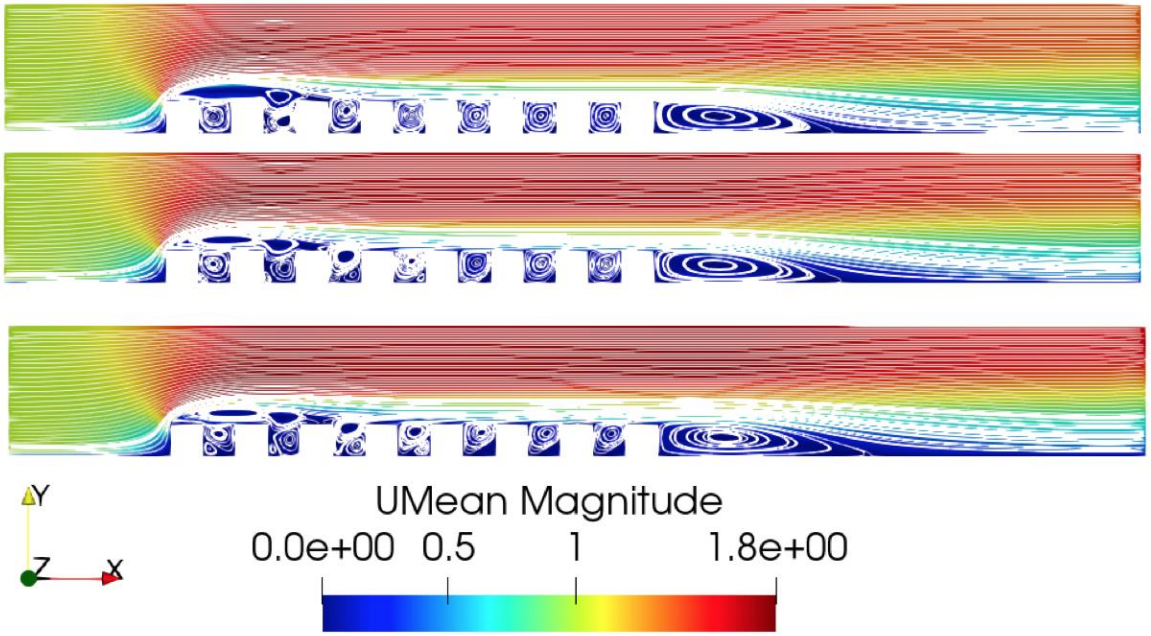

Figure 5-23. Streamlines of the domain for case 1 (From top to bottom: ΔT=2K, ΔT=6K, ΔT=12K)

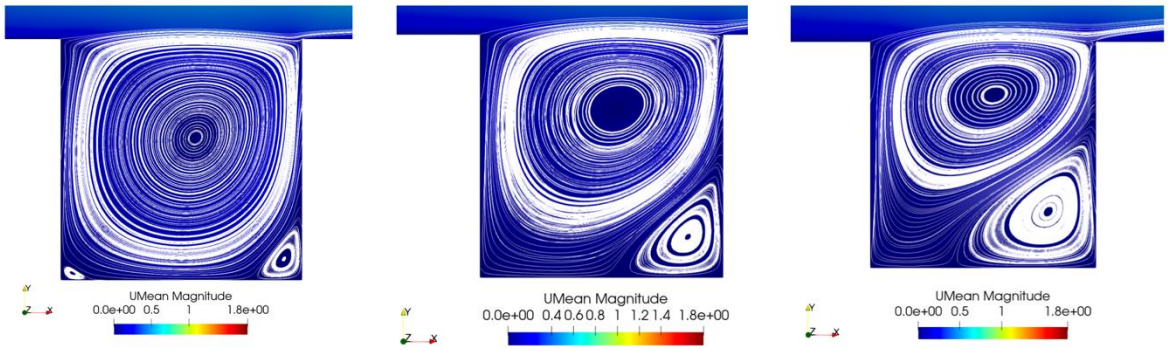

Figure 5-24. Streamlines in 4th canyon for case 1 (From left to right: ΔT=2K, ΔT=6K, ΔT=12K)

5.4.1.6 Mean pollutant concentration

Concerning the mean pollutant concentration in the complete domain, it is clearly appreciated how the pollutant removal increases with the temperature difference between walls and ambient air. In *Figure 5-26*, with the scale change, it can be observed how the pollutant concentration increases in the freestream as well as in the last three canyons of the model when the lower surfaces of the model are warmed up.

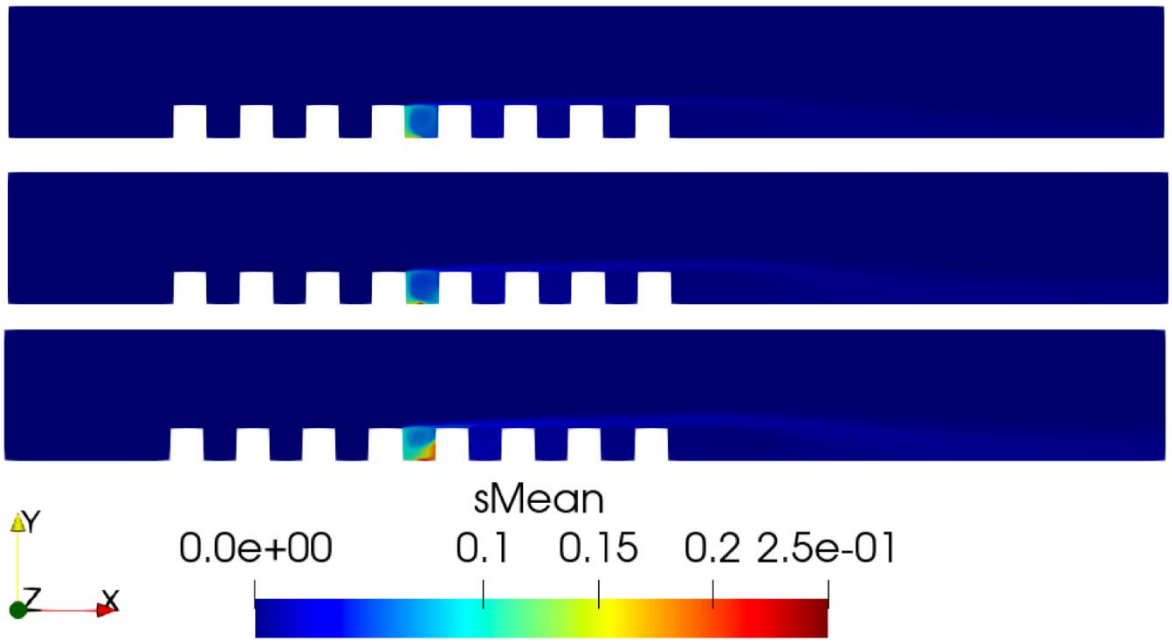

Figure 5-25. Mean pollutant concentration for case 1 (From top to bottom: ΔT=2K, ΔT=6K, ΔT=12K)

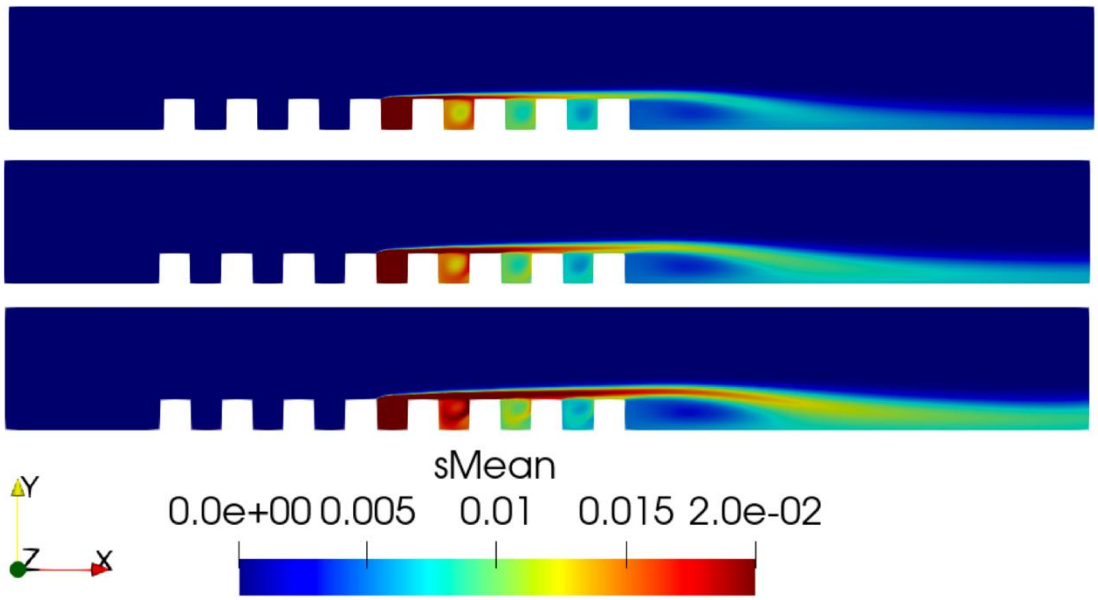

Figure 5-26. Mean pollutant concentration with a scale change for case 1 (From top to bottom: ΔT=2K, ΔT=6K, ΔT=12K)

Some interesting conclusions can be extracted from the detail views of the fourth canyon in *Figure 5-27*. As the temperature differences increases, the secondary counter-clockwise rotating vortex in the windward side grows and it extends beyond the center of the street to the leeward side. Therefore, the pollutants enters in the secondary vortex instead of the main vortex following the path of this secondary vortex and accumulating a bigger concentration of pollutants in the windward side than in the leeward side.

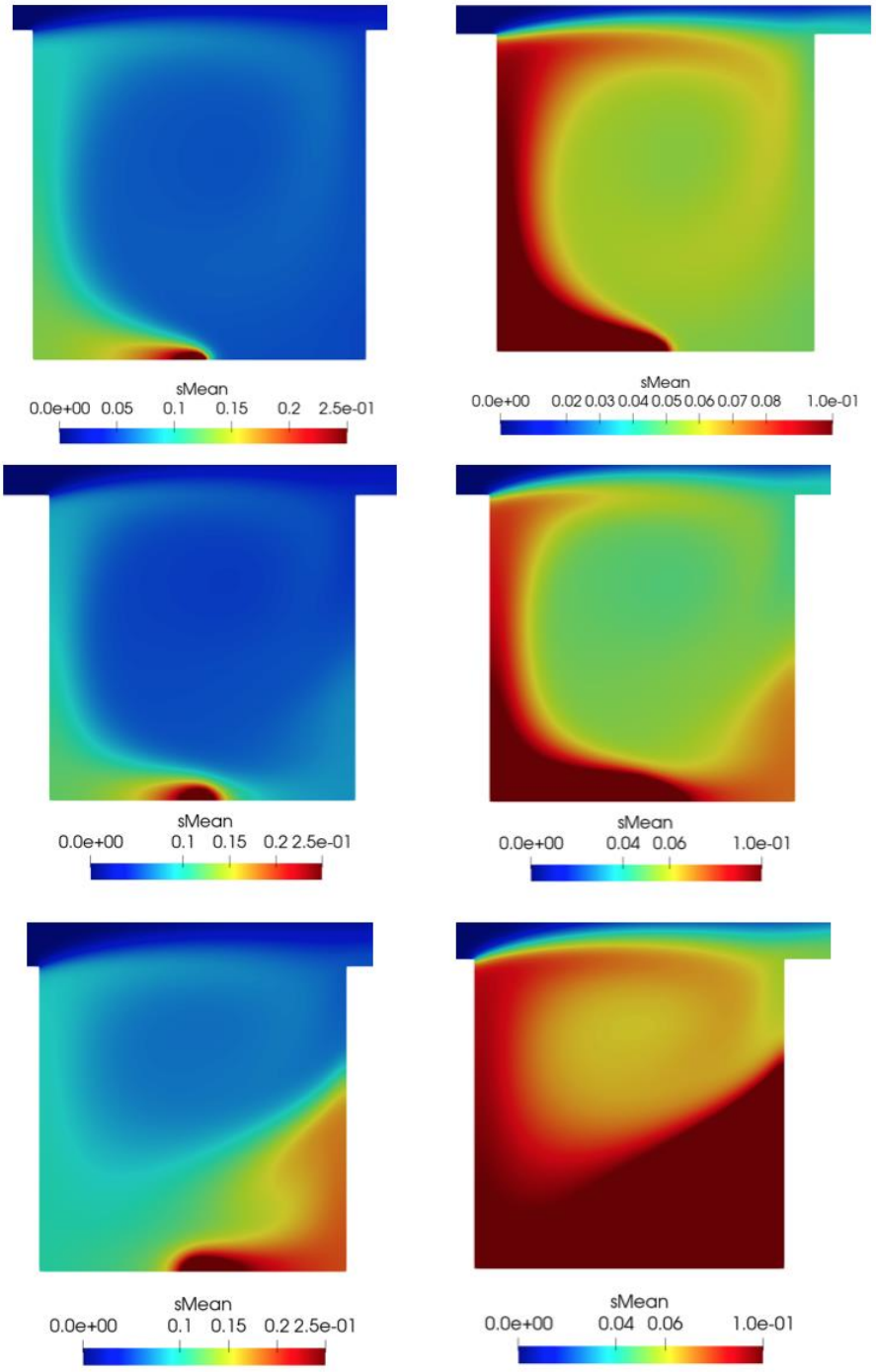

Figure 5-27. Mean pollutant concentration in 4th canyon with a scale change included for case 1 (From top to bottom: ΔT=2K, ΔT=6K, ΔT=12K)

5.4.1.7 Mean pollutant concentration fluxes

Figure 5-28 and *Figure 5-29* show the pollutant fluxes within the fourth canyon, which will depend on the pollutant concentration and fluctuating velocities in both main directions.

Regarding the horizontal pollutant fluxes, it can be observed how the direction of these fluxes is reversed as heating increases. On one hand, when ΔT = 2 K or ΔT = 6 K, the pollutants spread into the ambient follows the clock-wise primary vortex, although it can be appreciated how there is a negative flux lower leeward side corner that grows up as heating increases. When ΔT = 12 K, it can be seen how the pollutants are forced to enter the secondary vortex located at the windward lower side and there is a negative value along the contact line between both recirculation. This is expected since the pollutants will move to the upper vortex.

Regarding the vertical fluxes, stronger vertical fluxes at roof level are observed as difference of temperature between walls and ambient air increases. As it has been noticed for the horizontal fluxes, when ΔT = 12 K, an intermediate area located near the windward side with larger vertical fluxes appears at the connection of both primary recirculation since the pollutants will move upwards through windward side and will join the upper vortex via vertical turbulent transport at this area.

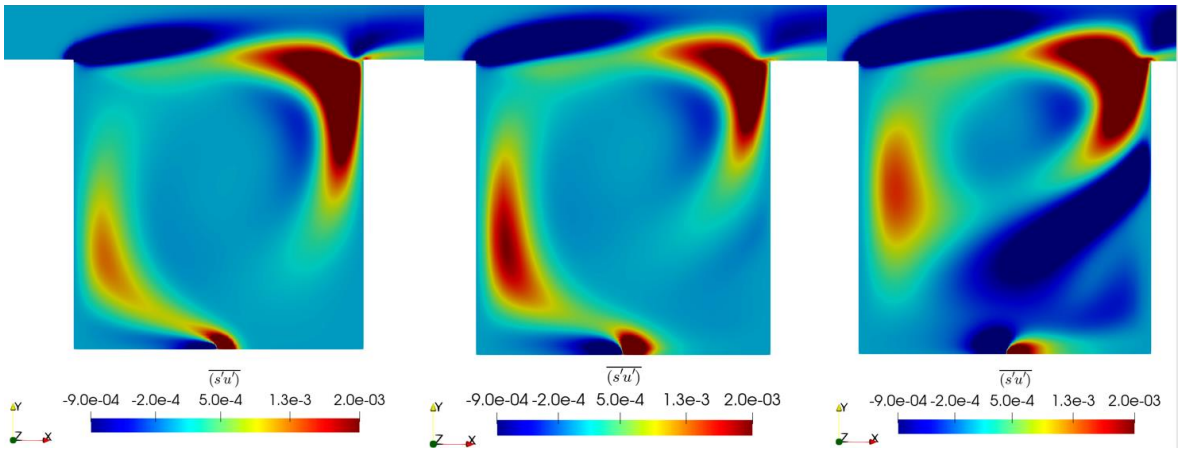

Figure 5-28. Mean pollutant concentration fluxes in horizontal direction for case 1 (From left to right: ΔT=2K, ΔT=6K, ΔT=12K)

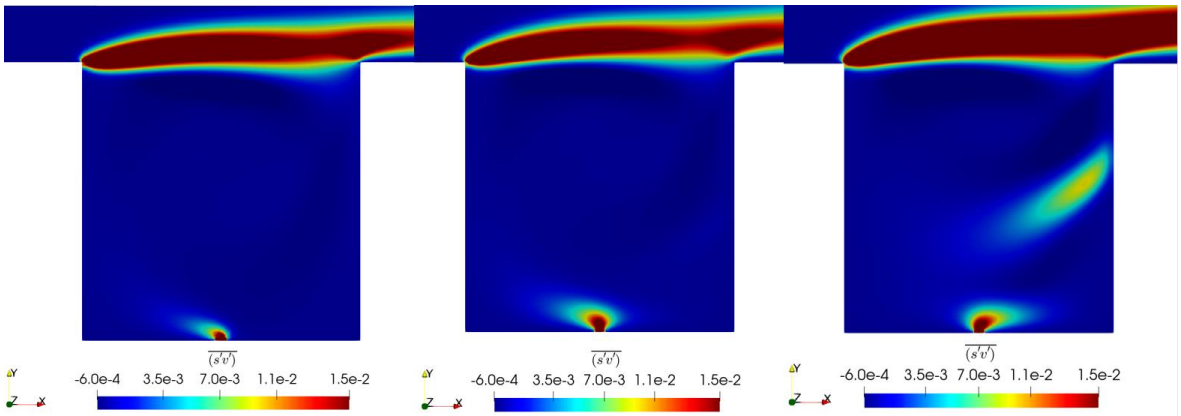

Figure 5-29. Mean pollutant concentration fluxes in vertical direction for case 1 (From left to right: ΔT=2K, ΔT=6K, ΔT=12K)

5.4.2 Case 2: Leeward side and ground heated

5.4.2.1 Residuals

In the following figures, it can be seen that the residuals have converged at 350s: the pressure is the first one to converge at a value around 10^{-3}, then the velocities in Y and X direction at values between 10^{-6} and 10^{-8} and, finally, the temperature at a value between 10^{-8} and 10^{-9} approximately.

In the simulations of the previous case (section 5.4.1) as well as in the first simulation of this section carried out with a temperature difference of 2K, the time-step used was 0.005s. However, the solution does not converge using this time-step with higher temperature differences such as 6K and 12K. Therefore, to achieve the convergence of the residuals in these scenarios a new time-step of 0.0025s was used.

It is also important to mention that prior to reducing the time-step, the relaxation factors were also modified to help the solution to converge. It did not fix the issue.

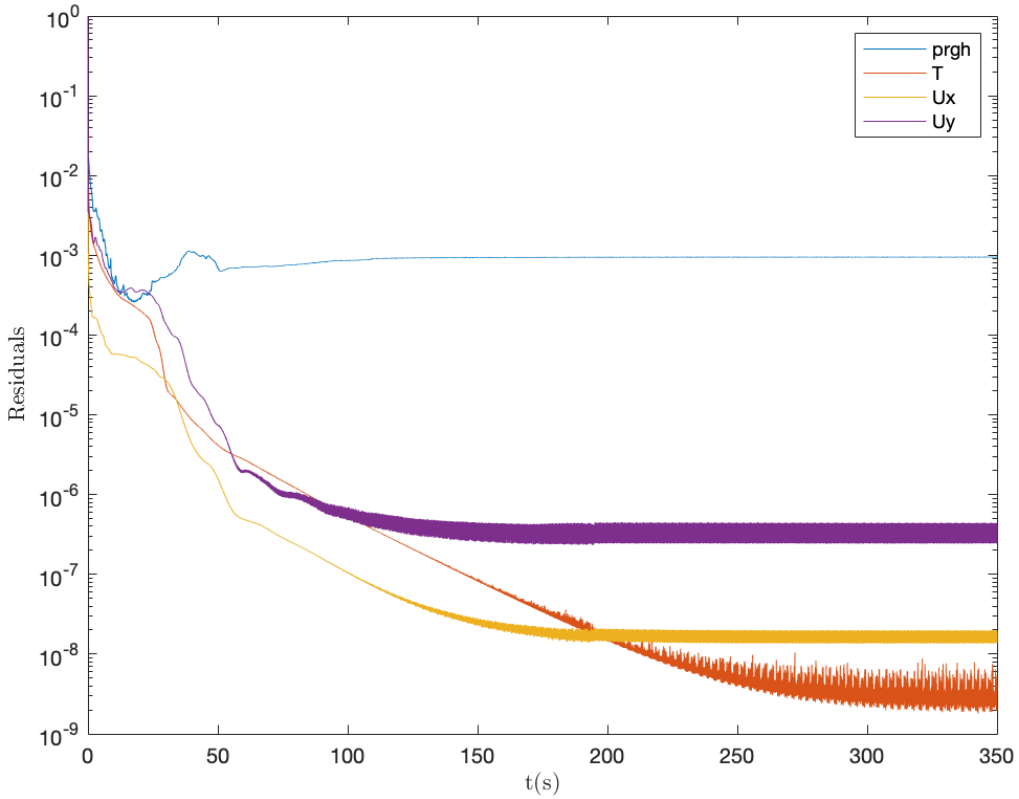

Figure 5-30. Residuals of simulation where leeward side, ground and roofs are heated (ΔT=2K)

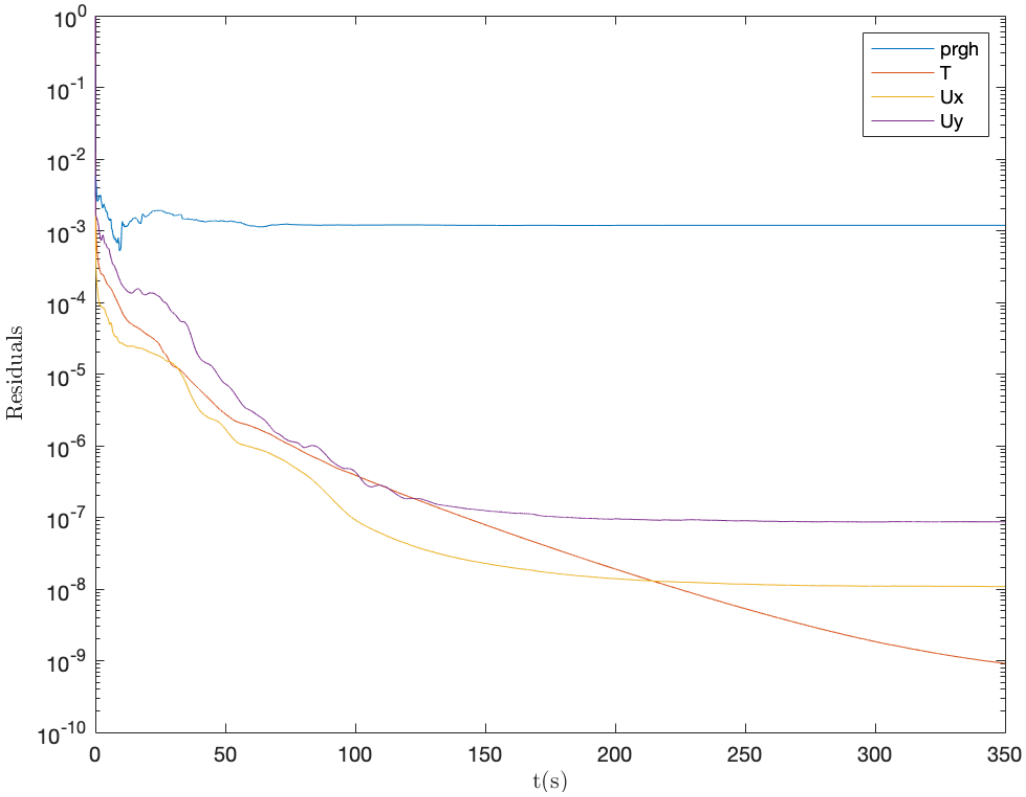

Figure 5-31. Residuals of simulation where leeward side, ground and roofs are heated (ΔT=6K)

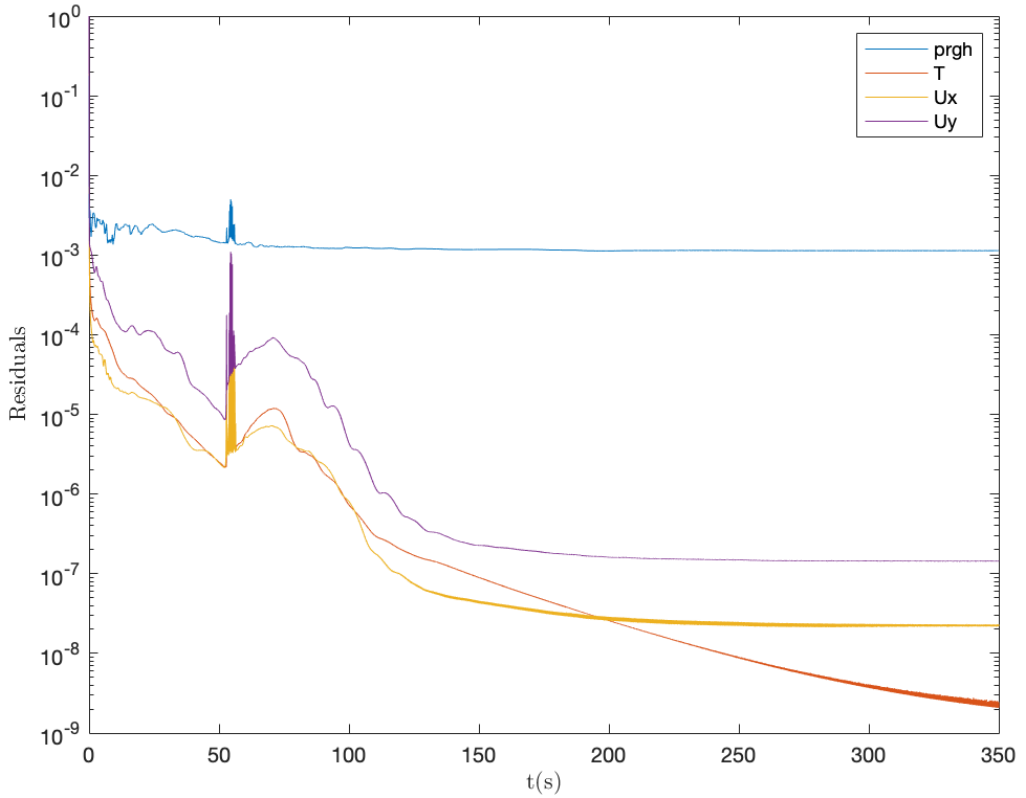

Figure 5-32. Residuals of simulation where leeward side, ground and roofs are heated (ΔT=12K)

5.4.2.2 *Pressure*

Concerning the pressure maps, it can be seen how the suction bubble generated after the stagnation point is strengthened when the leeward side and ground surfaces are heated achieving a minimum peak value of -1.8 m^2/s^2. In addition, from the fourth canyon till the last one it can be clearly appreciated that minor suction regions appears within them.

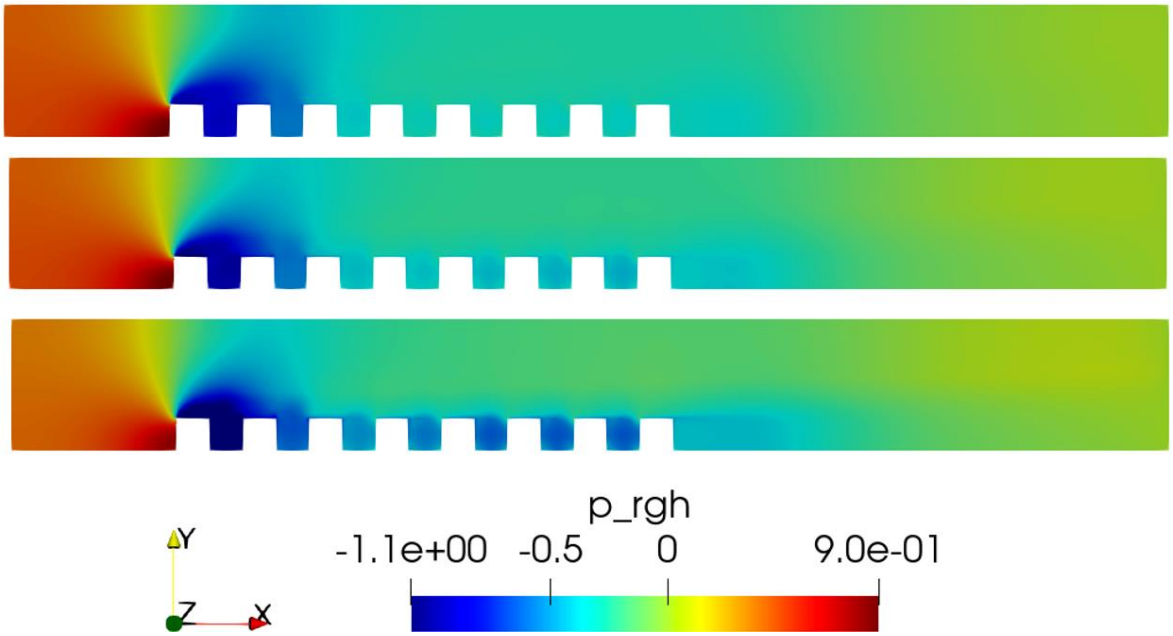

Figure 5-33. Pressure maps for case 2 (From top to bottom: ΔT=2K, ΔT=6K, ΔT=12K)

5.4.2.3 *Temperature*

The following images show how the temperature inside the canyons increases with temperature, however the temperature of the air outside the canyon does not seem to increase which means that the air is not mixing enough with the fresh air from the stream flow to cool it down so, the particles inside the canyon are getting hotter and hotter.

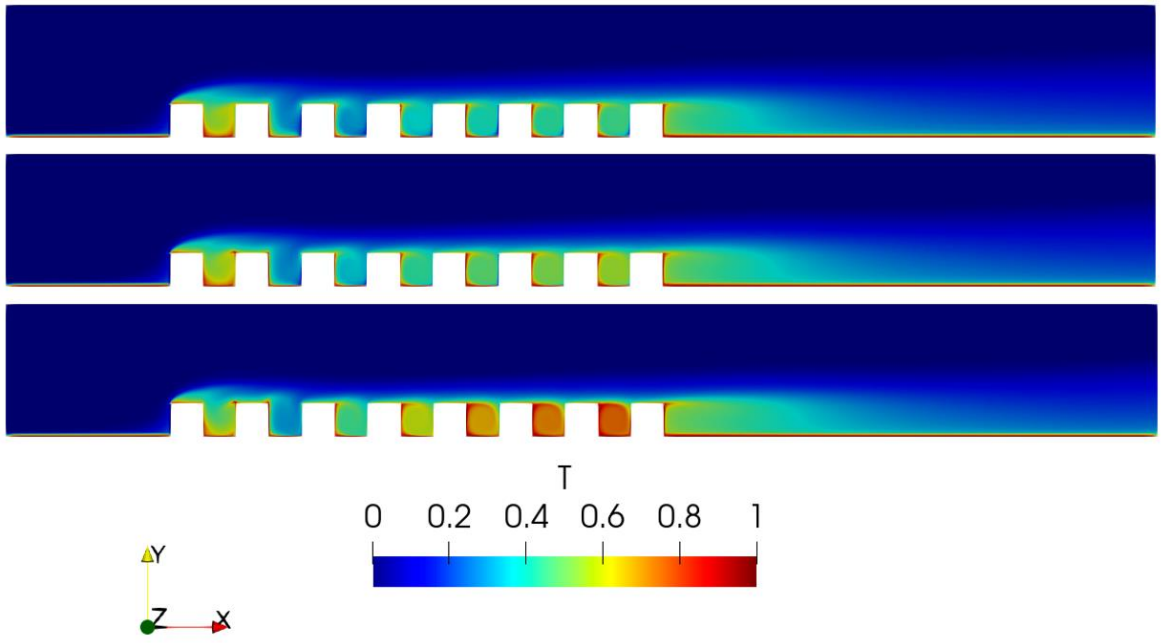

Figure 5-34. Normalized temperature map field for case 2 (From top to bottom: ΔT=2K, ΔT=6K, ΔT=12K)

5.4.2.4 *Velocity*

In *Figure 5-35*, the flow structure of the complete domain is shown. The flow structure does not have much difference compared to the simulations carried out with all the bottom surfaces at a higher temperature than the ambient air.

It is observed that in the last three canyons of the model, the mean velocity of the vortex increases as the temperature difference between the leeward wall and the windward wall also increases.

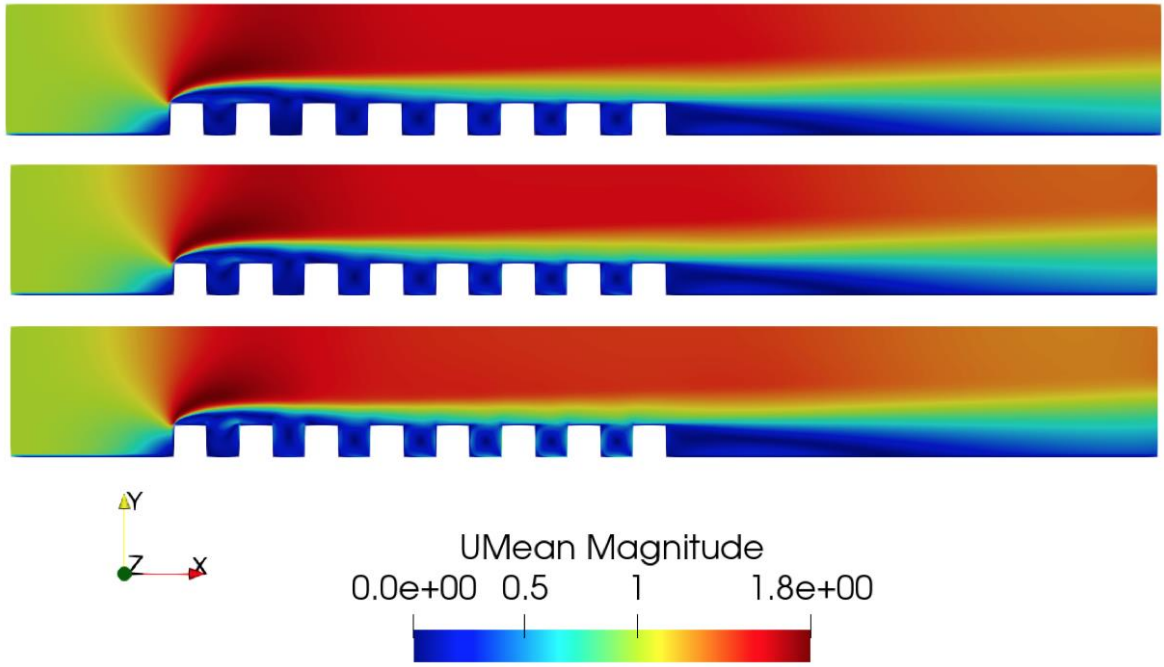

Figure 5-35 Mean velocity maps for case 2 (From top to bottom: ΔT=2K, ΔT=6K, ΔT=12K)

When analyzing the air movement in the urban canyon, it is observed that the average air velocity in the Y direction increases as the temperature difference also increases.

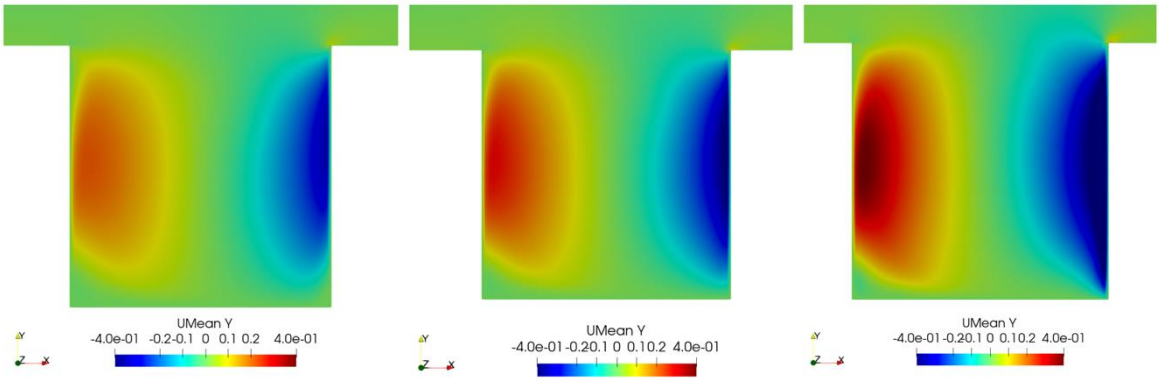

Figure 5-36. Mean velocity maps (Y direction) in the 4th canyon for case 2 (From left to right: ΔT=2K, ΔT=6K, ΔT=12K)

5.4.2.5 *Streamlines*

The streamlines of the complete domain presented in *Figure 5-37* show an important difference compared to the simulated scenarios in the previous case: the main vortex maintains its size and its position in the center of the canyon as can be seen from the fourth canyon on.

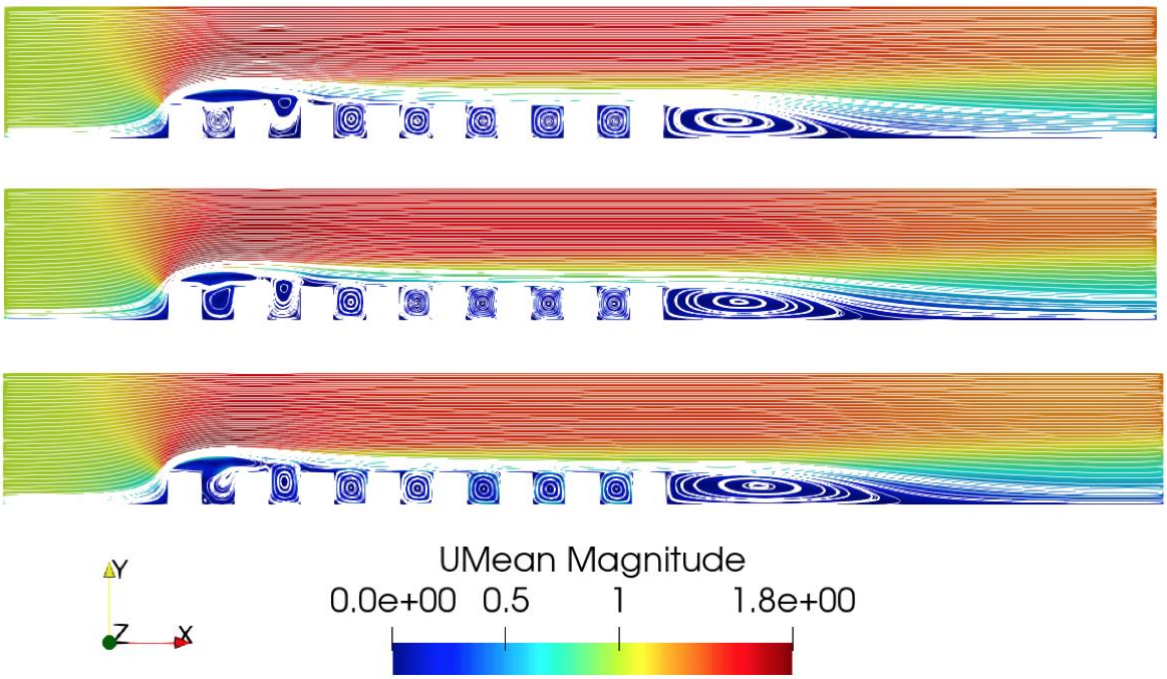

Figure 5-37. Streamlines of the domain for case 2 (From top to bottom: ΔT=2K, ΔT=6K, ΔT=12K)

When analyzing the streamlines in the fourth canyon, it can be better observed what has been previously commented: the presence of a main vortex perfectly centered in the canyon. In addition, a small counter-rotating vortex is observed in the lower corner of the leeward side.

Taking into account what it has been observed in the velocity maps, it can be concluded that for this case (leeward side, ground and roofs heated), the increase in temperature does not modify the air distribution in the canyon, but it does intensify the main vortex as its velocity increases.

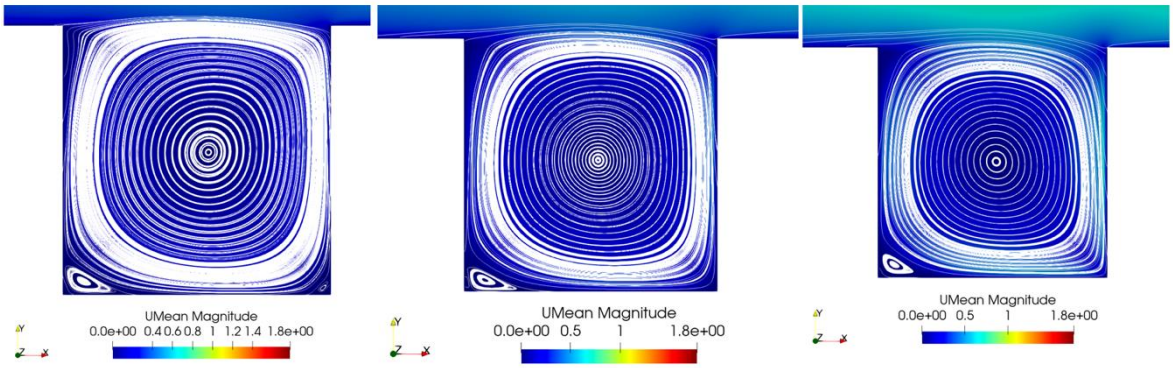

Figure 5-38. Streamlines in 4th canyon for case 2 (From left to right: ΔT=2K, ΔT=6K, ΔT=12K)

5.4.2.6 *Mean pollutant concentration*

Regarding the concentration of pollutants in the complete domain, it can be seen in *Figure 5-40* that the retention of pollutants in the canyon is high and the amount of pollutants that pass to the freestream and to the successive canyons is much lower. For this reason, a scale change is made to observe more clearly what is happening: on one hand, between 2K and 6K figures a significant difference is not observed. On the other hand, for a temperature difference of 12K it is clearly observed that the average concentration of pollutants in the freestream and in the rest of the canyons is considerably reduced, which indicates that the canyon retains more pollutants at higher temperatures.

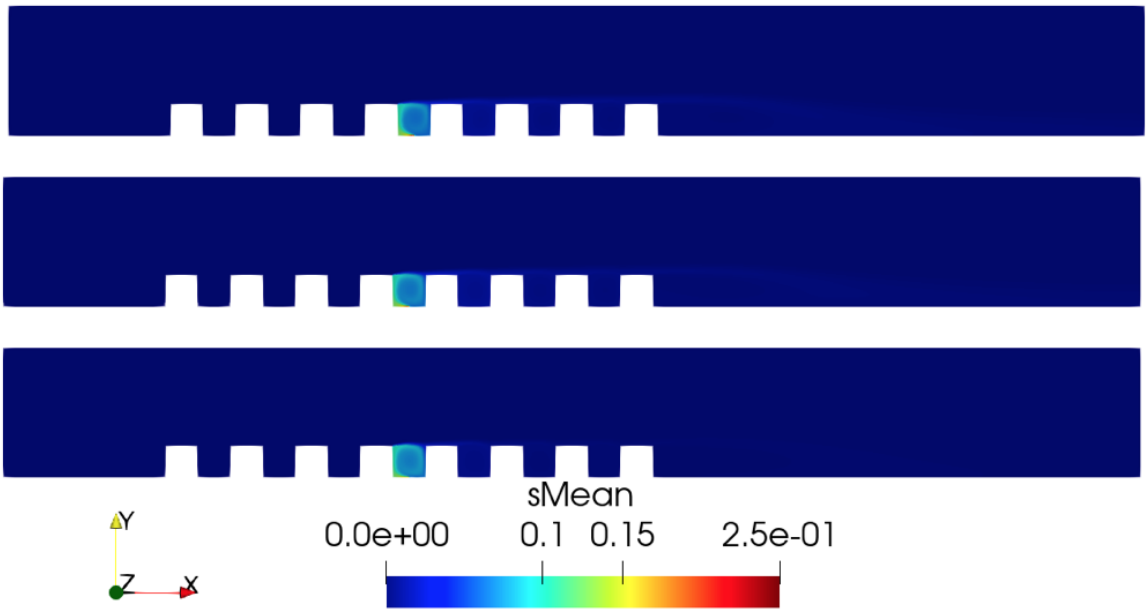

Figure 5-39. Mean pollutant concentration for case 2 (From top to bottom: ΔT=2K, ΔT=6K, ΔT=12K)

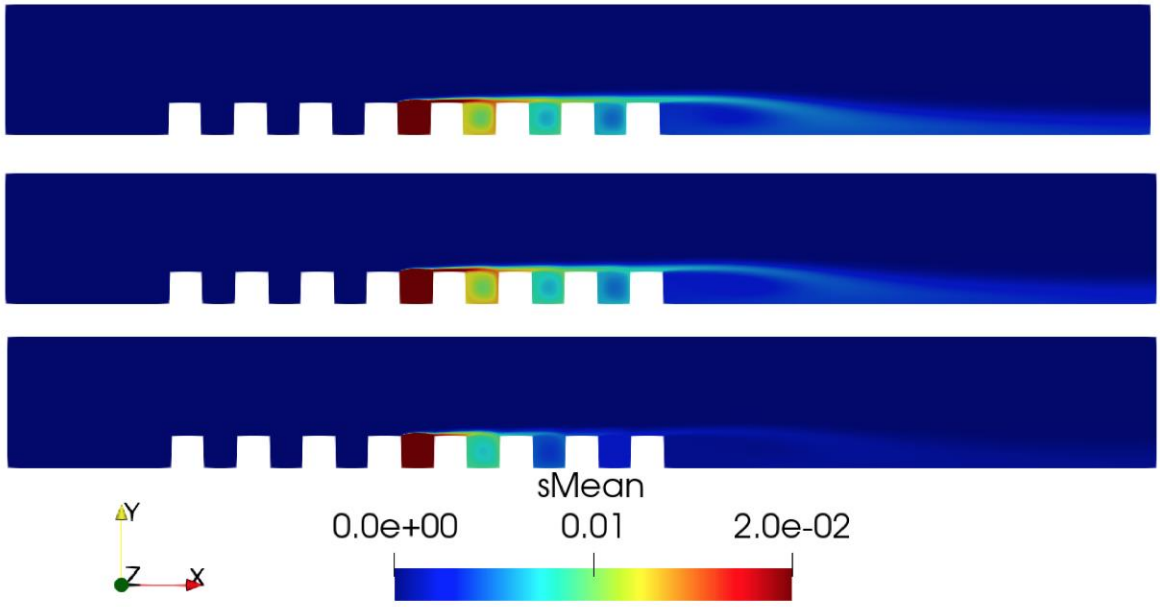

Figure 5-40. Mean pollutant concentration with a scale change for case 2 (From top to bottom: ΔT=2K, ΔT=6K, ΔT=12K)

As the temperature of the leeward side increases compared to the windward wall's temperature, the main vortex strengthens and increases its speed. This should be indicative of better air quality inside the canyon since the air flow structure is the same than for isothermal case. Nevertheless, it seems that if temperature increases it is more difficult to remove the pollutant particles from the urban canyon, so they accumulate and increase the average concentration within urban canyon. This can be clearly seen in detail in *Figure 5-41*:

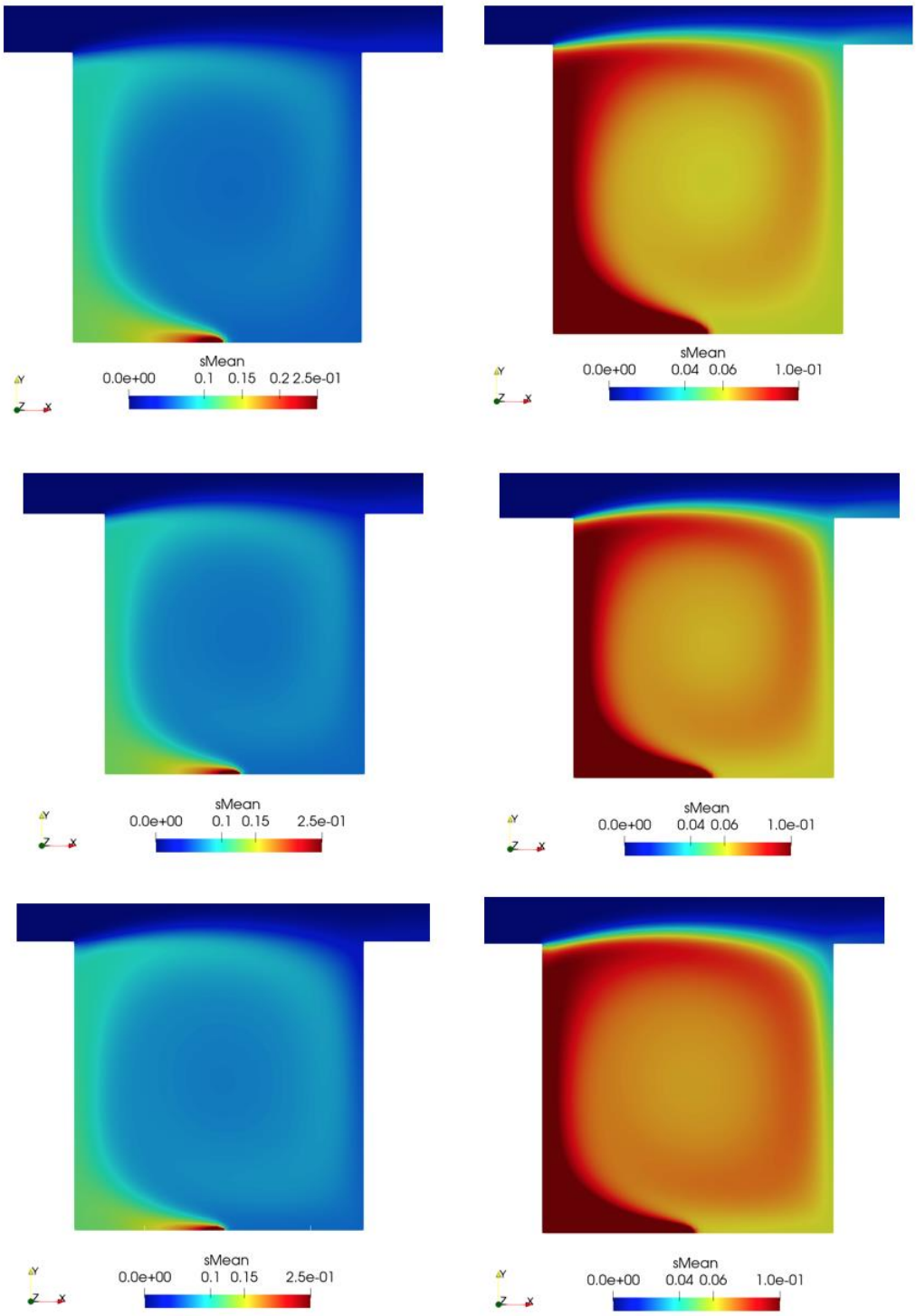

Figure 5-41. Mean pollutant concentration in 4th canyon with a scale change included for case 2 (From top to bottom: ΔT=2K, ΔT=6K, ΔT=12K)

5.4.2.7 Mean pollutant concentration fluxes

In this case it can be clearly seen how the mean pollutant concentration fluxes inside the canyon increases as the temperature of the leeward and ground surfaces rises up. On one hand, *Figure 5-42* shows that stream-wise turbulent transport in windward and leeward sides increases when temperature also increases. On the other hand, the vertical turbulent transport at roof-level decreases with temperature, which means that removal of pollutants is reduced.

Summarizing, this demonstrates what has been previously stated that pollutant removal decreases as long as the temperature of the leeward side increases.

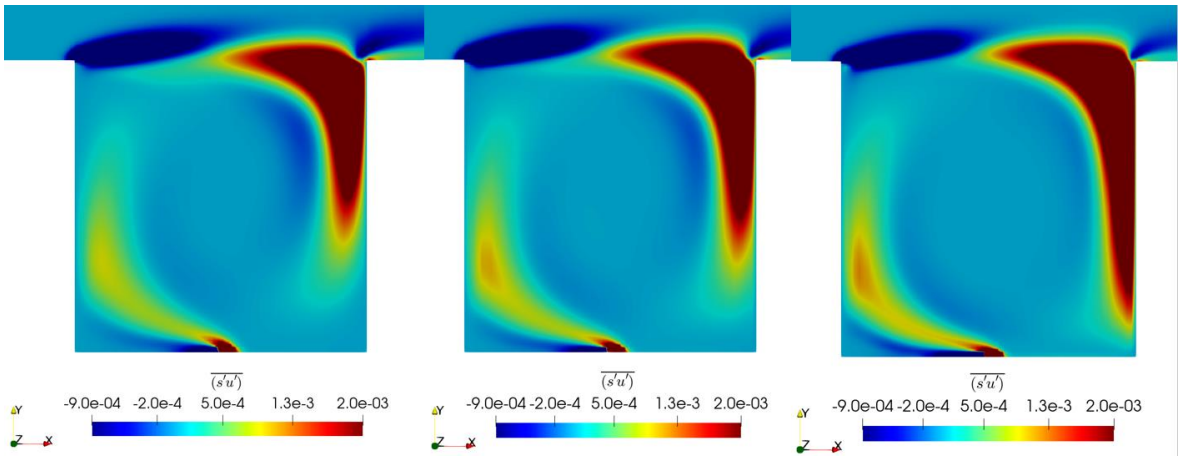

Figure 5-42. Mean pollutant concentration fluxes in horizontal direction for case 2 (From left to right: ΔT=2K, ΔT=6K, ΔT=12K)

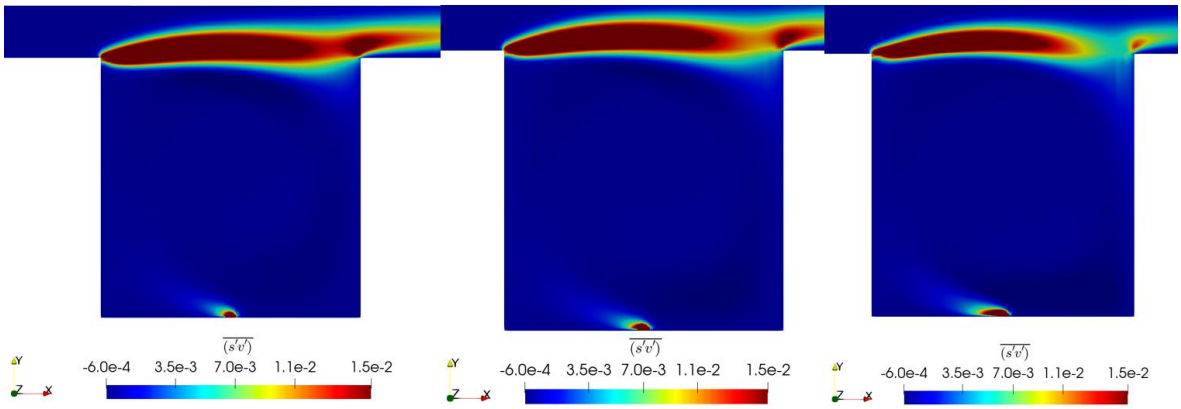

Figure 5-43. Mean pollutant concentration fluxes in vertical direction for case 2 (From left to right: ΔT=2K, ΔT=6K, ΔT=12K)

5.4.3 Windward side and ground heated

5.4.3.1 Residuals

As it has been done in previous sections, the following figures show that the results obtained have converged for the three different temperature scenarios (ΔT=2K, 6K and 12K). Due to the problem mentioned in section 5.4.2.1 with those simulations where the temperature differences were higher (ΔT=6K and ΔT=12K), the time-step has been defined equal to 0.0025 s in order to achieve convergence.

The following figures show that the last three simulations have converged at 350s, 300s and 400s respectively: the pressure is the first one to converge at a value around 10^{-3}, then the velocities in Y and X direction at values between 10^{-6} and 10^{-8} and, finally, the temperature at an approximate value between 10^{-8} and 10^{-9}.

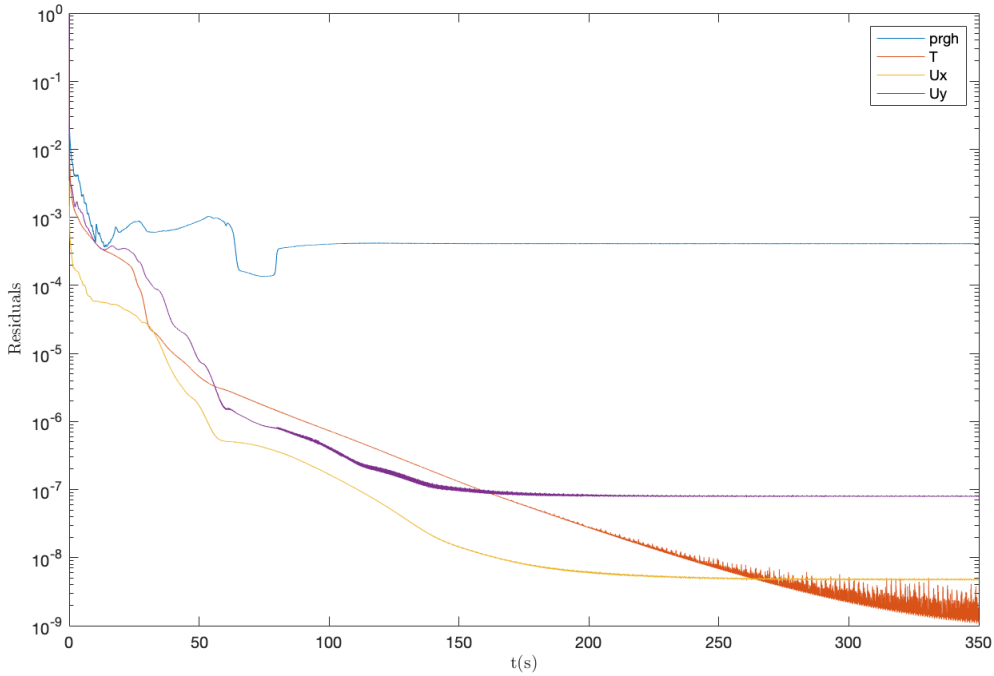

Figure 5-44. Residuals of simulation where windward side, ground and roofs are heated (ΔT=2K)

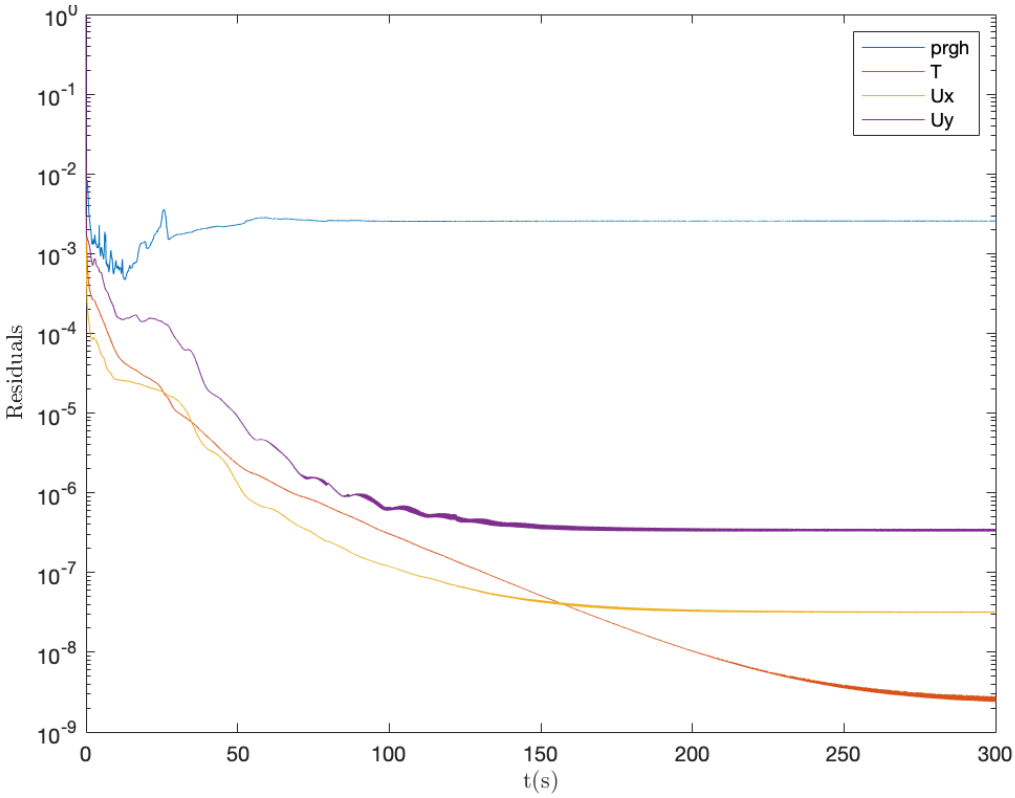

Figure 5-45. Residuals of simulation where windward side, ground and roofs are heated (ΔT=6K)

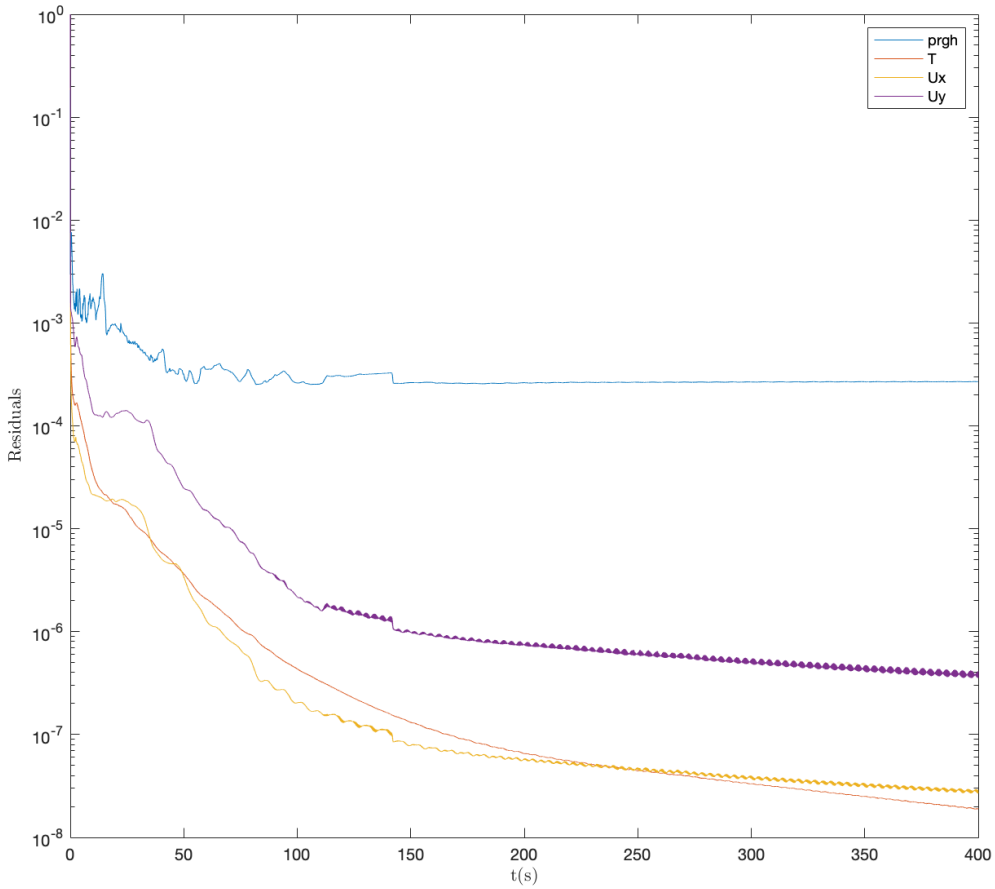

Figure 5-46. Residuals of simulation where windward side, ground and roofs are heated (ΔT=12K)

5.4.3.2 *Pressure*

Finally, the pressure maps for the last of the cases to be studied in this thesis are shown in *Figure 5-47*. A similar distribution of the pressure as the presented in previous case can be appreciated when leeward side were heated. However, the suction bubbles generated inside the canyons are stronger and they protrude through the roof level of the buildings into the flow stream. As it will be seen later, this is generated by the buoyancy forces that pushes the primary vortex of the canyons upwards.

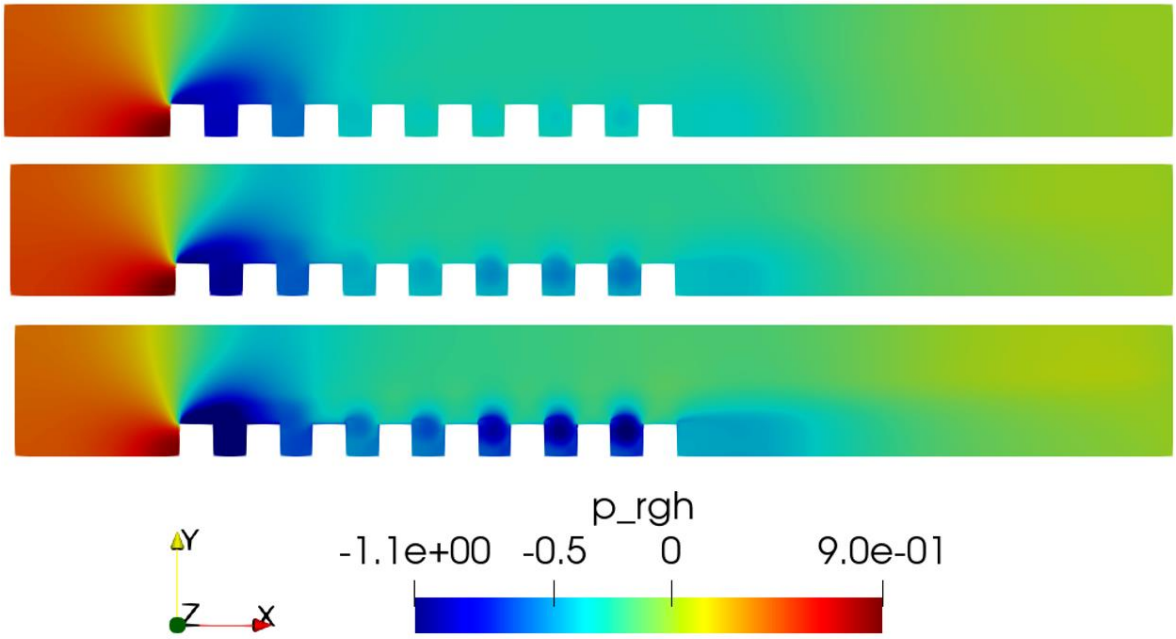

Figure 5-47. Pressure maps for case 3 (From top to bottom: ΔT=2K, ΔT=6K, ΔT=12K)

5.4.3.3 *Temperature*

The map fields of the normalized temperature for this scenario are similar to the ones presented in the previous scenario when the leeward side and the ground were heated. In this case, the temperature of the whole domain outside from the canyon does not change a lot for the different considered gradients, however, the temperature increases at the pedestrian level since the particles that enters to the secondary contra-rotating vortex remain retained for a longer time inside the canyon, thus their temperature increases.

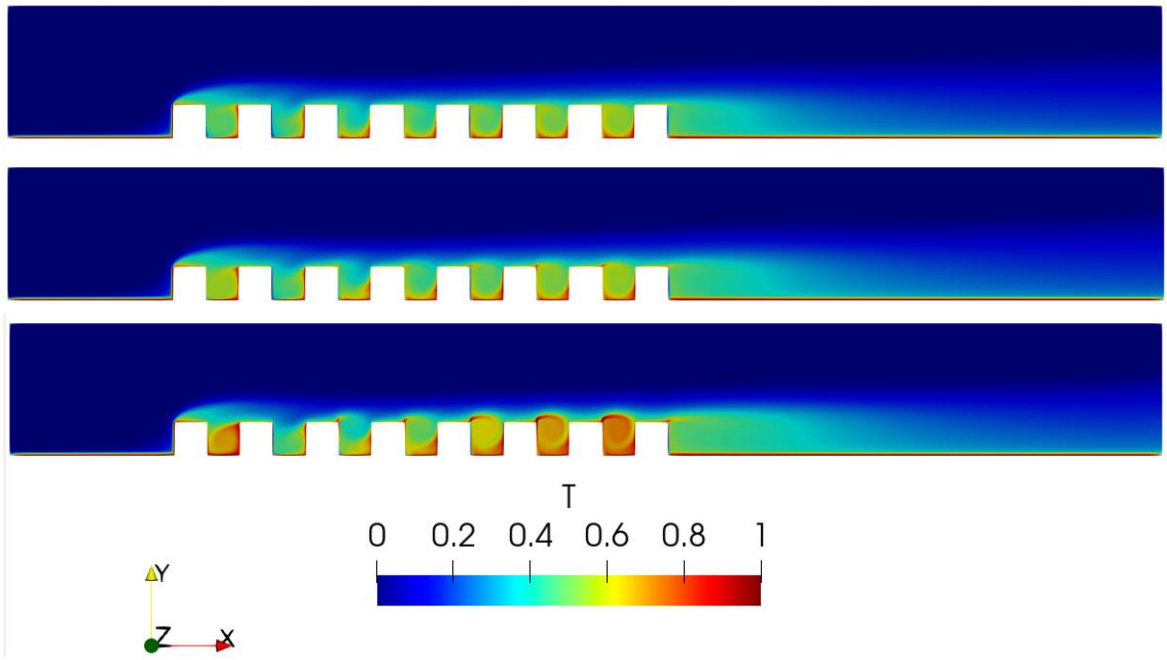

Figure 5-48. Normalized temperature map field for case 3 (From top to bottom: ΔT=2K, ΔT=6K, ΔT=12K)

5.4.3.4 *Velocity*

As can be extracted from the following velocity maps, no significant changes are observed in the flow structure of the simulated domain. An increase in velocity is observed in urban canyons as the temperature increases. Compared to the previous velocity maps, for a temperature difference of 12K the mean velocity inside the urban canyons is higher in the last simulated case.

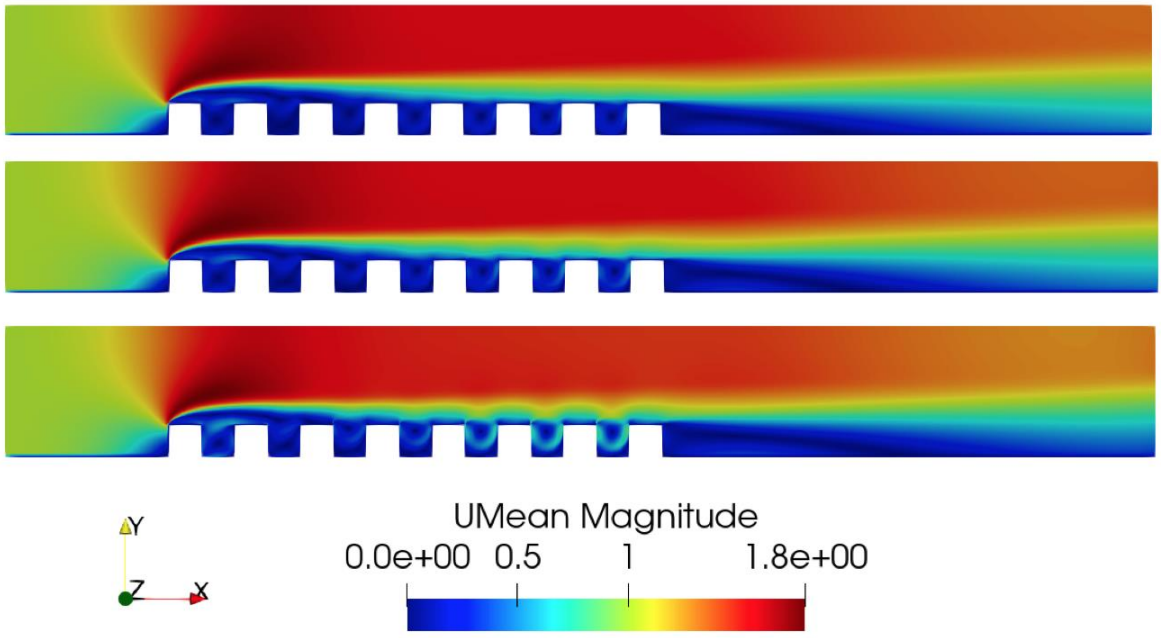

Figure 5-49. Mean velocity maps for case 3 (From top to bottom: ΔT=2K, ΔT=6K, ΔT=12K)

When analyzing the vertical component of the mean velocity in the fourth urban canyon, it can be seen that initially there are two regions with opposite speeds which intensify with the increase in temperature and, in addition, move upwards reaching out of the canyon. This means that the main vortex is displaced upwards, coming out of the canyon at roof-level. This is a consequence of the

increase in the size of the counter-rotating vortices of the lower corners. Consequentally, four differentiated regions are observed for the scenario with a higher temperature difference (ΔT=12K).

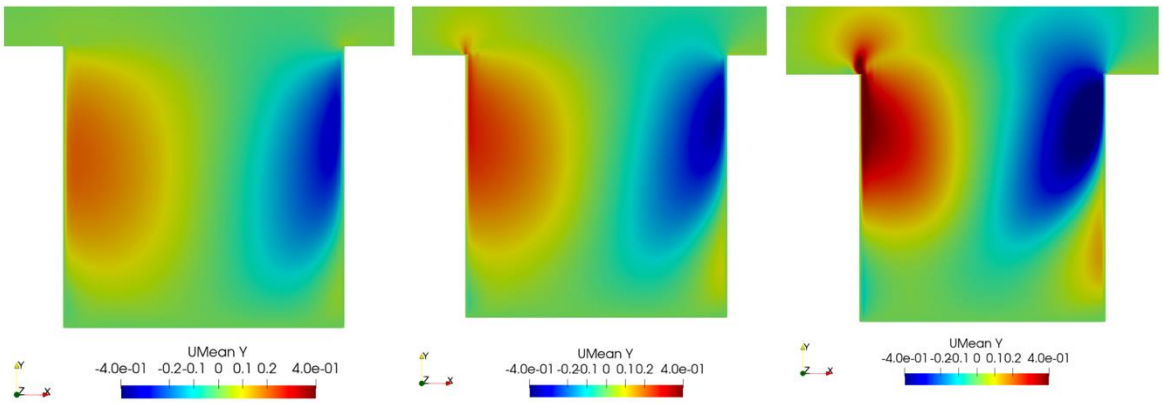

Figure 5-50. Mean velocity maps (Y direction) in the 4th canyon for case 3 (From left to right: ΔT=2K, ΔT=6K, ΔT=12K)

5.4.3.5 *Streamlines*

Studying the streamlines will help to better understand what is happening in this case. Regarding the stream lines of the complete domain, no big differences are observed with respect to those previously shown. It can be seen from the fourth canyon onwards how the increase in temperature moves the center of the main vortex upwards.

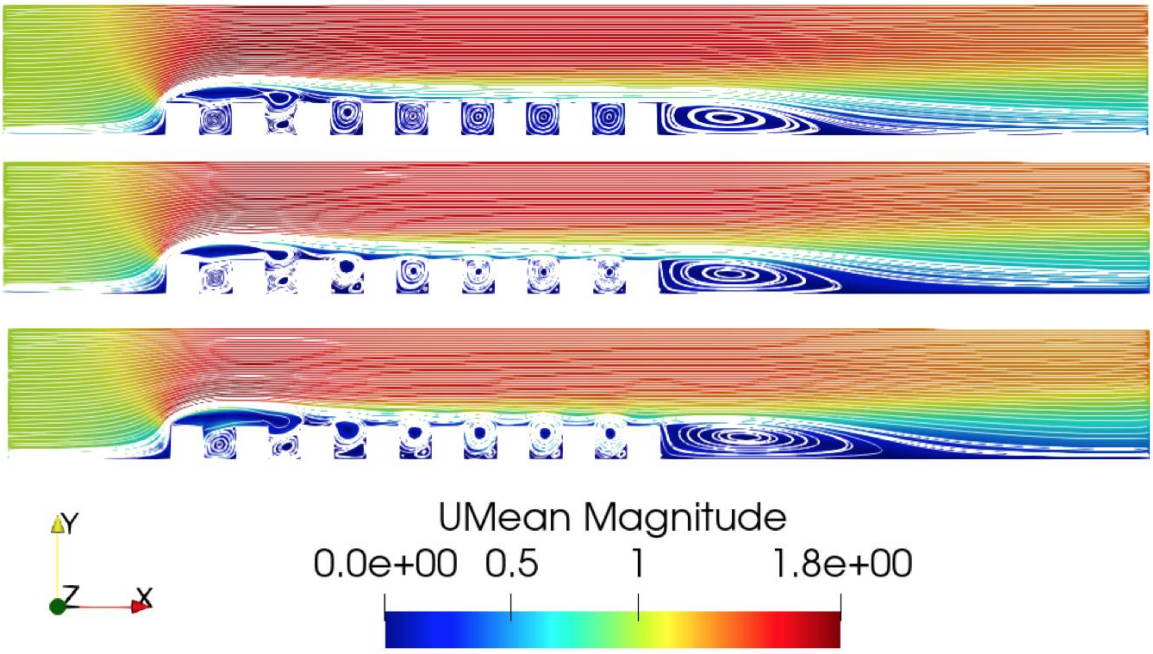

Figure 5-51. Streamlines of the domain for case 3 (From top to bottom: ΔT=2K, ΔT=6K, ΔT=12K)

Observing the streamlines in the fourth canyon, it can be appreciated how the counter-rotating vortices located in the lower leeward and windward corners grow with the increase of temperature, which joins for the scenario with a higher temperature difference. This increase in the size of the lower vortices moves the main vortex upwards taking part of the vortex out of the canyon into the freestream flow.

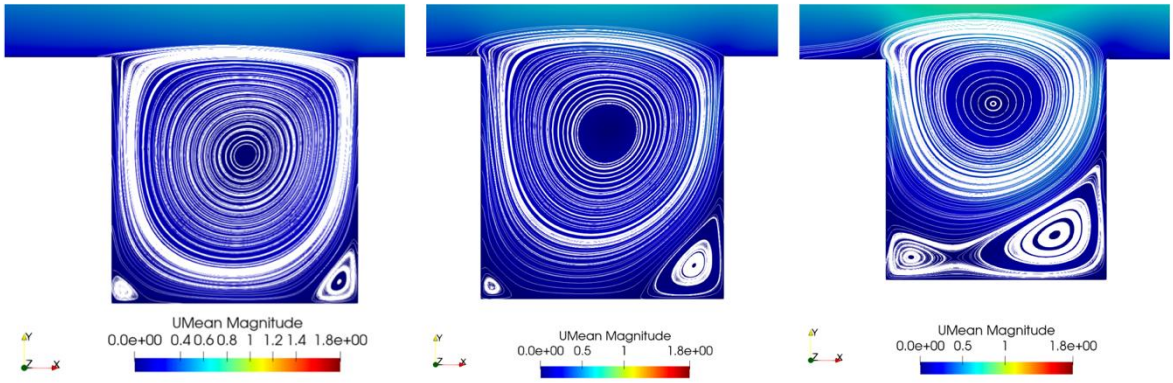

Figure 5-52. Streamlines in 4th canyon for case 3 (From left to right: ΔT=2K, ΔT=6K, ΔT=12K)

5.4.3.6 *Mean pollutant concentration*

In this case, as happened with case 2 in which the leeward side, the floor and the roofs were heated, the increase in the temperature difference causes a reduction in the concentration of pollutants reaching the canyons 5, 6 and 7 so the amount of contaminants that arrives to the end of the domain is also reduced.

With the change of scale, it can be seen that most of pollutants concentration accumulates in the lower half side of the canyon, which is considered the worst scenario since at the pedestrian level the quantity of pollutants will be high, so the quality of the air that people is going to breath will be very poor.

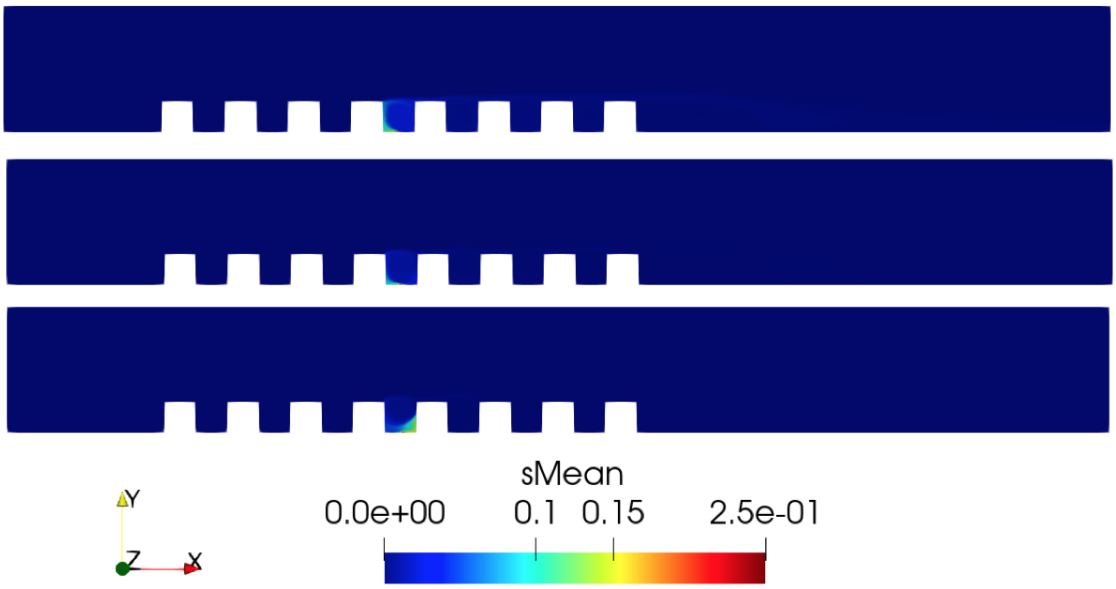

Figure 5-53. Mean pollutant concentration for case 3 (From top to bottom: ΔT=2K, ΔT=6K, ΔT=12K)

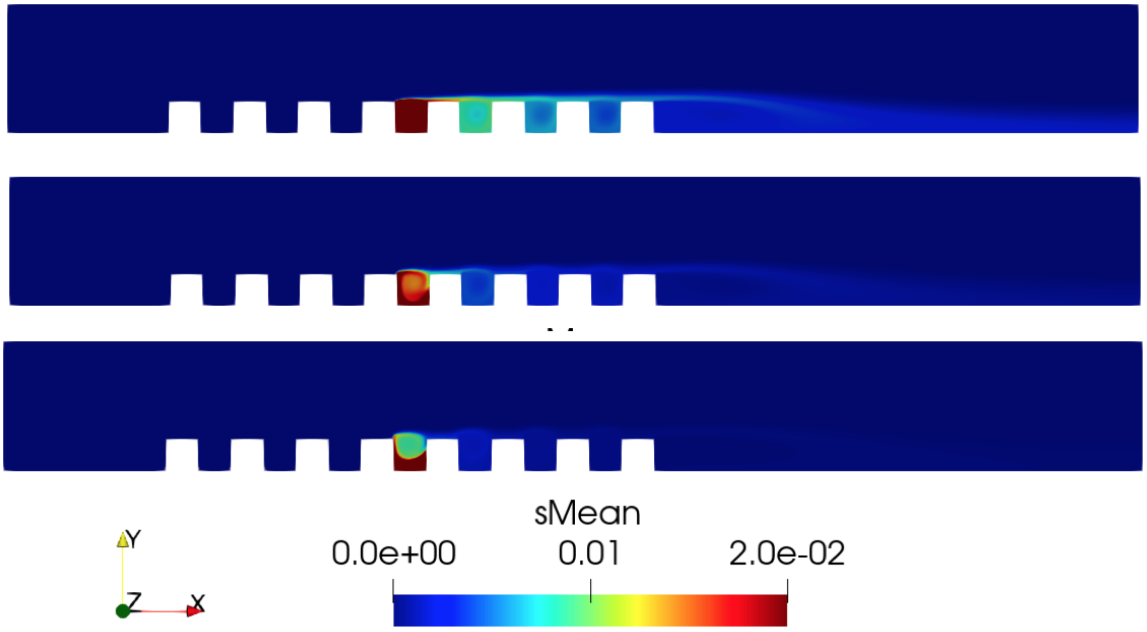

Figure 5-54. Mean pollutant concentration with a scale change for case 3 (From top to bottom: ΔT=2K, ΔT=6K, ΔT=12K)

The following figure shows in detail how as the temperature of the windward side increases, the concentration of pollutants in the canyon increases at the half lower side of the canyon. Therefore, the concentration of pollutants on this scenario will be high at pedestrian level.

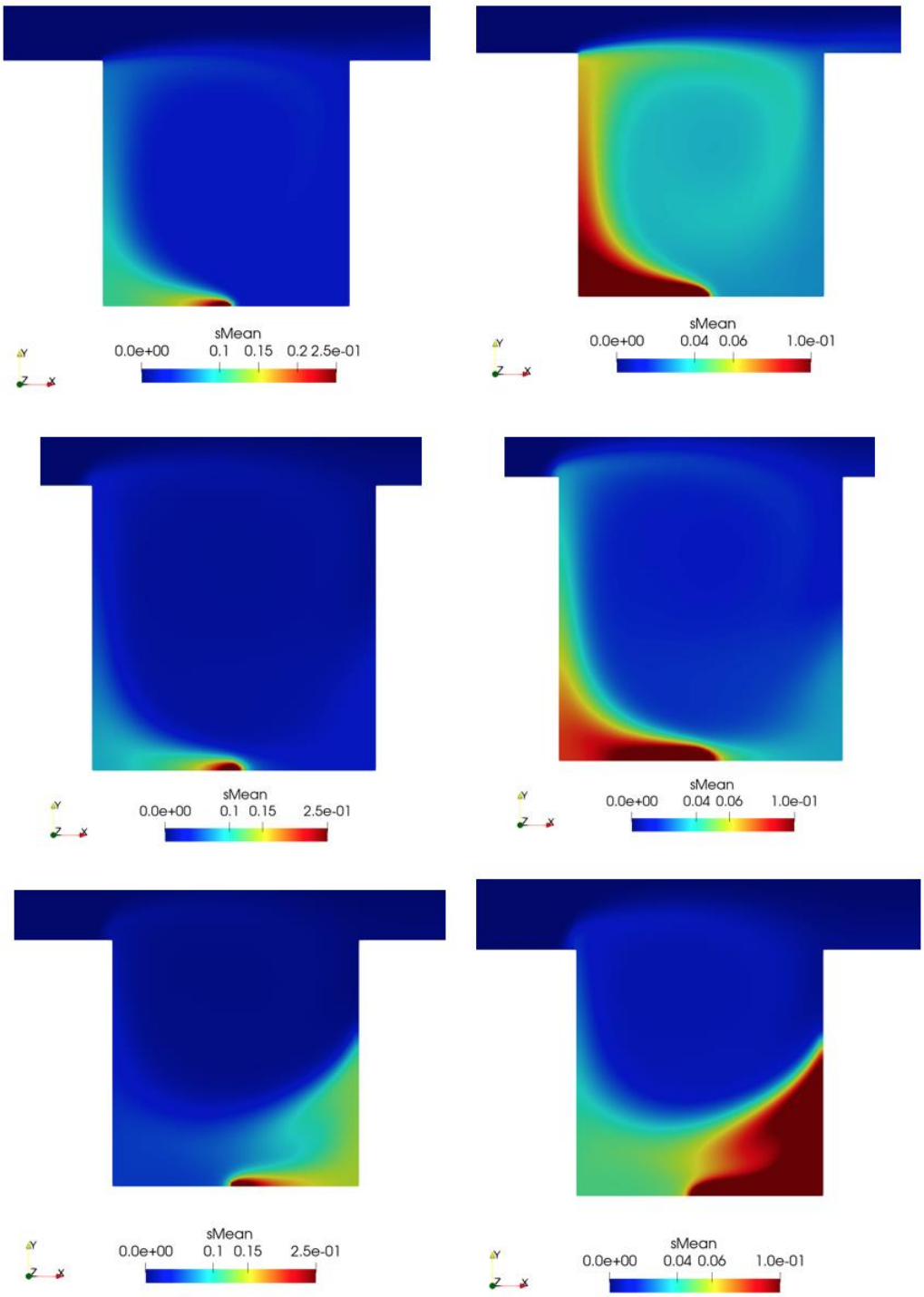

Figure 5-55. Mean pollutant concentration in 4th canyon with a scale change included for case 3 (From top to bottom: ΔT=2K, ΔT=6K, ΔT=12K)

5.4.3.7 Mean pollutant concentration fluxes

To end this chapter, the pollutant fluxes are presented in *Figure 5-56* and *Figure 5-57*.

These figures are similar to the ones obtained for case 1 where all bottom surfaces were heated; however, there are slightly differences. Concerning the vertical fluxes, the pollutant fluxes along the roof level line decrease as long as temperature gradient increases which means that a bigger amount of pollutants are retained at the canyon.

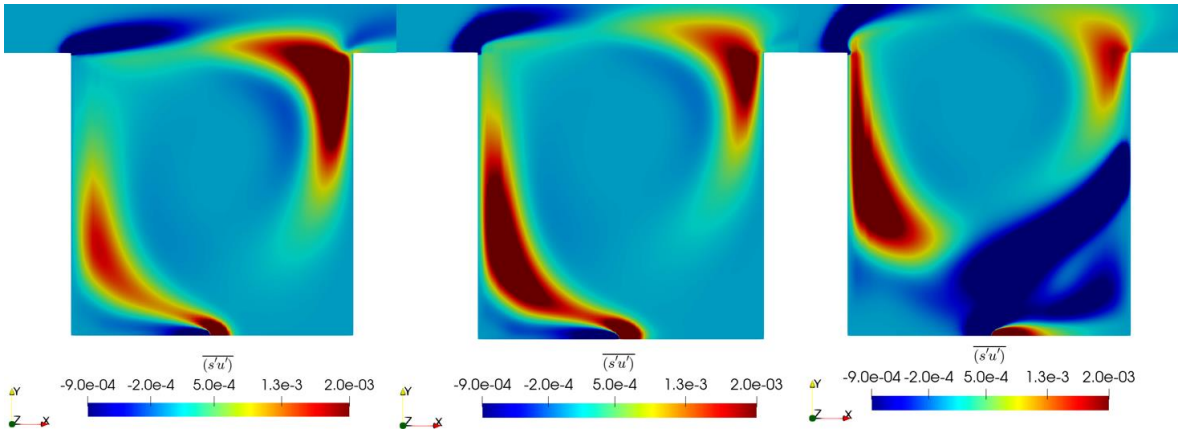

Figure 5-56. Mean pollutant concentration fluxes in horizontal direction for case 3 (From left to right: ΔT=2K, ΔT=6K, ΔT=12K)

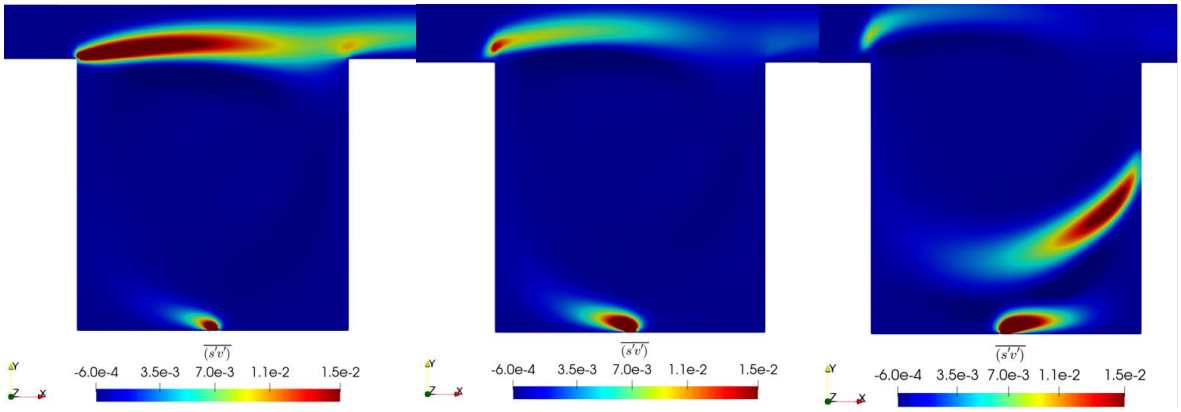

Figure 5-57. Mean pollutant concentration fluxes in vertical direction for case 3 (From left to right: ΔT=2K, ΔT=6K, ΔT=12K)

5.5 Validation

The first step to validate the model has been carried out comparing the normalized temperature and horizontal velocity with those obtained from wind tunnel experimental results conducted by Uehara and other four reports found in the literature where two-dimensional CFD simulations are used with a similar domain to the one used in this thesis.

As it has been previously explained, the experiment conducted by Uehara does not exactly use the same configuration that the one used in this thesis to get results. From the very beginning it was decided to maintain the model used by Pau and Jordi who previously worked in this field since three-dimensional simulations are out of the scope of this study.

To quantify the thermal effects, Uehara introduced a bulk Richardson number which was defined as:

$$Rb = \frac{gh}{U_r^2} \cdot \left(\frac{T_r - T_f}{T_0}\right) \tag{5.1}$$

Where T is the temperature at roof level, Ur is the horizontal velocity also at roof level, T_f is the temperature at the nearest grid point from the pedestrian level and T_0 is the mean temperature within the street canyon.

The simulation used to create the graphs below, considers a differential of temperature between the ground and ambient air of $\Delta T = 2ºC$. The computed Rb in the numerical simulation is -0.28.

The values of each variable have been collected from the lines indicated in section 4.5. It is important to note that these values are dimensionless in order to be able to compare them with those presented in other sources.

In the following lines the colours legend given for the results of each source in the graphic analysis can be found:

- Blue bullets (Rb = -0.21): experimental data from wind tunnel experiment conducted by Uehara.[10]

- Red line (Rb = -0.3): LES simulation from [34]. This study uses a LES based on a one-equation subgrid-scale model to investigate how the flow and pollutant transport is affected by ground heating in urban canyons of aspect ratio 1.

- Yellow line: RANS simulation from [35]. In this paper the authors have studied the effects of heating different surfaces of street canyons with different aspect ratios using a 2D RNG k-epsilon model. This paper is interesting because the authors try to understand which the effects of multi-surface heating are in an urban street canyon. It is also important to mention that these CFD simulations have been done with a Reynolds number of 12,000 and a temperature difference of 6K between heated surfaces and the ambient air.

- Magenta line (Rb = -0.27): RANS simulation from [36]. This paper is mainly focused on understanding which is the interrelationship between aspect ratio, diurnal heating scenario, wind speed and dispersion of reactive gases. In here, the authors have develop a model to couple a CFD model with NO-NO_2-O_3 photochemistry, which differs from the pollutant source used in this thesis where no specific reactive gas have been used.

- Green line (Rb = -0.21): RANS simulation from [37]. In this report, the author tries to analyse the thermo-fluid dynamic effects inside and above street canyon. It is interesting to mention the implementation of the atmospheric boundary layer profiles of velocity, k and epsilon at the inlet of the two-dimensional domain.

- Cyan line (Rb = -0.28): RANS simulation from this thesis.

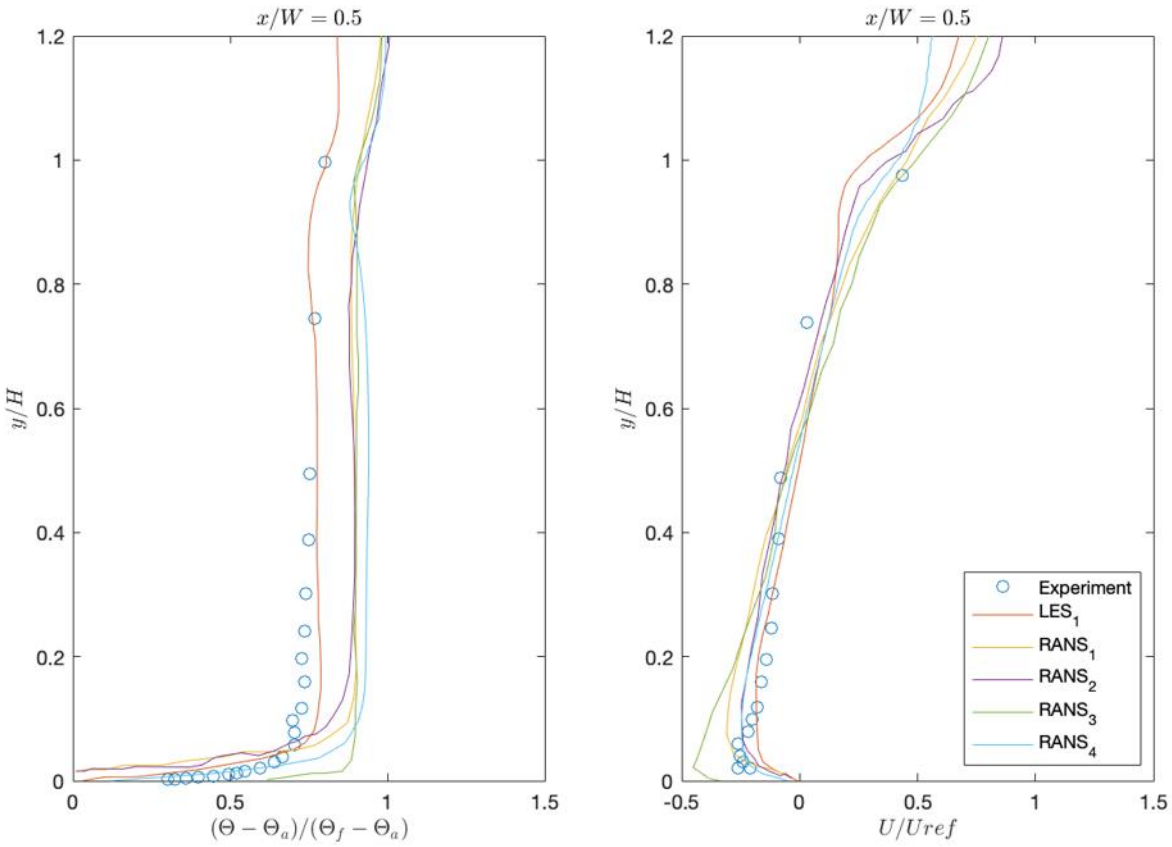

Figure 5-58. Adimensionalized temperature and velocity comparisons at the center line of the canyon

Comparing the temperature values with those extracted from the experiment, the current model provides under-predicted values for temperature along the height of the canyon. In the near-ground level the temperature results obtained with this model are very close to the experimental ones. In the horizontal velocity measured in a line at the center of the canyon, it can be seen how the current model follows with precision the experimental results measured at the same line.

Furthermore, as it can be appreciated, the CFD simulations made by the author of this thesis follows with high precision the other RANS simulations found in the literature. However, there is a bit of divergence when comparing the normalized temperature between RANS simulations and LES simulations.

On one hand, the divergence with the experimental results might be attributed to the differences in the simulation conditions and experimental set up due to the experimental model containing roughness elements which have not been included in the model of this thesis. Furthermore, the experimental model was comprised of city block arranged in a three-dimensional space while the simulation model of this thesis is two-dimensional.

On the other hand, the deviation regarding LES results might be related to the gradient diffusion hypothesis, i.e. how temperature fluctuations are modelled in the RANS model.

Nevertheless, despite some differences, the overall results have been accepted and the model is considered valid to proceed with the simulations considering thermal conditions.

The second part of the validation consists on a comparison of the plots obtained in this thesis with the ones presented in previous mentioned studies as well as in some other papers from the literature: the first one is the study done by Jonas Allegrini, Viktor Dorer and Jan Carmeliet [38] in 2013, called "*Buoyant flows in street canyons: Validation of CFD simulations with wind tunnel measurements*", where the authors try to validate CFD simulations for buoyant flows in urban canyons by comparing the results obtained for 2D steady RANS simulations with wind tunnel measurements. In addition to this paper, the second source that is going to be used is [39]. These studies will help to analyse and validate the results obtained.

Regarding the wind flow structure, on the one hand, the results obtained agree partially with the results presented in [35] since for every simulated case (ground heated, leeward façade and ground heated, windward façade and ground heated and all surfaces heated) two contra-rotating vortexes are found while in this study this happens only for cases where windward façade is heated (windward heated, windward and ground heated or all surfaces heated). On the other hand, in [38] the authors found that one main vortex is formed at the center of the urban canyon when ground or leeward side are heated, while two contra-rotating vortexes appear when the windward side is heated; thus, these results are more similar to the ones found in this thesis. Also, Allegrini found that for ground heating or leeward heating, the main vortex is strength compared to the isothermal case and the same performance can be also appreciated in results obtained in this study.

Furthermore, in *Figure 4* and *Figure 5* from [34] and in *Figure 10* from [39] the results obtained when ground is directly heated differs from those presented in [35] for the same heating scenario since only one main vortex located at the center of the canyon appears and this is strength when the temperature of the ground increases such as it can be appreciated in horizontal and vertical velocity maps.

Regarding the pollutant concentration, similar results are obtained in [34] since the ground heating increase the mixing across the roof level, therefore the mean pollutant concentration inside the canyon is lower than for the isothermal case. The same conclusions are obtained in this thesis comparing *Figure 4-20* and *Figure 5-12* for direct ground heating scenario. Concerning the cases where one of the building facades is heated, major differences are found with the results obtained from literature: when the windward side is heated, independently of the scenario (all surfaces heated, windward and ground heated or only windward heated), the conclusions obtained in [35] agree with the plots presented in this thesis since a bigger quantity of pollutants accumulates in the windward side. However, for the rest of the scenarios where leeward side is heated up, the higher pollutant concentration is not found in the windward side such as it happens in [35], but in the leeward side. This may be also related with the flow stream velocity considered which changes completely the flow structure inside the canyon. For example in [36], where the flow stream velocity is 6.5 m/s, on the one hand, one main vortex appears at the center of the canyon when leeward is heated and the higher concentration of pollutants is found in the leeward side which fits better with the results presented in this thesis; on the other hand, there is also a higher concentration of pollutants in leeward side when windward side is heated up.

To conclude, the results obtained in this thesis show similarities in some aspects and some differences compared to the results obtained from literature. The differences between the results presented in this thesis and the ones obtained from other sources may be due to different aspects: the level of refinement of the mesh both inside the canyon and in the shear layer at the roof level, the turbulence model used to run the simulation e.g. RANS-based, LES… or even in how the pollutant source is modelled.

6 Discussion

This section contains a discussion of the results obtained both for the isothermal case, which is an ideal case in which all the walls of the model and the ambient air remain at the same temperature (T = 296 K), and for the rest of scenarios where some walls are at a higher temperature to mimic solar radiation in the city and see how it can affect the pollutants removal in an urban canyon.

In the results obtained, it has been observed how the effect of temperature has caused changes in the air movement resulting in changes in the pollutant concentration inside the canyon.

Firstly, when analysing the air velocity and distribution within the canyon in the isothermal case, the appearance of a clockwise vortex in the center of the canyon is observed. In addition, two small counter-clockwise vortices in the corners at pedestrian level are also identified.

On one hand, regarding single-surface heating scenarios, when the leeward side or the ground are heated the air flow structure inside the canyon is almost the same than for isothermal case. However, when the windward side is heated the flow structure is completely different since a bigger counter-rotating vortex appears at the lower corner of the windward wall due to the buoyancy. These simulations have also shown that if leeward or ground walls are heated the vortex accelerates. Conversely, when the windward side is heated the air flow reduces its velocity.

On the other hand, regarding multi-surface heating scenarios, it has been seen that in the all surfaces heated scenario when the temperature differences are low, the same vortices were obtained as for the isothermal case. Nonetheless, as the temperature gradient increases, the main vortex is displaced upwards losing speed and the secondary counter-rotating vortex of the windward side grows in strength. This is a result of the upward buoyancy flow due to a stronger diurnal heating.

The velocity map fields of the scenario where leeward and ground are heated up show that the main vortex is neither modified nor displaced, although the air speed in the canyon increases as temperature difference increases, thus the main vortex strengthens. When considering the opposite scenario, in which there is a higher temperature on the windward side and the ground, the main vortex is displaced upwards due to the upward buoyancy flow. In this case, both secondary contra-rotating vortices grow until they form a second counter-clockwise vortex below the main one.

Finally, conclusions can be drawn from the comparisons carried out so far regarding velocity maps and airflow structure for a Reynolds number of 12000 which is moving itself in a perpendicular direction to an urban canyon of aspect ratio 1:

- The heating of ground and/or leeward wall strengthens the main vortex.
- The heating of windward wall tends to create a secondary contra-rotating vortex at the lower corner of windward side which strengthens with the increase temperature difference due to the upward buoyancy flow.

Regarding the pollutant concentration in single-surface heating scenarios, it is observed that when the ground is considered at a higher temperature, pollutant levels in the canyon are lower than for the isothermal case. When the leeward side is considered to be heated up, the mean concentration in the canyon increases with respect to both isothermal and ground heating cases. This is remarkable, since the structure of the airflow in the canyon is the same for these three cases, having a more intense vortex than in the isothermal case, but less than in ground heating scenario.

In the case where the windward side was heated above the rest of the walls, most of pollutants were concentrated at pedestrian level with a higher concentration than in other cases.

In the following lines, the mean pollutant concentration of multiple-heating surfaces scenarios is going to be compared. When the leeward side and ground are heated, the pollutant concentration maps show a similar effect as when only leeward side is heated up: the pollutant concentration increases with temperature, thus the removal of pollutant particles decreases with temperature in this case. When windward side and ground are heated, an effect similar to the one observed for the case

where only the windward side is heated up happens: as the temperature increases, the pollutant concentration accumulates at a pedestrian level. Therefore, the higher the difference of temperature, the higher the mean concentration at low heights.

Finally, when all surfaces are considered at a higher temperature than ambient air, the quantity of contaminants that passes to the following canyons and reaches the end of the domain increases with temperature gradient. The higher it is, the further distances pollutant particles are displaced. This can be explained because buildings and streets have a higher temperature than ambient air so the urban heat plume in this case is larger than in the rest of scenarios (see *Figure 5-20*). Thus, the main flow stream speeds up affecting the transport of pollutants. Also, inside the canyon where the source of contaminants is located, as the temperature increases, a greater concentration appears in the lower corner of the windward side due to a counter-rotating vortex that grows up when the temperature increases because of the upward buoyancy flow.

In order to give an estimate value of pollutant removal from the urban canyon, the concept of ACH (Air Changes per Hour) is introduced. This represents the volume of air renewed per unit of time in the canyon. This concept is widely used in the literature, with the relation with urban street canyons being outlined in [41] by C. Liu, D. Leung and M. Barth. This method uses the integration of the fluctuating velocities along the ventilation area above the canyon to obtain ACH. In this thesis the model considered is a two-dimensional domain. Thus, the values of the fluctuating velocities are obtained from a line at the roof level (y/H = 1).

$$\overline{ACH_+} = \overline{ACH_-} = \frac{1}{2}\int_A (\overline{v'v'})^{\frac{1}{2}}\, dA \tag{6.1}$$

It is important to mention that positive ACH represents the air removal from the canyon, while the negative ACH represents the clean air that enters to the canyon. Due to mass conservation principle inside the canyon, they must have the same absolute value.

To make the results dimensionless, the volume of the urban street canyon as well as the reference time scale shall be known. The volume can be obtained using the height of the buildings which in this case are 1 meter-height, the width of the street which is also 1-meter-wide since the aspect ratio is 1 and the length which for a 2D canyon is also 1m. Since the volume is the same for all simulated cases due to the aspect ratio being the same for each case and the reference time scale ($T = H/U_{ref}$) is also the same for each case, the non-dimensional values are as follows:

$$\frac{\overline{ACH_+}}{\frac{HwL}{T}} = \overline{ACH_+} = \frac{1}{2}\int_{\frac{y}{H}=1} (\overline{v'v'})^{\frac{1}{2}}\, dx \tag{6.2}$$

Then, applying the appropriate post-processing tools, the graphs of the fluctuating velocities along the roof level can be obtained as well as the integrals that will provide an approximation of the levels of pollutants removed from the canyon.

The fluctuating velocity plots for the case where all the walls are heated show quite similar behaviour with some differences. When the temperature difference between the walls and the ambient air is 2K, the removal of contaminants is slightly higher than when the difference increases to 6K. Instead, as the temperature increases and the center of the main vortex is displaced upward to the top-right side of the canyon, vertical fluctuations near the windward side increase. The fluctuating peak velocity on the windward side is caused by the increase of turbulent kinetic energy generated by the mechanical wind shear. The figure below shows how the growth of the counter-rotating secondary vortex slightly decreases the ACH in the canyon.

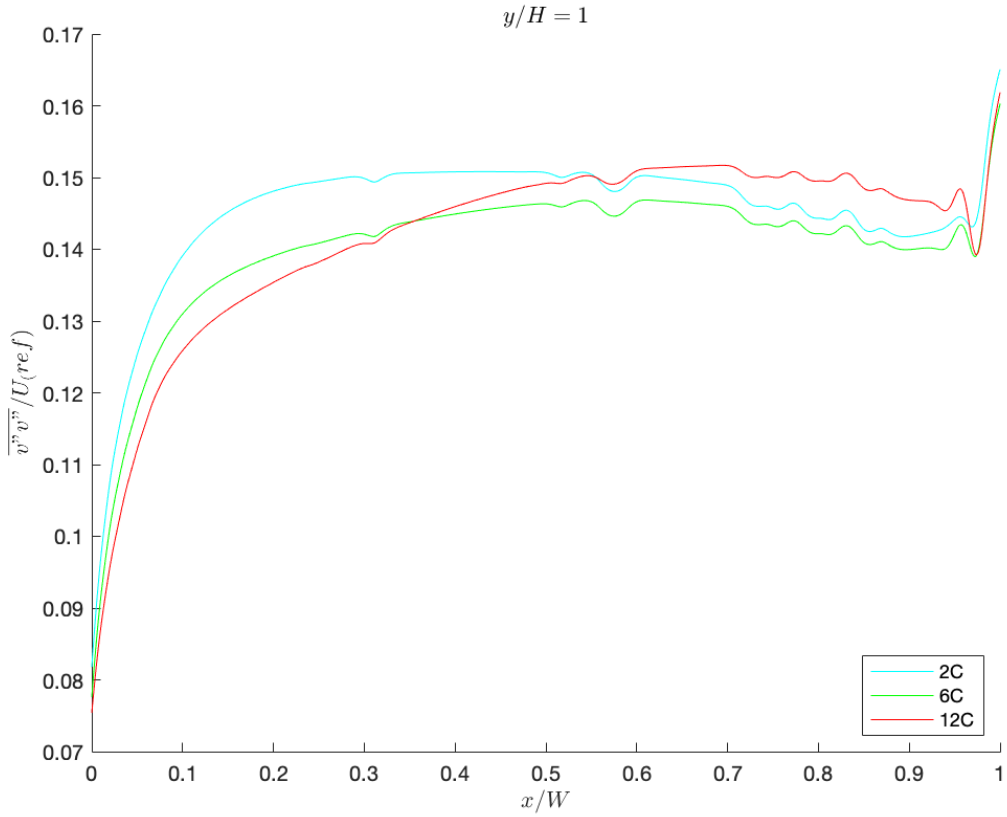

Figure 6-1. All surfaces heated

In *Figure 6-2*, it can be clearly observed how the increase of the leeward side temperature decreases the pollutant transport along the roof of the canyon. Also, the highest vertical fluctuations are found at the windward side and at this point, the values reached by all three scenarios are practically the same. This graph is in line with the results presented in map fields of *Figure 5-40* and *Figure 5-41* where, the pollutant concentration outside the canyon decreases when temperature of leeward side increases while, the pollutant concentration inside canyons increases. Also, the vertical mean pollutant concentration fluxes shown in *Figure 5-43* are related with the figure below since these fluxes decrease as the temperature increases.

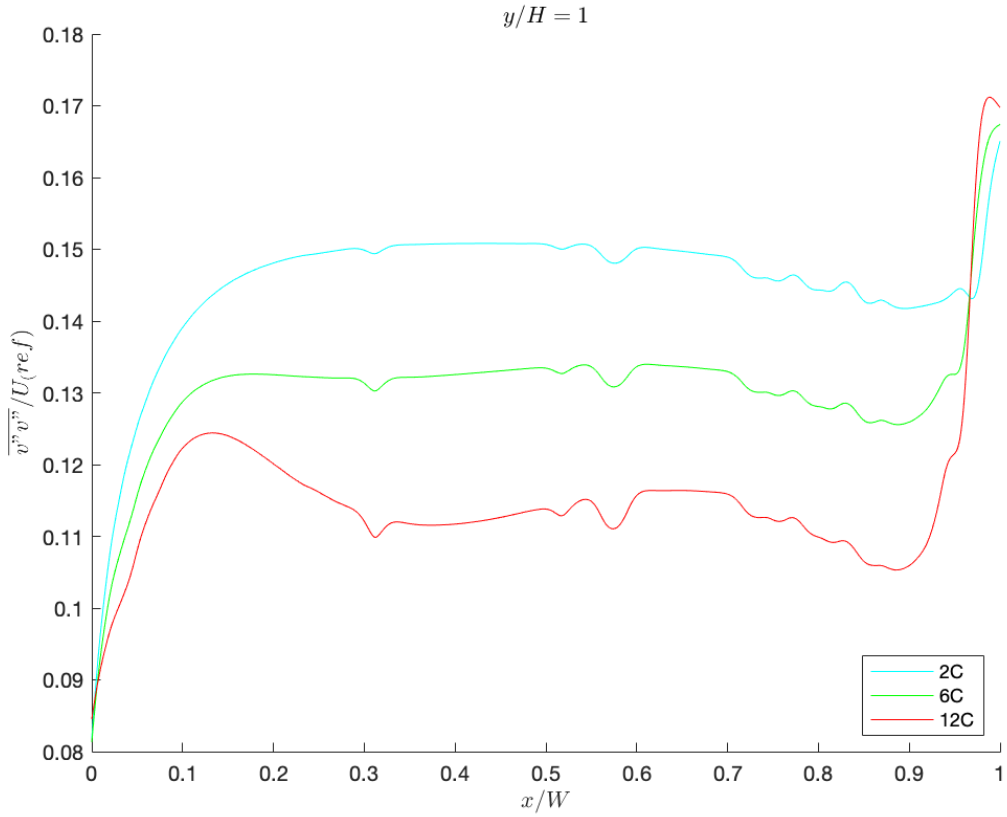

Figure 6-2. Leeward, ground and roof surfaces heated

The fluctuating velocities at roof level for the case where windward, ground and roofs are heated are shown in *Figure 6-3*. Here, it can be seen how with the increase of temperature gradient, the vertical fluctuating velocities increase considerably at both sides of the street at roof level, while decrease at the middle. This happens due to the fact that with the increase of temperature, the counter-rotating secondary vortex grows due to the upward buoyancy force and the main vortex is pushed upwards, approaching its center closer to the middle of the roof level. Thus, higher fluctuating velocities are found in the top corner of the leeward and windward sides. This graph confirms that the fluctuating velocities decrease when temperature difference increases and, ultimately, the quantity of pollutants leaving the canyon as can also be observed in *Figure 5-57*.

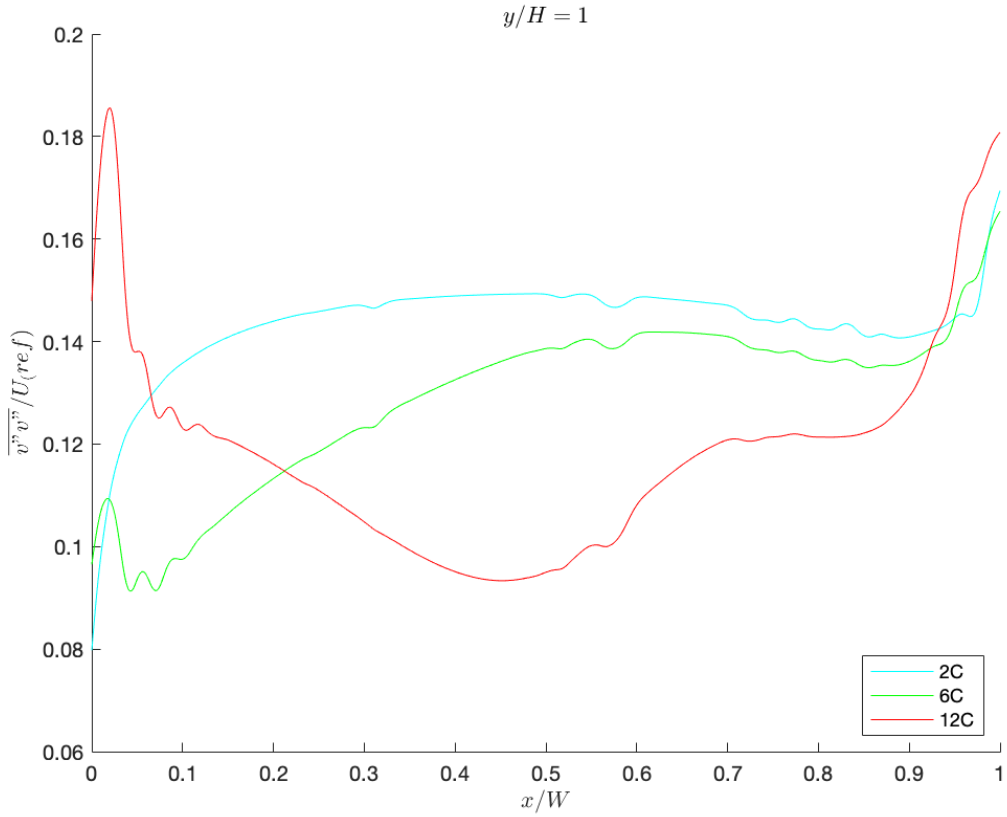

Figure 6-3. Windward, ground and roof surfaces heated

The ACH related with the figures above are obtained from the integrals previously mentioned and they have been summarized in the following table:

Table 6-1. ACH values of multi-heating surface scenarios considered

Case	ΔT [K]	ACH/(HwL/T)
All surfaces heated	2	0.0726
	6	0.0701
	12	0.0709
Leeward side, ground and roofs heated	2	0.0726
	6	0.0653
	12	0.0576
Windward side, ground and roofs heated	2	0.0717
	6	0.0644
	12	0.0593

As previously noted, when analyzing the plots, the ACHs were reduced in the scenarios where the leeward and windward sides were heated, while in the scenario where all bottom walls were heated the ACHs were also reduced, although very minor. The reduction in air quality inside the urban canyon in any of the scenarios where the windward side warmed up is normal because the counter-rotating secondary vortex located in the downwind building is strengthened, causing an accumulation of contaminants at pedestrian level and making it difficult for them to reach roof level. However, in the case of the leeward side, the fact that the air quality is reduced differs from what was observed in simulations of other reports, which may be due, as previously mentioned, to the level of refinement in the shear layer at roof level.

7 Budget

A total amount of 400 hours were needed to carry out this thesis. The project can be divided into different work packages/tasks and the dedicated time for each one has been represented in *Figure 7-1*.

Most of the time used to develop the project was dedicated to the setting up and running of CFD simulations of the different cases with OpenFOAM. This task is followed by the writing of the report. Nevertheless, if all training tasks are considered in the same group (formation in different softwares), then the second task with the biggest amount of hours would be the training. This was to be expected given that great part of the time employed was dedicated to learning to use the necessary tools to carry out this project.

A reference cost per hour of 25 €/h was considered. However, the amount of formation hours have not been considered in the budget as they are considered tasks more proper of a student than a professional engineer. Furthermore, the energy costs related to the energy consumption of the computer as well as the light required to finish this thesis have been estimated.

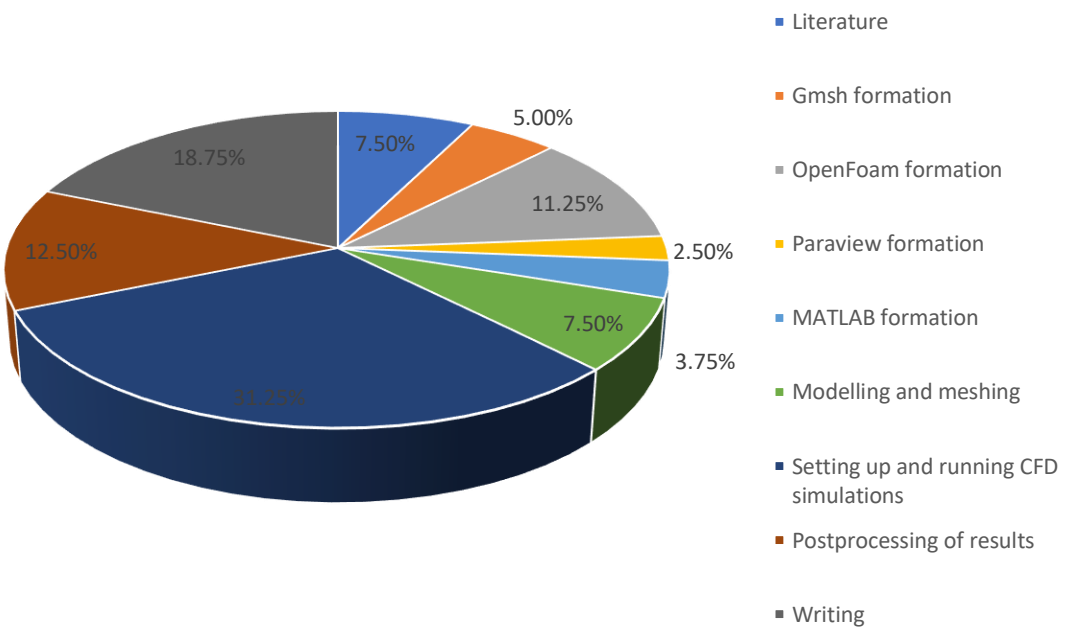

Figure 7-1. Distribution of spent time by engineer on each task

The license prices of the employed softwares shall also be included in the budget:

- Gmsh. License price: free.
- OpenFOAM. License price: free.
- Paraview. License price: free.
- MATLAB Student version. License price: free (University agreement)
- Microsoft Office. License price: free.

Eventually, table 7-1 show the total amount of the disaggregated costs. The detailed table may be found in *Annex*.

Table 7-1. Total costs of the project

Reason	**Total amount [€]**
Training	0
Engineer work	7000
Energy	8.37
Licenses	0
TOTAL	**7008.37**

Therefore, the final budget of this thesis is 7008.37 €.

8 Environmental impact

In recent years, the importance of our actions have over the environment has increased and it has become in a moral responsibility to take actions in order to reduce our environmental footprint. In a similar manner, when carrying out a project, the impact that this work has on the environment must also be taken into account.

This master thesis was developed with a laptop computer MacBook Pro 11.4 which charger has a DC output of 20.0V and 4.25A. The total amount of hours used to finish this project were approximately 400 hours. Therefore, the energy used can be calculated as:

$$E = 20V \cdot 4.25A \cdot 400\ h \cdot \frac{3600s}{1h} = 122400kJ \tag{8.1}$$

Then, if it is assumed that the total amount of electricity used has been generated through non-renewable sources, the CO_2 emitted to the atmosphere can be calculated according to the carbon intensity of energy production in Spain [33]:

$$m_{CO_2} = 122400kJ \cdot \frac{0.16kgCO2}{kWh} \cdot \frac{1kWh}{3600kJ} = 5.44\ kgCO_2 \tag{8.2}$$

Therefore, the environmental impact is low.

9 Conclusions

In this study several two-dimensional RANS-based CFD simulations of an urban street canyon with AR = 1 have been carried out. In order to analyse how the temperature affects the airflow structure and the pollutant transport, different case scenarios using the same domain were created. A first one without including thermal effects (isothermal case), a second one including only one surface at a higher temperature than the rest (single-surface heating cases) and a third one, more realistic, where different surfaces have a higher temperature than the ambient air and shadowing effects were also included. Therefore, in this thesis all the steps to carry out a CFD study were followed: creating geometry with a CAD software, meshing of this geometry, configuring each different case and running the CFD simulations, post-processing of the results and validating them.

The first case analysed, the isothermal one, can be considered as a preliminary problem. The aim of including this case was to get an idea of how the pollutant transport and the airflow structure are inside an idealized canyon where all the surrounding walls are at the same temperature than ambient air in order to make comparisons with the rest of cases simulated afterwards. The results obtained for this case have been corroborated and they are in accordance with the results found in literature as seen in the validation section. Mainly, one main vortex appears at the center of the urban street canyon and two little counter-rotating vortexes are found at the lower side of the upwind and downwind building facades.

The second case analysed, the single-surface heating one, comprises three different scenarios: ground heating, leeward heating and windward heating. In all these cases the difference of temperature considered was 6K. In these simulations, it is not as easy to corroborate the results as for the isothermal case since there are a lot of different combinations which may affect in different ways the air flow structure and pollutant transport: the established air flow stream velocity, the gradient of temperature considered or the heated wall can change the results obtained completely. Nevertheless, the results have been contrasted with several different sources and they fit quite well.

The air flow structure remains similar to the one presented in the isothermal case when the leeward side or the ground are heated, but it is observed that the main vortex is strengthened, while when the windward side is heated the secondary counter-rotating vortex of the windward side increases in size and becomes stronger compared to the same vortex in the other scenarios. In addition, this causes the main vortex to weaken, losing velocity. These changes also affect the distribution of contaminants inside and outside of the canyon. It has been observed that when the leeward side or the ground are heated, the path followed by pollutants inside the canyon is the same as for the isothermal case. However, the quantities vary in each case: first, when ground is directly heated, there is a lower concentration of pollutants inside canyon. Second, when leeward side is heated there is a higher concentration of pollutants in the upwind building façade that reaches the roof and leaves the canyon, although part of them are re-entrained the canyon. Therefore, a higher concentration of pollutants throughout the canyon is observed. Third, when the windward side is heated, the pollution inside the canyon worsens because they have to follow a longer path to leave the canyon since most quantity of pollutant particles enters the secondary vortex on the windward side before passing to the main one to reach the roof level.

The third case analysed, the multi-surface heating one, comprises also three different scenarios: ground and leeward heated, ground and windward heated and all surfaces heated. In all these scenarios three different gradients of temperature were studied: 2K, 6K and 12K. Here, more discrepancies were found regarding the results obtained compared to those presented in other similar studies. For the multi-surface heating scenarios, there are not as many studies to validate the current results as for the single-surface heating scenarios.

In this case, it was observed that in those scenarios in which the windward side was not heated, the air distribution was practically identical to the one obtained for the isothermal case, regardless of the applied temperature difference. Conversely, in those cases in which the windward side was one of the surfaces heated, the counter-rotating secondary vortex located in the lower side of the downwind

building façade grew and pushed the main vortex upwards. It was observed that the temperature of the urban heat plume was higher when all bottom surfaces were heated and due to this fact, the flow stream velocity speed up favouring a higher concentration of pollutants reaching the last urban canyons as well as the end of domain. On the other hand, concerning the other two cases, the temperature outside of the canyon practically did not change, while the temperature inside of the canyons increased when the temperature of the walls also increased.

In terms of pollutant concentration, this is where the author has found more discrepancies since it has been observed that with the increase in temperature of the leeward side and the ground, the maps show a larger amount of mean pollutant concentration inside the canyon and a lower renewal of the air, while in different studies from the opposite is indicated. However, in the rest of simulated cases, results are in line with what has been shown in other studies, since when the windward side is heated, the appearance of a second large counter-rotating vortex below the main one increases the retention of pollutants at pedestrian level and, ultimately, reduces the removal of contaminants from the canyon.

Additionally, the ACHs of the multi-heating surface scenarios were calculated. Despite no values were found from other sources with similar simulations in order to compare them, the author of this thesis considers that it is interesting to be able to give an estimate value of the air renewal for each simulated case. In line with the maps presented, it was observed that the greatest renovation occurred in the scenario where all bottom walls were heated, while for the scenarios in which leeward and windward sides were heated, the air quality inside the canyons worsened as wall temperatures increased; thus, ACH decreased.

Finally, but not less important, it is important to comment that the model chosen to carry out this study has been the RNG k-epsilon, which is a RANS based turbulence model and is used in most of the studies that have been consulted to develop this thesis. On one hand, the results show that for the isothermal case the model gives close results to the experimental ones and to other simulations that use both RANS and LES turbulence models. On the other hand, the model shows some limitations when thermal effects are included, which causes certain differences with the experimental results because the buoyant flow fields have three-dimensional flow characteristics and they cannot be correctly captured with a two-dimensional RANS simulation, but 3D CFD simulations are required. Furthermore, it has been seen that there is a deviation in the prediction of the air temperature in the center of the canyon (x=12.5m) between the experimental results and those obtained by LES and RANS simulations which might be related to the gradient diffusion hypothesis, i.e. how temperature fluctuations are modelled.

There are many different ways and paths to continue improving this project:

The first recommended step would be to increase the refinement level at the shear layer of roof level in order to see if there are some improvements regarding deviations previously mentioned. It is important to correctly model the shear layer since it is the area where the air exchange is produced.

Another interesting step would be to carry out 3D simulations modifying the current domain and modelling a real street canyon considering side inflows because they also play an important role. An alternative option would be to repeat this study but using a Large Eddy Simulation model instead of a Reynolds-Averaging Navier-Stokes model in order to make a comparison between the results obtained in here with the new ones. To carry out these modifications bigger computational power would be needed.

Also, some changes may be implemented in this model such as introducing different aspect ratios to the current domain or even changing the shape of building's roofs in order to see how they affect air velocity, temperature and pollutant distribution inside and outside urban street canyons.

These improvements will help other authors who want to continue studying the effect of pollution inside cities, which is one of the biggest problems today and will continue to be as there are more and more cities and they are more and more populated.

To conclude this final thesis, I would like to remark that, regarding the engineering behind of computational fluid dynamics, there is not a unique way to solve the problem but many of them. In this field, progress in this type of projects is slow because it requires a lot of resources and time and

each advance is treated as a small victory. Despite all, the engineer must find the way to solve the problem even when deviating from the initial path.

10 References

[1] Jordi Galí. Air distribution in street canyons: a cfd study (2019).

[2] Pau García. Air distribution in street canyons: a cfd study (2021).

[3] Emission of air pollutant from transport. [Online]. Available: : https://www.eea.europa.eu/data-and-maps/indicators/transport-emissions-of-air-pollutants-8/transport-emissions-of-air-pollutants-8, 11/10/2021.

[4] M. Nunez and T. Oke, "The Energy Balance of an Urban Canyon", *Journal of Applied Meteorology*, vol. 16, no. 1, pp. 11-19, 1977.

[5] T. Oke, "Street design and urban canopy layer climate", *Energy and Buildings*, vol. 11, no. 1-3, pp. 103-113, 1988.

[6] J. Sini, S. Anquetin and P. Mestayer, "Pollutant dispersion and thermal effects in urban street canyons", *Atmospheric Environment*, vol. 30, no. 15, pp. 2659-2677, 1996.

[7] J. Kim and J. Baik, "A Numerical Study of Thermal Effects on Flow and Pollutant Dispersion in Urban Street Canyons", *Journal of Applied Meteorology*, vol. 38, no. 9, pp. 1249-1261, 1999.

[8] X. Li et al., "Large-Eddy Simulation of Flow and Pollutant Transport in Urban Street Canyons with Ground Heating", *Boundary-Layer Meteorology*, vol. 137, no. 2, pp. 187-204, 2010.

[9] M. Pavageau and M. Schatzmann, "Wind tunnel measurements of concentration fluctuations in an urban street canyon", *Atmospheric Environment*, vol. 33, no. 24-25, pp. 3961-3971, 1999.

[10] K. Uehara, S. Murakami, S. Oikawa and S. Wakamatsu, "Wind tunnel experiments on how thermal stratification affects flow in and above urban street canyons", *Atmospheric Environment*, vol. 34, no. 10, pp. 1553-1562, 2000.

[11] Población Mundial: 7.9 Billones de Personas (2022) - Worldometer, *Worldometers.info*, 2022. [Online]. Available: https://www.worldometers.info/es/poblacion-mundial/#table-historical, 20/01/2022

[12] Urban heat island, *En.wikipedia.org*, 2022. [Online]. Available: https://en.wikipedia.org/wiki/Urban_heat_island#:~:text=The%20main%20cause%20of%20the%20urban%20heat%20island,expand%20its%20area%20and%20increase%20its%20average%20temperature, 12/10/2021

[13] H. Taha, "Heat Islands and Energy", *Encyclopedia of Energy*, pp. 133-143, 2004.

[14] Urban canyon, *En.wikipedia.org*, 2022. [Online]. Available: https://en.wikipedia.org/wiki/Urban_canyon, 20/09/2021

[15] M. Dirksen, R. Ronda, N. Theeuwes and G. Pagani, "Sky view factor calculations and its application in urban heat island studies", *Urban Climate*, vol. 30, p. 100498, 2019.

[16] Navier-Stokes Equations. [Online]. Available: https://www.grc.nasa.gov/WWW/k-12/airplane/nseqs.html, 01/10/2021

[17] Boussinesq approximation (buoyancy), *En.wikipedia.org*. [Online]. Available: https://en.wikipedia.org/wiki/Boussinesq_approximation_(buoyancy), 01/10/2021.

[18] The Boussinesq approximation. [Online]. Available: https://www.comsol.com/multiphysics/boussinesq-

approximation#:~:text=The%20Boussinesq%20approximation%20is%20a%20way%20to%20solve,the%20full%20compressible%20formulation%20of%20the%20Navier-Stokes%20equations , 01/10/2021.

[19] *What is computational fluid dynamics (CFD)?, Simscale,* [Online]. Available: https://www.simscale.com/docs/simwiki/cfd-computational-fluid-dynamics/what-is-cfd-computational-fluid-dynamics/, 20/09/2021

[20] Finite Volume Method, *En.wikipedia.org*. [Online]. Available: https://en.wikipedia.org/wiki/Finite_volume_method#:~:text=Finite%20volume%20method%20From%20Wikipedia%2C%20the%20free%20encyclopedia,differential%20equations%20in%20the%20form%20of%20algebraic%20equations, 03/10/2021

[21] Josep M. Bergadà Granyó, Mecánica de fluidos breve introducción teórica con problemas resueltos, 2a ed. Barcelona: Universitat Politècnica de Catalunya. Iniciativa Digital Politècnica, 2015.

[22] S. Pope,Turbulent Flows. Cambridge: Cambridge University Press, 2000.

[23] F. Moukalled, L. Mangani and M. Darwish, "Boundary Conditions in OpenFOAM® and uFVM", *The Finite Volume Method in Computational Fluid Dynamics*, pp. 694 - 695, 2015.

[24] Turbulence models in CFD – RANS, DES, LES and DNS, [Online]. Available https://www.idealsimulations.com/resources/turbulence-models-in-cfd/, 10/10/2021

[25] G. Alfonsi, "Reynolds-Averaged Navier–Stokes Equations for Turbulence Modeling", *Applied Mechanics Reviews*, vol. 62, no. 4, 2009.

[26] Fluent k-epsilon, *Courses.washington.edu*, 2022. [Online]. Available: https://courses.washington.edu/mengr544/handouts-10/Fluent-k-epsilon.pdf#:~:text=The%20RNG%20theory%20provides%20an%20analytical%20formula%20for,e%0Bective%20viscosity%20that%20ac-%20counts%20for%20low-Reynolds-number%20e%0Bects, 15/10/2021

[27] V. Nguyen, T. Nguyen and J. Nguyen, "Numerical Simulation of Turbulent Flow and Pollutant Dispersion in Urban Street Canyons", *Atmosphere*, vol. 10, no. 11, p. 683, 2019.

[28] X. Li, D. Leung, C. Liu and K. Lam, "Physical Modeling of Flow Field inside Urban Street Canyons", *Journal of Applied Meteorology and Climatology*, vol. 47, no. 7, pp. 2058-2067, 2008.

[29] J. Tu, G. Yeoh and C. Liu, "Practical Guidelines for CFD Simulation and Analysis", Computational Fluid Dynamics, pp. 219-273, 2013.

[30] 2.1 File structure of OpenFOAM cases, *OpenFOAM*, [Online]. Available: https://www.openfoam.com/documentation/user-guide/2-openfoam-cases/2.1-file-structure-of-openfoam-cases, 25/09/2021.

[31] OpenFOAM: API Guide: applications/solvers/heatTransfer/buoyantBoussinesqPimpleFoam/buoyantBoussinesqPimpleFoam.C Source File, *Openfoam.com*, 2022. [Online]. Available: https://www.openfoam.com/documentation/guides/latest/api/buoyantBoussinesqPimpleFoam_8C_source.html, 15/10/2021.

[32] Y. Nakamura and T. Oke, "Wind, temperature and stability conditions in an east-west oriented urban canyon", *Atmospheric Environment* (1967), vol. 22, no. 12, pp. 2691-2700, 1988.

[33] Greenhouse gas emission intensity of electricity generation by country, 2022. [Online]. Available: https://www.eea.europa.eu/data-and-maps/daviz/co2-emission-intensity-9/#tab-chart 2 filters=%7B%22rowFilters%22%3A%7B%22ugeo%22%3A%5B%22Spain%22%5D%7D%3B%22columnFilters%22%3A%7B%7D%7D, 02/10/2021.

[34] X. Li et al., "Large-Eddy Simulation of Flow and Pollutant Transport in Urban Street Canyons with Ground Heating", *Boundary-Layer Meteorology*, vol. 137, no. 2, pp. 187-204, 2010.

[35] X. Xie, C. Liu and D. Leung, "Impact of building facades and ground heating on wind flow and pollutant transport in street canyons", *Atmospheric Environment*, vol. 41, no. 39, pp. 9030-9049, 2007.

[36] N. Tong and D. Leung, "Effects of building aspect ratio, diurnal heating scenario, and wind speed on reactive pollutant dispersion in urban street canyons", *Journal of Environmental Sciences*, vol. 24, no. 12, pp. 2091-2103, 2012.

[37] G. Battista and L. Mauri, "Numerical Study of Buoyant Flows in Street Canyon Caused by Ground and Building Heating", *Energy Procedia*, vol. 101, pp. 1018-1025, 2016.

[38] J. Allegrini, V. Dorer and J. Carmeliet, "Buoyant flows in street canyons: Validation of CFD simulations with wind tunnel measurements", 2022. .

[39] L. Li, L. Yang, L. Zhang and Y. Jiang, "Numerical study on the impact of ground heating and ambient wind speed on flow fields in street canyons", *Advances in Atmospheric Sciences*, vol. 29, no. 6, pp. 1227-1237, 2012.

[40] T. Oke, "The energetic basis of the urban heat island", *Quarterly Journal of the Royal Meteorological Society*, vol. 108, no. 455, pp. 1-24, 1982.

[41] C. LIU, D. LEUNG and M. BARTH, "On the prediction of air and pollutant exchange rates in street canyons of different aspect ratios using large-eddy simulation", *Atmospheric Environment*, 2005.

[42] Energy cascade - Wikipedia, *En.wikipedia.org*, 2022. [Online]. Available: https://en.wikipedia.org/wiki/Energy_cascade, 11/11/2021.

[43] Convection–diffusion equation - Wikipedia, *En.wikipedia.org*, 2022. [Online]. Available: https://en.wikipedia.org/wiki/Convection%E2%80%93diffusion_equation, 28/09/2021